ISTANBUL TECHNICAL UNIVERSITY ★ GRADUATE SCHOOL OF SCIENCE ENGINEERING AND TECHNOLOGY

ELECTROSPUN NANOFIBERS OF METHYL METHACRYLATE AND BUTYL ACRYLATE COPOLYMERS

M.Sc. THESIS

Merih Zeynep AVCI

Department of Polymer Science and Technology

Polymer Science and Technology Programme

JANUARY 2012

ISTANBUL TECHNICAL UNIVERSITY ★ GRADUATE SCHOOL OF SCIENCE ENGINEERING AND TECHNOLOGY

ELECTROSPUN NANOFIBERS OF METHYL METHACRYLATE AND BUTYL ACRYLATE COPOLYMERS

M.Sc. THESIS

Merih Zeynep AVCI
(515091050)

Department of Polymer Science and Technology

Polymer Science and Technology Programme

Thesis Advisor: Prof. Dr. A. Sezai SARAÇ

JANUARY 2012

İSTANBUL TEKNİK ÜNİVERSİTESİ ★ FEN BİLİMLERİ ENSTİTÜSÜ

METİL METAKRİLAT VE BÜTİL AKRİLAT KOPOLİMERLERİNDEN ELEKTROSPUN YÖNTEMİ İLE NANOLİF ELDESİ

YÜKSEK LİSANS TEZİ

Merih Zeynep AVCI
(515091050)

Polimer Bilim ve Teknolojileri

Polimer Bilim ve Teknolojileri Programı

Tez Danışmanı: Prof. Dr. A. Sezai SARAÇ

OCAK 2012

Merih Zeynep AVCI, a M.Sc Student of ITU **Institute of Science and Technology/Graduate School of Istanbul Technical University student** ID 515091050, succesfully defended the **thesis** entitled **"ELECTROSPUN NANOFIBERS OF METHYL METHACRYLATE AND BUTYL ACRYLATE COPOLYMERS"**, which she prepared after fulfiling the requirements specified in the associated legislations, before the jury whose signatures are below.

Thesis Advisor :	**Prof. Dr. A.Sezai SARAÇ** İstanbul Technical University	.....
Jury Members :	**Prof. Dr. Ahmet AKAR** Istanbul Technical University	.....
	Prof. Dr. Hale KARAKAŞ Istanbul Technical University	.....

Date of Submission : 19 December 2011
Date of Defense : 24 January 2012

To my family,

FOREWORD

I would like to express my gratitude to my thesis supervisor, Prof. Dr. A.Sezai SARAÇ for his continuous encouragement, guidance, helpful critics and discussions in my studies.

I would like to thank Prof. Dr. H.Yıldırım ERBİL and Res. Ass. Uğur CENGİZ in Gebze Institue of Technology for offering invaluable help in all possible ways, encouragement throughout this research.

I would like to give my special thanks to my laboratory friends Timucin BALKAN, Derya ÇETECİOĞLU, Nazif Uğur KAYA, Fatma Gül GÜLER, Suat ÇETİNER, Başak DEMİRCİOĞLU, Selda ŞEN, Burcu ARMAN, Keziban HÜNER, Hacer DOLAŞ and Bilge KILIÇ for their collaborative and friendly manner.

I would like thanks to my collegues Gözde ÖZKARAMAN, Seher UZUNSAKAL, Selim ZEYDANLI, Merve ZAKUT, Fatma CÖMERT, Atılay TUZER and Damla GÜLFİDAN from Istanbul Technical University.

I would like to thanks to my flatmate Betül ÇEVİK for everything.

My personal thanks goes to Yusuf ÇETİN for his full support, patience, understanding and being always with me during these ten years.

Most of all, I would like to thanks my family, especially my mother Esen Gül AVCI, my father Mehmet AVCI, my sister Ebru KILIÇ and my brother in law Tufan KILIÇ. For all those times they stood by me and heartedly supported. I was able to accomplish everything in my life thanks to their eternal love.

Finally, I would like to thank all of my other friends for all their emotional assists and motivation during this extremely difficult accomplishment.

January 2012

Merih Zeynep AVCI
Chemist

TABLE OF CONTENTS

Page

ABBREVIATIONS

AIBN	**:** Azobisisobutyronitrile
BA	**:** Butyl Acrylate
BT-1	**:** 9.2 % Flor Containing Polymer
BT-4	**:** 8.6 % Flor Containing Polymer
BT-9	**:** 6.6 % Flor Containing Polymer
DMF	**:** Dimethylformamide
DSC	**:** Differential Scanning Calorimetry
FTIR-ATR	**:** Fourier Transform Infrared Spectroscopy
GPC	**:** Gel Permeation Chromatography
KPS	**:** Potassium Peroxydisulfate
MMA	**:** Methyl Methacrylate
M_n	**:** Number Average Molecular Weight
M_v	**:** Viscosity Average Molecular Weight
M_w	**:** Weight Average Molecular Weight
NMR	**:** Nucleear Magmetic Resonance
PDI	**:** Polydispersity Index
PMMA	**:** Poly (methyl methacrylate)
P(BA-co-MMA)	**:** Poly Butyl Acrylate-Methyl Methacrylate Copolymer
P(PFMA-MMA-BA)	**:** Perfluoroethyl Alkyl Methacrylate Containing n-Butyl Acrylate/Methyl Methacrylate Copolymer
r	**:** Reactivity Ratio
SDS	**:** Sodium Dodecyl Sulfate
SEM	**:** Scanning Electron Microscopy
THF	**:** Tetrahydrofuran
T_g	**:** Glass Transition Temperature
η	**:** Intrinsic Viscosity
ε	**:** Dielectric Constant
θ^o	**:** Contact Angle

LIST OF TABLES

Page

LIST OF FIGURES

Page

ELECTROSPUN NANOFIBERS OF METHYL METHACRYLATE AND BUTYL ACRYLATE COPOLYMERS

SUMMARY

This study can be categorized into two parts. The first parts aims to obtain Nanofibers of n-Butyl Acrylate/Methyl Methacrylate copolymer by electrospinning method which can be used for adhesives and coatings. Emulsion polymerization of n-Butyl Acrylate (BA) and Methyl Methacrylate (MMA) initiated by Potassium Persulfate (KPS) in the aqeuos medium was performed. Processing parameters effects on the morphology such as fiber diameter and its uniformity of electrospun polymer nanofibers was investigated. Effects of solutions properties and processing conditions on the electrospun nanofiber morphology were investigated. Polymer solution concentration and dielectric of solvents were found as dominant parameters to control the morphology. Based on the parameter study, electrospun P(BA-co-MMA) fibers as small as 390±30 nm were successfully produced. The diameters of the fibers increase slightly as the concentration of the P(BA-co-MMA) solution is increased and Bead-free nanofibers and smaller fiber can be obtained for the polymer solutions having high dielectric constant. Moreover, processing conditions were examined and as the flow rate is increased, fiber diameter increases. This is apparent that there is a greater volume of solution fiber is drawn away from the needle tip. The diameter values range from 390 nm to 1180 nm for the P(BA-co-MMA) nanofibers. Spectroscopic, morphological and thermal characterization of nanofibers were performed by Fourier Transform Infrared-Attenuated Total Reflectance (FTIR-ATR), Nuclear Magnetic Resonance Spectrometric Measurements (^{1}H-NMR), Scanning Electron Microscopy (SEM), Differential Scanning Calorimetry (DSC) . Number average (M_n) and weight average (M_w) molecular weights were determined in ultra pure THF solvent using Gel Permeation Calorimetry (GPC).

The second aim was to obtain perfluoroethyl alkyl methacrylate containing n-Butyl Acrylate/Methyl Methacrylate copolymer nanofibers. Thus, Statistical copolymers of poly(PFMA-ran-MMA-ran-BA) were synthesized in supercritical carbon dioxide at 200 bar and 80 ^{o}C using AIBN as an initiator in a heterogeneous free radical copolymerization medium at Gebze Institue of Technology. The morphology of the resulting nanofibers was analyzed by scanning electron microscopy (SEM). The structural properties of electrospun poly(PFMA-ran-MMA-ran-BA) composite nanofibers, monomers and copolymers were analyzed spectroscopically i.e. Fourier Transform Infrared-Attenuated Total Reflectance spectroscopy (FTIR-ATR), Nuclear Magnetic Spectroscopy (NMR) and thermal characterization by Differantial Scanning Calorimetry (DSC). The glass transition temperature of the copolymer decreases as a function of BA content due to the increasing free volume of the copolymer. The effect of Fluorine content on the properties of nanofibers were investigated as the Fluorine content increase in the copolymer resulted a decrease in the diameter of nanofibers. The contact angle measurements indicated that the

electrospun nanofiber copolymers were superhydrophobic with a water contact angle of 172^0±1. For oils with surface tension higher than ~45 mN/m, the nanofibers are superoleophobic with a glycerol and ethylene glycol contact angle of 167^0±1 and 163^0±1 are obtained, respectively.

BUTİL AKRİLAT VE METİL METAKRİLAT KOPOLİMERİNDEN ELEKTROSPUN YÖNTEMİYLE NANOLİF ELDESİ

ÖZET

Bu çalışma iki bölümden oluşmaktadır. Birinci bölümde, yapıştırıcı ve yüzey kaplama uygulamalarında kullanılmak üzere, elektrospun yöntemi ile Butil akrilat (BA)/Metil metakrilat (MMA) kopolimerinden nanolif eldesi amaçlanmıştır. Bunun için öncelikle BA ve MMA'ın emülsiyon polimerizasyonu, potasyum persülfat başlatıcısı kullanılarak sulu ortamda yapılmıştır. Lif çapı gibi, nanolif morfolojisini etkileyen elektrospun işlem parametreleri ve çözelti parametreleri incelenmiştir. İşlem parametresi olarak; besleme hızı, çözelti parametresi olarak; Polimer çözelti konsantrasyonu ve çözücünün dielektrik sabiti incelenmiştir. Besleme hızları; 1ml/h, 3ml/h, 5ml/h ve 7ml/h olarak değiştirilmiş, besleme hızı arttıkça nanolif çaplarında artış meydana gelmiş ve nanolif morfolojisi önemli ölçüde değişmiştir. En yüksek besleme hızına sahip nanolifler oluşurken, jet ucundan çıkan polimer çözeltisi toplayıcıya ulaşana kadar, çözelti içindeki çözücünün tamamı buharlaşamadığı için, oluşan lifler birbirine geçmiş, iç içe geçmiş gibi oluşmaktadır. Çözelti konsantrasyonu arttırıldığında, çözelti viskozitesi de artmış ve nanolif eldesi kolaylaşmıştır. Nanolif eldesinde çözelti viskozitesi oldukça önemli bir etkiye sahiptir ve nanolif elde edebilmek için optimum viskoziteye ihtiyaç vardır. Bu çalışmada çözelti konsantrasyonları; 1 wt%, 3wt%, 5wt%, 8wt% ve 10wt% olarak değiştirilmiştir. En düşük konsantrasyona sahip polimer çözeltisi için yapılan elektrospun işleminde, nanoliflerin oluşmadığı gözlenmiştir. Çözelti konsantrasyonu artmaya başladıkça nanolifler oluşmaya başlamış ve oluşan lif çaplarının arttığı gözlenmiştir. Elektrospun işleminin devamlılığı ve oluşan çapların nano boyutta olmasından dolayı, optimum çözelti konsantrasyonu olarak 5wt% belirlenmiştir. Son parametre olarak, çözelti parametresi incelenmiş ve DMF,THF,Aseton gibi üç farklı çözücü kullanılmış, DMF/THF, DMF/Aseton ve THF/Aseton gibi çözücü karışımları aynı oranlarda karıştırılıp polimer çözeltileri hazırlanmıştır. Ayrıca farklı oranlarda DMF/THF çözelti karışımları hazırlanmış ve onların dielektrik sabitleri hesaplanmış, dielektrik sabitleri ve lif morfolojisi arasındaki ilişki incelenmiştir. Hazırlanan farklı çözeltiler için dielektrik sabitleri hesaplanmış ve dielektrik sabiti arttıkça oluşan nanoliflerin çaplarının inceldiği ve dielektrik sabiti fazla olan çözeltiden elde edilen liflerin boncuksuz, homojen yapıda olduğu gözlenmiştir. Sentezlenen BA, MMA kopolimerinin yapısını incelemek için FTIR-ATR ve NMR analizi kullanılmıştır. Daha sonra elde edilen nanolifler, kopolimer yapısını incelemek için FTIR-ATR ve NMR analizlerinde, Termal olarak DSC analizinde, morfolojik olarak SEM analizlerinde ve molekül ağırlığını belirlemek için GPC analizinde kullanılmıştır. Sentezlenen kopolimerin FTIR-ATR ve NMR sonuçları, elde edilen nanoliflerden ölçülen FTIR-ATR ve NMR sonuçları ile kıyaslandığında, her 2 numuneden ölçülen sonuçlar birbirlerinin tam olarak aynısı çıkmış ve bu sonuçlar nanolif numunlerinde çözücünün tamamen buharlaştığını kanıtlamıştır. FTIR-ATR grafiğinde, PMMA'a ait 2950 cm^{-1}, 1728 cm^{-1}, 1435 cm^{-1}ve 1149 cm^{-1} de C-H esneme, C=O esneme,

CH_3 esneme and O-CH_3 esneme titreşimi pikleri gözlenmiş, 962 cm^{-1} de BA'a ait karakteristik pik gözlenmiştir. NMR spektrumu incelendiğinde, 3.99 ppm'de BA'a ait metilen piki, 3.64 ppm'de MMA'a ait metil piki gözlenmiş ve bu piklere ait integral değerleri kullanılarak, polimerizasyon sonucu elde edilen kopolimerin içerikleri hesaplanmıştır. MMA'ın reaktivite oranının BA'dan daha fazla olmasından dolayı, MMA polimerizasyona daha fazla katılmıştır. Bu nedenle elde edilen kopolimerde MMA içeriği daha fazladır. MMA'ın yapıda daha fazla bulunması, kopolimer yapısını olumlu yönde etkilemiş, elde edilen lifler renksiz, transparan ve yüksek ışık geçirgenliğine sahip olmuşlardır. Poli(BA-co-MMA) emülsiyon polimerizasyonu ile elde edildiği için çok yüksek molekül ağırlığına sahip olmuş ve electrospun için oldukça viskoz çözelti elde edilmesini sağlamıştır. Poli(BA-co-MMA) lifleri ilk defa bu çalışmada elde edilmiştir. Elde edilen bu liflerin, hidrofobik özelliklerinden dolayı, gözlük camı kaplama malzemesi olarak kullanılması ve gözlük camının yüzeyinde suyun ve lekenin tutulmadan, akıp gitmesini sağlaması amaçlanmıştır.

Tezin ikinci bölümünde, BA, MMA ve perfloroetil alkil metakrilatları içeren kopolimerlerden nanolif eldesi amaçlanmıştır. Bu yüzden Zonil-TM, BA ve MMA içeren yeni perfloroetil alkil metakrilat terpolimerinin [poli(PFMA-MMA-BA)] nanolifleri ilk kez electrospun yöntemiyle elde edilmiştir. Çalışmaya başlarken ilk olarak Poli(PFMA-MMA-BA) kopolimeri süper kritik CO_2 ortamında, 200 bar'da ve 80 ^oC'de başlatıcı olarak AIBN kullanılarak serbest radikal polimerizasyonu ile Gebze Yüksek Teknoloji Enstitüsünde sentezlenmiş, bu kopolimerler hazır olarak Gebze Yüksek Teknoloji Enstitüsünden temin edilmiştir. Bu çalışma için üç farklı özellikte kopolimerler kullanılmış, onların nanolif oluşumuna etkileri ve hidrofob özellikleri araştırılmıştır. Kullanılan kopolimerler, içerdikleri Flor, BA ve MMA bakımından birbirlerinden farklı özelliklere sahiptir. Tüm kopolimerler için elektrospun yöntemi kullanılarak, nanolifler elde edilmiştir. Oluşan nanolifler morfolojik olarak SEM ile analiz edilmiş ve yapısal olarak FTIR-ATR, ve NMR analizlerinde kullanılmıştır. DSC'de yapılan termal analiz sonucuna göre camsı geçiş sıcaklıkları, kopolimerdeki artan serbest hacimden dolayı, BA içeriğinin fonksiyonu olarak azalmaktadır. Ayrıca literatür çalışmalarında olduğu gibi, Kopolimer yapısındaki Flor içeriği arttıkça, camsı geçiş sıcaklığının azaldığı gözlemlenmiştir. Poli(BA-co-MMA) liflerinin FTIR-ATR spektrumu ve [poli(PFMA-MMA-BA)] liflerinin FTIR-ATR spektrumları karşılaştırıldığı zaman, F içeren kopolimerlerin FTIR-ATR grafiğinde 2 farklı pik gözlenmiştir. C-F bağının Esneme titreşimine ait piki 1190 cm^{-1} ve dalgalanma titreşimine ait piki 690 cm^{-1} de gözlenirken, Flor içermeyen kopolimerin FTIR-ATR spektrumunda bu piklere rastlanmamıştır. NMR spektrumu incelendiğinde 4.25 ppm de Zonil-TM grubuna ait metilen piki, 3.6 ppm de Metilmetakrilat grubuna ait metil piki ve 4.00 ppm de Bütilakrilat grubuna ait metilen piki gözlenmiş ve kopolimerizasyonun başarılı bir şekilde gerçekleştiği sonucuna varılmıştır. Ayrıca NMR sonuçları göz önünde bulundurularak, metil ve metilen piklerine ait integral oranları kullanılmış ve kopolimerlerin ne kadar Flor, BA ve MMA içerdikleri hesaplanmıştır. Ayrıca kullanılan üç farklı kopolimerlerin FTIR-ATR'si de incelenmiş, tüm piklerin birbiri ile örtüştüğü, ancak artan çözelti konsantrasyonları ile absorbansın arttığı gözlenmiştir. Elde edilen liflerin morfolojisi incelendiğinde, artan Flor içeriğinin çözelti viskozitesini düşürdüğü ve lif çapını azalttığı gözlenmiştir. En yüksek Flor içeriğine sahip olan BT-1 polimerinin molekül ağırlığı en düşük bulunmuş ve nanolif elde etmek için BT-1'in konsantrasyonu en yüksek tutulmuştur, böylece çözelti elektrospun işlemi için yeterli viskoziteye sahip olmuş, ancak BT-1 çözeltisinden elde edilen nanoliflerde boncuklu yapılar

gözlenmiştir. BT-1 kopolimerine ait çözelti konsantrasyonu en yüksek derişime sahip olmasına rağmen, nanolif eldesi için yeteri kadar viskoz olmamıştır. Bu yüzden BT-1 nanolifleri; boncuklu yapıyı ve nano boyutta lifleri yapısında bulunduran, hiyerarşik morfolojiye sahip olmuşlardır. Elde edilen Nanoliflerden Kontak açı ölçümleri yapılmış ve oluşan liflerin süperhidrofobik (172^0±1) olduğunu, yağlar için yüzey geriliminin~45 mN/m'den fazla ve nanoliflerin gliserol ve etilen glikole karşı süperolefobik (167^0±1 ve163^0±1) özellik gösterdiğni kanıtlamıştır. BT-1 lifleri hem hiyerarşik yapıda olduğu için, hem de en yüksek Flor içeriğine sahip olduğundan en yüksek kontak açıya sahip olmuştur. Diğer yandan BT-9 kopolimerinin kontak açısı BT-4'in kontak açısından daha fazla bulunmuştur, oysa Flor içeriği bakımından BT-4, BT-9'dan daha fazladır. Ancak, bu çalışmada nanolif elde etmek için konsantrasyonlar farklı kullanılmış, bu nedenle BT-9'un kontak açısı BT-4'ten daha fazla çıkmıştır. Ayrıca artan nanolif çapları kontak açıyı olumsuz yönde etkilemiş, nanolif çapı arttıkça kontak açı değeri düşmüştür. Elektrospun yöntemi ile nanolifler elde edilirken, genellikle boncuksuz, homojen dağılıma sahip nanolifler oluşsun istenir, ancak hidrofob özelliğe sahip liflerin oluşması, kontak açı değerinin yüksek elde edilmesi isteniyorsa; elde edilecek olan lifler boncuklu yapıda olmalıdır. Böylece yüzey hiyerarşik morfolojiye sahip olur ve hidrofob özellik gösterir. Bu nedenle bu çalışmada hiyerarşik morfolojiye sahip olan BT-1 çözeltisinden elde edilen lifler süperhidrofob olmuştur.

Elde edilen lifler süperhidrofob ve süperoleofob özelliklere sahip oldukları için, davlumbazların iç yüzey kaplamasında, otomobil ön camlarında ve gemilerin alt yüzeyindeki kaplamalar için kullanılabilme imkanı sağlamaktadır. Davlumbazların iç yüzeyine kaplanıldıkları takdirde, yağı ve suyu tutamayacaklar, otomobil ön camlarında kullanıldıkları için sileceklere gerek kalmayacak ve otomobil yapımında maliyeti azaltacaklardır ve son olarak gemilerin alt yüzeyini kaplamada kullanıldığı takdirde, suyu tutmayacağı için sürtünme etkisini ortadan kaldırıp yakıt tasarrufu sağlayacaklardır.

1. INTRODUCTION

The fabrication of polymer nanofibers by electrospinning has received much attention in recent years. This method uses electrically charged jet of polymers or liquid states of polymers in order to make fibers from micro dimensions to nano dimensions. Polymer nanofibers exhibit several properties that make them favorable for many applications. Nanofibers have extremely high specific surface area due to their small diameters, and nanofiber mats can be highly porous with excellent pore interconnection. These unique characteristics plus the functionalities from the polymers themselves impart nanofibers with many desirable properties for advanced applications such as tissue engineering scaffolds, filtration devices, sensors, materials development, and electronic applications [1]. Thus, nanofiber production is prefered from several polymers such as polyacrylates and Fluorine containing polymers. The polyacrylates are highly heat and oil resistant polymers. Acrylate and methacrylate esters are used to make polymers for textiles, latex paints, surgical cements and dental resins.Butyl acrylate/Methyl methacrylates (BA/MMA), emulsion copolymers are versatile materials extensively used as adhesives (BA homopolymers and BA rich copolymers) and coatings (BA/MMA 50/50 wt/wt copolymers). In spite of their commercial importance, only a few literature reports dealing with the microstructural properties of BA/MMA emulsıon copolymers have been published [2]. Fluorine containing polymers constitute a unique class of materials with a combination of interesting properties that have attracted significant attention of material chemists over the last few decades [3-5]. In general, these polymers have high thermal stability, improved chemical resistance and lower surface energy when compared to their non-fluorinated counterparts. The small size of the fluorine atom with its 2s and 2d electrons close to the nucleus is the most electronegative element. A strong C–F bond leads to high thermal and chemical stabilities of fluorinated polymers. The low polarizability of the C–F bond along with its hydrophobic character (low moisture uptake) together results in low dielectric constant of these materials. Moreover, low surface energy of fluorine helps in oil-repellence resulting in increased resistance to

wear and abrasion [6]. Fluorinated polymers are also highly solvophobic and which also are used for nonstick coating applications. Hydropbicity of a material is a key property that depends on both surface chemistry and surface roughness. Hydrophobic polymers (with water contact angle above 90^{o}C) are useful in many applications such as inert biomaterials, environmentally resistant coatings, and low friction devices, whereas suprehyrophobic materials (with water contact angles above 150^{o}C) are of special interest as self-cleaning surfaces and stain-resistant textiles [7].

The first part of this study, the electrospinning method was applied to produce Nanofibers of n-Butyl Acrylate/Methyl Methacrylate which can be used for adhesives and coatings. Emulsion polymerization of n-Butyl Acrylate (BA) and Methyl Methacrylate (MMA) initiated by Potassium Peroxydisulfate (KPS) in the aqeuos medium was performed. Processing parameters effects on the morphology such as fiber diameter and its uniformity of electrospun polymer nanofibers was investigated. In this study, electrospun nanofibers of P(BA-co-MMA) are first obtained.

The second part of this study, the electrospinning method was applied to produce Nanofibers of perfluoroethyl alkyl methacrylate containing n-Butyl Acrylate/Methyl Methacrylate copolymers and then contact angles were measurement with use the electrospun mats. Beaded nanofiber is the highest contact angle 172±1^{o}C due to it has the hierarchical structure. Moreover, relationship between contact angle and fiber diameter were examined and increasing contact angle caused by decrasing nanofiber diameter is determined. In this study, electrospun nanofibers of poly(PFMA-ran-MMA-ran-BA) are first obtained.

2. THEORETICAL PART

2.1 Polyacrylates

The polyacrylates are highly heat and oil resistant polymers. Acrylate and methacrylate esters are used to make polymers for textiles, latex paints, surgical cements and dental resins. The esters of acrylic and methacrylic acid are unsymmetrically substituted ethylenes of the general formula;

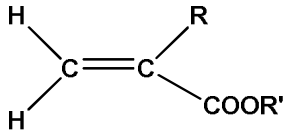

Figure 2.1 : General Formula of Acrylates

with R:H for acrylates and R:CH_3 for methacrylates. The substituents R' may be of a great variety: from n-alkyl chains to more complicated functional groups [8].

Esters of acrylic acid CH_2:CHCOOH and methacrylic acid CH_2:C(CH_3)COOH. Both are crystalline solids at low ambient temperatures, becoming liquid at slightly higher temperatures. These acids polymerise and copolymerise extremely readily, being frequently employed in copolymers to obtain alkalisoluble polymers. Whilst both acids are water soluble, methacrylic acid, as might be expected because of its angular methyl group, is more soluble in ester monomers, and to some extent in styrene, and as such is more useful in copolymerisation, especially if water based [9].

The first report of a polymeric acrylic ester was published in 1877 by Fittig and Paul [10] and in 1880 by Fittig and Engelhorn [11] and by Kahlbaum [12], who observed the polymerization reaction of both methyl acrylates and methacrylates. But it remained to O. Röhm [13] in 1901 to recognize the technical potential of the acrylic polymers. He continued his work and obtained a U.S. patent on the sulfur vulcanization of acrylates in 1914 [14]. In 1924, Barker and Skinner [15] published details of the polymerization of methyl and ethyl methacrylates. In 1927 [16], based on the extensive work of Röhm, the first industrial production of polymeric acrylic

esters was started by the Röhm & Haas Company in Darmstadt, Germany (since 1971, Röhm GmbH, Darmstadt). After 1934, the Röhm & Haas Co. in Darmstadt was able to produce an organic glass (Plexiglas) by a cast polymerization process of methyl methacrylate [17]. Soon after, Imperial Chemical Industries (ICI, England), Röhm & Hass Co. (United States), and Du Pont de Nemours followed in the production of such acrylic glasses [18].

One of the first uses of acrylic polymers was as an interlining for automobile windshields, but poly(methyl methacrylate) sheet (Plexiglas, Lucite) soon became the principal use of acrylic plastics. Poly(methyl methacrylate) (PMMA), [-CH_2-$CH(CH_3)COOCH_3$-], has a light transmittancy of about 92% and has good resistance to weathering. It is widely used in thermoformed signs, aircraft windshields, bathtubs [19], electron beam or ion beam resists in the manufacture of microelectronics chip [20,21]. Poly(methyl methacrylate) is used as an automobile lacquer and polyacrylonitrile, (-CH2-CHCN-)$_n$, is used as a fiber. Poly(ethyl acrylate),(-CH_2–$CHCOOC_2H_5$-)$_n$, is more flexible and has a lower softening temperature than PMMA. Poly(hydroxyethyl methacrylate), is used for contact lenses, and poly(butyl methacrylate) is used as an additive in lubricating oils[19].

Whilst esters of acrylic acid give soft and flexible polymers, except for those with long alkyl chains, methyl methacrylate polymerises to an extremely hard polymers. The polymers in this series become softer with increasing alkyl chain lengths up to C_{12}. The highest alkyl chain acrylics in both series tend to give side chain crystallisation.

The methacrylic ester series closely parallels the acrylics, but boiling points tend to be somewhat higher, especially with the short chain esters. Methyl methacrylate is by far the most freely available and least costly of the monomers of the series. As an alternative to the simple alkyl esters, several alkoxyethyl acrylates are available commercially, e.g. ethoxyethyl methacrylate CH_3:$C(CH_3)COOC_2H_4OC_2H_5$ and the corresponding acrylate. The ether oxygen which interrupts the chain tends to promote rather more flexibility than a simple carbon atom.

Some technical perfluorinated alkyl acrylates are as following they include N-ethylperfluorooctanesulfonamido)ethyl acrylate $C_nF_{2n+1}SO_2N(C_2H_5)$–CH_2O–C(O)–$CH=CH_2$ (n approximately 7.5, fluorine content 51.7 %), the corresponding

methacrylate and the corresponding butyl derivatives. The ethyl derivatives are waxy solids, the ethyl acrylate and the corresponding methacrylate derivative having a melting range of 27–42 °C. The butyl acrylic derivative is a liquid, freezing at -10 °C. Butyl acrylate/Methyl methacrylates (BA/MMA), emulsıon copolymers are versatile materials extensively used as adhesives (BA homopolymers and BA rich copolymers) and coatings (BA/MMA 50/50 wt/wt copolymers). In spite of their commercial importance, only a few literature reports dealing with the microstructural properties of BA/MMA emulsıon copolymers have been published [2].

Polyacrylate elastomers can be prepared by the water emulsion system, suspension system, solvent solution method, or even the mass (bulk homogenous) polymerization process. Most are made by the water emulsion (latex) or the suspension method. Peroxides or persulfate initiated free radical systems are most commonly used in the presence of heat. Polymerization is usually taken to completion. Coagulation is best with salts, followed by water washing and drying with hot air, vacuum, or extrusion [22].

2.2 Polymerization of Acrylates and Emulsion Polymerization

Emulsion polymerization involves the reaction of free radicals with relatively hydrophobic monomer molecules within submicron polymer particles dispersed in a continuous aqueous phase. This unique polymerization process that is heterogeneous in nature exhibits very different reaction mechanisms and kinetics compared to bulk or solution free radical polymerization. Surfactant is generally required to stabilize the colloidal system; otherwise, latex particles nucleated during the early stage of polymerization may experience significant coagulation in order to reduce the interfacial free energy. This feature may also come into play in determining the number of reaction loci (i.e., polymer particles) available for the consumption of monomer therein.

2.2.1 Free radical polymerization

Free radical polymerization of vinyl monomers containing carbon – carbon double bonds has been widely used in industry to manufacture a variety of polymeric materials such as low - density polyethylene, polystyrene, polyvinyl chloride, polyvinyl acetate, acrylic polymers, and synthetic rubbers, which can be

accomplished in bulk, solution, suspension, or emulsion processes. The generally accepted free radical polymerization mechanism involves three kinetic steps in sequence, namely, initiation, propagation, and termination [23-25].

Initiation

$$I \xrightarrow{k_d} 2R^* \qquad \textbf{(2.1)}$$

$$R^* + M \xrightarrow{k_i} P_1^* \qquad \textbf{(2.2)}$$

Propagation

$$P_1^* + M \xrightarrow{k_p} P_2^* \qquad \textbf{(2.3)}$$

$$P_2^* + M \xrightarrow{k_p} P_3^* \qquad \textbf{(2.4)}$$

$$P_n^* + M \xrightarrow{k_p} P_{n+1}^* \qquad \textbf{(2.5)}$$

Termination

$$P_m^* + P_n^* \xrightarrow{k_{tc}} P_{m+n}^* \qquad \textbf{(2.6)}$$

$$P_m^* + P_n^* \xrightarrow{k_{td}} P_m + P_n \qquad \textbf{(2.7)}$$

where I, R * , M, P_n^* (n = 1, 2, 3, . . .), and P_n represent the initiator, initiator radical, monomer, free radicals with n monomeric units, and dead polymer chains with n monomeric units, respectively. The kinetic parameters k_d,k_i,k_p,k_{tc} and k_{td} are the thermal decomposition rate constant for the initiator, the initiation rate constant for the primary radical, the propagation rate constant for the reaction between one free radical with n monomeric units and one monomer molecule, the combination termination rate constant, and the disproportionation termination rate constant for the reaction between two free radicals, respectively. The above three reaction mechanism reflects its characteristic chain addition polymerization; the rate of

consumption of monomer is relatively slow, but the molecular weight of polymer builds up rapidly.

Chain transfer reactions are also a part of the free radical reaction system. These reactions, as the name implies, transfer the radical activity from a growing chain to another species such as monomer, polymer, initiator, solvent, or a deliberately added chain transfer agent. For example, chain transfer of a propagating radical to monomer or polymer can be represented as follows:

$$P_n^* + M \xrightarrow{k_{tr,m}} P_n + P_1^* \qquad \textbf{(2.8)}$$

$$P_n^* + P_m \xrightarrow{k_{trp}} P_n + P_m^* \qquad \textbf{(2.9)}$$

where $k_{tr,\,m}$ and $k_{tr,\,p}$ are the rate constants for the chain transfer reaction of a propagating radical with monomer and polymer, respectively. Both P_1^* and P_m^* may reinitiate the free radical chain polymerization to form linear and branched polymer chains, respectively, or participate in the termination reactions [25].

2.2.2 Emulsion polymerization

There is a way to suspend even smaller monomer particles in water such that the monomer droplets are stable and do not aggregrate to form a separate layer. Essentially, a surfactant is used to form an emulsion. Surfactant molecules consist of a polar head (hydrophilic) group attacched to a non-polar (hydrophobic) tail, such that it looks something like a tadpole, as depicted in Figure 2.2.

Figure 2.2 : Schematic representation of a surfactant molecule with a hydrophilic head and a hydrophobic tail.

In water, soap molecules arrange them selves so as to keep the polar groups in contact with water molecules, but the non-polar tails as far from the water as possible (at concentrations above a certain level, called the critical micelle concentration). One way of doing this is to form a micelle, which usually has a spherical or rod-like shape, as illustrated in Figure 2.3.

Figure 2.3 : Two dimensional schematic representation of a spherical micelle.

In this micelle, which is about 10^{-3} to 10^{-4} μm in diameter, the polar groups are on the outside surface while the non-polar tails are hidden away inside. The non-polar groups are compatible with non-polar monomer, however,if monomer is added to the water and dispersed by stirring, the very small amounts of monomer that dissolve in the water can diffuse to the micelles and enter the interior, non-polar hydrocarbon part (then more monomer enters the aqueous phase to replace that which has departed). In the same way, surfactant molecules can diffuse to the dispersed monomer droplets (whose size depends upon the stirring rate, but usually in the range of 1-10mm), where they are absorbed onto their surface, thus stabilizing them. Unlike suspension polymerization, where a water insoluble initiator is used, in emulsion polymerization a water soluble initiator is used. The polymerization, for the most part, occurs in the swollen micelles, which can be thought of as a meeting place for ,the water soluble iniator and the (largely) water insoluble monomer (Figure 2.4).

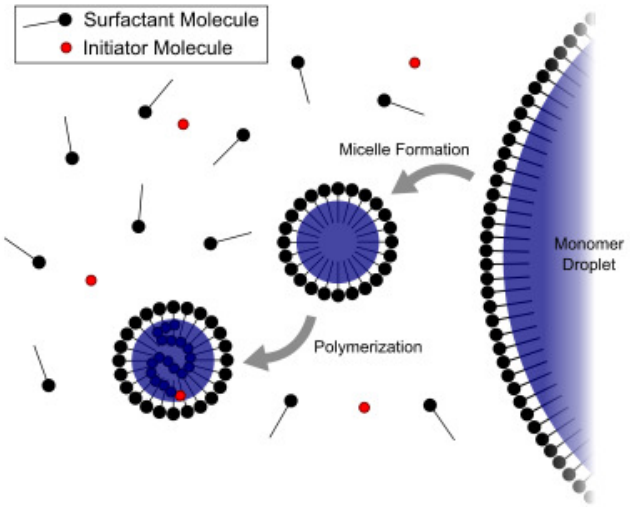

Figure 2.4: Schematic representation of Emulsion polymerization.

A small amount of polymerization sometimes occurs in the monomer droplets and almost certainly in solution, but the latter does not contribute significantly, due to the

low monomer concentration in the water phase. As the polymerization proceeds, the micelles grow by addition of new monomer diffusing in form the aqeous phase.

At the same time, the size of the monomer droplets shrinks, as monomer diffuses out into the aqeous phase. The micelles where polymerization is occuring grow to about 0.5 mm in diameter and at this stage are called polymer particles. After a while (~15% conversion of monomer to polymer) all the micelles become polymer particles and a while later (40-60% monomer conversion) the monomer droplets phase finally disseappears which is all quite remarkable. Termination occurs when a radical (usually from the initiator) diffuses in from the aqueous phase. This is major advantage of the emulsion technique for the polymerization of monomers such as butadiene, which can not be polymerized easily by free radical means using homogeneous (single-phase) polymerization, because it has a fairly high rate of termination. The termination step in an emulsion polymerization is controlled by the rate of arrival of radicals at the polymer particles, which depends only an the concentration of surfactant. There are some obvious additional advantages to emulsion polymerization; as in suspension polymerization, the viscosity is always low and heat control is relatively straightforward. Also, the final product is an emulsion of 100 nm diameter polymer particles that is typically 50% by volume polymer and 50% water. This makes it almost immediately applicable as a surface coating (paint). The major disadvantage is the presence of the surfactant, which is diffucult to completely remove even if the polymer product is precipitated and washed [26].

2.3 Fluorinated Polymers

Fluorine containing polymers constitute a unique class of materials with a combination of interesting properties that have attracted significant attention of material chemists over the last few decades [3-5]. In general, these polymers have high thermal stability, improved chemical resistance and lower surface energy when compared to their non-fluorinated counterparts. The small size of the fluorine atom with its 2s and 2d electrons close to the nucleus is the most electronegative element. A strong C–F bond leads to high thermal and chemical stabilities of fluorinated polymers. The low polarizability of the C–F bond along with its hydrophobic character (low moisture uptake) together results in low dielectric constant of these

materials. Moreover, low surface energy of fluorine helps in oil-repellence resulting in increased resistance to wear and abrasion [6].

Generally, Fluoropolymers are categorized as main-chain and side chain fluoropolymers, and most of the side-chain fluoropolymers are synthesized from the polymerization reaction of the methacrylate monomers [27]. The introduction of fluorinated groups through the acrylic monomers which have perfluoroalkyl side groups, decreases the surface tension of the obtained copolymer films [28,29]. Fluoro methacrylate (FMA) copolymers have been used increasingly in a wide range of applications including surface coatings for textile, paper and leather industries, biomaterials, microelectronics and antifouling [30,31]. Some of statistical FMA copolymers with methyl methacrylate (MMA) were synthesized by using bulk copolymerization [32], solution copolymerization in $scCO_2$ [33] and in polar solvent mixtures such as α,α,α-trifluorotoluene/1,1,2-trichlorotrifluoroethane [34].

Fluorinated surfaces derive their characteristics from the unique molecular properties associated with the C–F bond that impacts a specific chemistry and physics at interfaces. Their low surface tensions, low electrostatic loading and low friction coefficient can play an essential role in microelectronics, antifogging and antifouling applications and are promising in medical field. Physicochemical and structural studies of acrylate/methacrylate polymers with perfluoroalkyl side chains have been reported in literature and have shown a direct relationship between the organization of the fluorinated side chains and the surface properties of the coatings prepared with the various polymers [35].

Fluorinated polymers are highly solvophobic. For improving the solubility of fluorinated polymers in solvents, hybrid compounds with non-fluorinated moieties are synthesized. Then, amphiphilic copolymers are soluble and self-associated in solvents. Incorporation of fluorinated moieties in polymers is carried out using different methods: (1) participation of fluorinated unit in main chain; (2) modification of polymer terminals by fluorinated derivatives; and (3) fluorination of polymer side chains [36].

Fluorinated polymers are used for nonstick coating applications due to the fluorine atom is the most electronegative of the elements and strongly attracts electrons to it in any bond that it forms. The electrons around fluorine are held tightly thus forming very stable bonds with low chemical reactivity. Therefore, an inherent property of

fluoropolymers is that they do not bond readily with other materials, a property that is popularly called *nonstick* [36].

The tightly held electrons in fluorocarbons result in very high electrical resistances and the lowest electrical permitivity. Hence fluoropolymers are used extensively as wire insulation. The presence of fluorine atoms also makes fluoropolymers inherently nonflammable. This property enhances the value of fluoropolymers in electrical insulation, bearing assemblies, and many electrical and mechanical devices in sensitive aerospace applications.

The presence of fluorine atoms presents a problem if the fluoropolymers decomposes. The resulting products can be toxic. Fortunately, the service temperatures of fluoropolymer are quite high, ranging to 260^{o}C for continuous use and they show hydrophobic properties.

2.4 Contact Angle

The contact angle is an important parameter in surface science. It is a common measure of the hydrophobicity of a solid surface. In the literature [37-39], it is well established that meaningful contact angle measurements can be used in the calculation of solid surface tensions. In the past several decades, numerous techniques [40-44] have been used to measure contact angle which were inspired by the idea of using the equation first derived by Thomas Young in 1805 [43]. Young's equation governs the equilibrium of the three interfacial tensions and the Young contact angle (C.A) θ of a liquid drop on a solid (see Fig. 2.5):

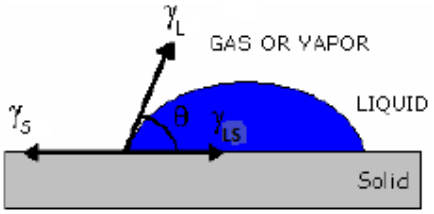

Figure 2.5 : Vectorial Equilibrium for a Drop of a Liquid Resting on a Solid Surface [45].

$$\cos\theta = (\gamma_S - \gamma_{LS})/\gamma_L \qquad (\mathbf{2.10})$$

where γ_L and γ_S are the liquid and the solid surface energies, and γ_{LS} is the liquidsolid interfacial energy. The Young equation in the form of equation (1.1), a

thermodynamic proof based on the minimization of the free energy was given by Johnson [36]. It is now well understood that the contact angle obtained from Young equation corresponds to the thermodynamic equilibrium state, as long as the solid surface is perfectly homogenous and flat. In addition to homogeneity and flatness, the liquid should not penetrate into the solid and no reactions should occur between the two as well. These conditions are violated to some extent in all real systems, and care must be taken in determining surface/interfacial energies from measured contact angle values. Nevertheless contact angle measurement is the most direct method of putting wettability in a quantitative scale. It is yet the wettability, not the surface energies; one is usually concerned with in practical studies [36].

Figure 2.6 shows three cases for $\theta = 60^\circ$, 90° and 120°. When $\theta = 0^\circ$ the liquid is said to wet the solid. Partial wetting corresponds to $0^\circ < \theta < 90^\circ$. For $\theta > 90^\circ$ the solid is not wetted by the liquid. $\theta = 90^\circ$ is the transition between partial wetting and nonwetting cases. A solid that is not wetted by water is called hydrophobic (water contact angle > 90º). As θ increases, the area of the liquid-solid interface shrinks and the interaction between the drop and the solid surface weakens. This can cause the drop roll off or slide down the surface when a small force is applied. As a subclass of hydrophobic surfaces, surfaces on which water drops can easily move and have contact angles > 150º are commonly called superhydrophobic [41].

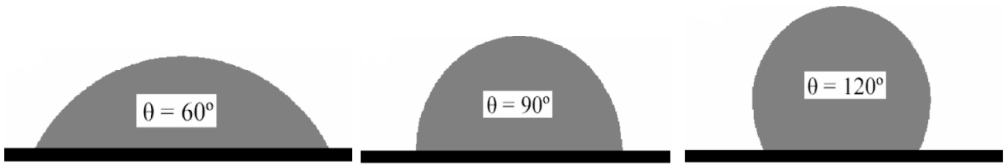

Figure 2.6 : Shape of a liquid drop on a solid surface for $\theta = 60^\circ$, $\theta = 90^\circ$, and $\theta = 120^\circ$. Drawn to scale with the drop volume same in all cases.

The measurement of a single static contact angle to characterize the solid-liquid interaction is not adequate because, in practice, there is no single equilibrium contact angle, θ_e, on a solid surface. There may be a range of static contact angles, depending on the location of the drop and on the application type of the measurement. Static contact angle is the contact angle when all participating phases gas, liquid, solid have reached their natural equilibrium positions and the three phases line is not moving anymore [47].

Experimentally, only two types of C.A measurement technique are standardized:

1- When a liquid drop is formed by injecting the liquid from a needle connected to a syringe onto a substrate surface, it is allowed to advance on the fresh solid surface and the measured angle is said to represent the *advancing contact angle*, θ_a,

2- The receding contact angle, θ_r, can be measured when a previously formed sessile drop on the substrate surface is contracted by applying a suction of the drop liquid through the needle. Precise measurement of θ_r is very difficult because of the drop evaporation effect. These contact angles fall within a range where the advancing contact angles approach a maximum value and receding angles approach minimum value ($\theta_a > \theta_r$) [47].

Contact angle hysteresis is the difference between the advancing and receding contact angles:

$$H \equiv \theta_a - \theta_r \qquad \textbf{(2.11)}$$

Hysteresis of the contact angle results from the system under investigation not meeting ideal conditions. In order to apply Young's equation, the solid should be ideal: it must be chemically homogeneous, rigid, flat at an atomic scale and not perturbed by chemical interaction or by vapor or liquid adsorption. If such an ideal solid surface is present, there would be a single, unique contact angle. On the contrary, it is common to find contact angle hysteresis on practical non-ideal surfaces, in the region of 10^o or larger; and 50^o or more of hysteresis has sometimes been observed. In general, there appear to be five causes of contact angle hysteresis. Surface roughness and microscopic chemical heterogeneity of the solid surface are the most important ones, and the others such as drop size effect, molecular reorientation and deformation at the solid surface are less important [47]. When wetting with water the hydrophobic regions will repel the water and the hydrophilic regions will attract the water. Thus when advancing in a hydrophobic region the contact angle increases (the solid tries to limit the area touched by water) and similarly when receding in a hydrophilic region the contact angle decreases (the solid tries to hold on to the water). From this analysis it can be seen that with water

advancing angles characterize hydrophobic regions and receding angles characterize hydrophilic regions [48].

2.5 Nanofiber

Generally, fibers can be defined as objects or materials that have an elongated structure as shown in Figure 2.7. There are other definitions according to the field they are used such as textile industry, biochemistry, physiology, botany, and anatomy [49]. With regard to fibers, "nano" refers to the diameter of the fiber. According to the National Science Foundation (NSF), nano materials are matters that have at least one dimension equal to or less than 100 nanometers [50]. However some scientists accept the nanofibers as less than 1 micron, while others describe them as less than 100 nanometers [51]. In the industry, up to 500nm, it is acceptable to classify fibers with the prefix 'nano' whereas some scientists use the term 'sub-micron' in the academic world Nanofibers have several superior characteristics. They present a high surface area to volume ratio, better mechanical properties, e.g. good directional strength, and flexibility so they can be utilized for a wide variety of materials and applications including for their mechanical, biomedical, optical, electronical, and chemical properties [1].

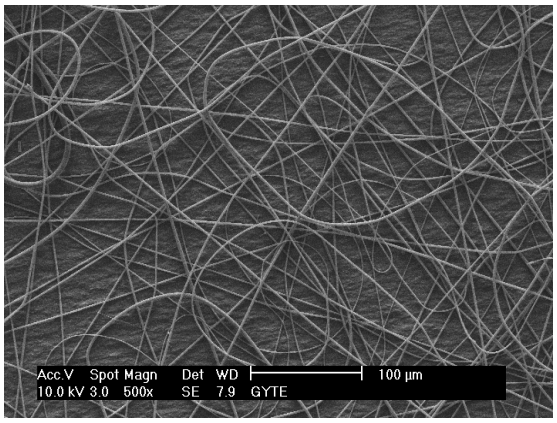

Figure 2.7 : SEM photograph of fibers from this study**.**

The comparison between different techniques was given in Table 2.1. Among all, electrospinning is the best candidate for further development with a wide range of opportunities to be utilized in all types of polymers (both synthetic and natural), and ceramics. Also, in this thesis study, electrospinning was used for fabrication of non-

woven fibers. Therefore, electrospinning process was given in the next section in detail.

Table 2.1: Advantages and disadvantages of various processing techniques [53].

Process	Advantages	Disadvantages
Drawing	Requires simple equipment	No continuous fibers, no control on fiber dimension
Template Synthesis	Fibers of different diameters can be easily achieved by using different templates.	Process cannot be scaled-up
Phase Separation	Process can directly fabricate a nanofiber matrix. Batch-to-batch consistency is achieved easily. Mechanical properties of the matrix can be tailored by adjusting polymer concentration.	For only specific polymers
Self-Assembly	Good for obtaining smaller (7- 8 nm) nanofibers.	Not controllable on fiber diameter and complexity of the process
Electrospinning	Cost effective. Long, continuous nanofibers can be produced.	Jet instabilit, Controllable on fiber diameter

2.6 Electrospinning

Fiber production using electrostatic forces, or electrostatic spinning is described as a novel approach for fiber collection which has become important in the last decades. This method uses electrically charged jet of polymers or liquid states of polymers in order to make fibers from micro dimensions to nano dimensions. In contrast to fibers created from conventional melt spinning, dry spinning or wet spinning, they possess

several unique properties. Electrospun fibers are smaller in diameter and longer in length so that they have very high surface area to volume ratios and fibers are placed closer to each other on the mat when compared to fibers produced from dry or wet spinning Technologies [49].

In late 1800's Lord Rayleigh investited the hydrodynamic stability of a liquid jet, with and without an applied electric field. In 1882, he studied the condition of instability occuring in electrically charged liquid droplets. He showed that when the electrostatic force overcomes the surface tension force, which acts in the opposite direction of the electrostatic force, liquid is thrown out in fine jets [58].

Although the term "Electrospinning", derived from "electrostatic spinning", was used relatively recently (in around 1994), its fundamental idea dates backmore than 60 years earlier. From 1934 to 1944, Formhals published a series of patents [59-63], describing an experimental setup for the production of polymer filaments using an electrostatic force. A polymer solution, such as cellulose acetate, was introduced into the electric field. The polymer filaments were formed, from the solution, between two electrodes bearing electrical charges of opposite polarity. One of the electrodes was placed into the solution and the other onto a collector. Once ejected out of a metal spinnerette with a small hole, the charged solution jets evaporated to become fibers which were collected on the collector. The potential difference depended on the properties of the spinning solution, such as polymer molecular weight and viscosity. When the distance between the spinnerette and the collecting device was short, spun fibers tended to stick to the collecting device as well as to each other, due to incomplete solvent evaporation [64].

Since 1980s and especially in recent years, the electrospinning process essentially similar to that described has regained more attention probably due in part to a surging interest in nanotechnology. As ultrafine fibers or fibrous structures of various polymers with diameters down to submicrons or nanometers can be easily fabricated with this process [64].

To the mid-1990s, after Reneker and his group [69-71] began to study about electrospinning process, many researchers intensified on this subject as well. It is obvious that after 1990s, this method was investigated intensively. Still, there is much to understand about the electrospinning process itself.

2.6.1 Electrospinning process

The Experimental setup of electrospinning shown in Figure 2.8. Electrospinning apparatus, consists of a nozzle, a high voltage power supply, a container for polymer fluid and an electrode collector. An AC/DC high voltage equipment which creates high electrical potential, a capillary tube, and a collecting screen. High voltage supplier has two electrodes. One is positive and the other one is negative. In the electrospinning, positive end is attached to polymer solution or polymer melt and negative end is connected to the collecting ground. By adjusting the voltage a required electric field for spinning can be created between the positive and negative sides. Polymer fluid (solution or melt) is filled to a capillary tube where positive electrode wire is inserted into. Capillary tube can be a pipette, micropipette, a glass capillary, a syringe with needle or nozzle. If a metal needle is used for electrospinning, the positive end is wrapped around the metallic needle. Capillary tube position can be vertical with or without using a metering or syringe pump [72]. Polymer fluid holder can be placed horizontally or with various angles [73]. Negative end of the voltage power supplier is connected to a collector opposite to the polymer fluid container. Most fiber collection screens are metallic and covered with an aluminum foil. The shape of the metal collectors is usually flat but in some cases, for specific fiber production (e.g. aligned fibers) dynamic collectors are utilized instead of stationary ones. Rotating drums, discs, or rotating cylindrical collectors are examples of dynamic screens. Conductive parallel plates are also potential candidates for aligned nanofiber production [74].

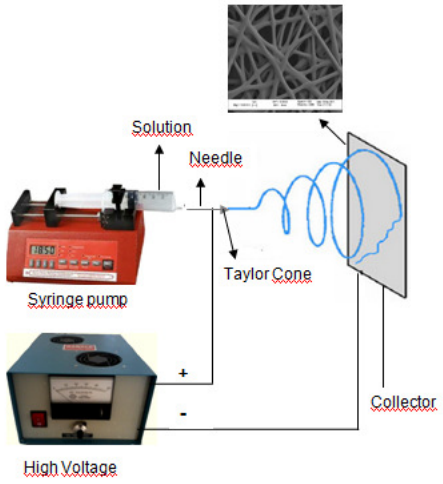

Figure 2.8 : Experimental setup of electrospinning.

Electrospinning process has four different phases. In the first phase, electrically charged liquid polymer jet emerges from the tip of the needle. A whipping process occurs in the second phase. Splaying or multi jet formation is accepted as the third phase and grounding of the thin dried fibers to the collector is the last phase [71]. When an electrostatic force is applied by a high voltage source, an electric field is formed at the tip of the syringe where polymer liquid is held by its surface tension. The accumulation of the charges in the tip causes repulsion which opposes the surface tension forces and the higher the voltage the stronger the mutual repulsion of the charges at the tip. With the increase of the electric field the pendant polymer drop at the tip of the needle changes its hemispherical shape and takes a conical shape which is called as Taylor cone [76]. Taylor stated that a conductive liquid can stay in equilibrium with a cone angle of 49.3° under an electric field. Some recent researches have shown that Taylor cone angle is valid for only to a specific self-similar solution. Cone angle of 33.5° have been reached both experimentally and theoretically with the initiation of a critical electric field [77]. Surface tension can no longer resist mutual repulsive electrostatic forces and charged jet of polymer solution or melt protrudes from the tip of needle at a point of Taylor cone. Polymer jet goes through a short stable region and then immediately gains a chaotic motion or instable region starts. In this region solvent evaporation occurs, leaving a thin dried fiber behind. Fibers are generally collected at the negative polar end as non woven mats[49].

2.6.2 Parameters effecting of electrospinning

In the electrospinning process, the following three parameter classes have relative effects on the resulting fiber properties:

1. Polymer solution parameters

2. Polymer processing parameters

3. Ambient parameters

Solution conductivity, surface tension, dielectric effect, solutionviscosity which is closely related to molecular weight of the polymer, solution concentration and polymer chain entanglement, and volatility of the solvent are the properties of the spinning solution. Applied voltage (or electrical potential), flowrate of the polymer solution (or feedrate), diameter of the tip, distance between the tip and the collector,

and geometry of collector are the processing parameters. Ambient parameters are thought as temperature of spinning environment, humidity, air velocity in the media, pressure, and atmosphere around the area [64,65,74,77].

2.6.2.1 Polymer solution parameters

The property of the solution plays a significant part in the electrospinning process and the resultant fiber morphology. During the electrospinning process, the polymer solution will be drawn from the tip of the needle. The electrical property of the solution, surface tension and viscosity will determine the amount of stretching of the solution. The rate of evaporation will also have an influence on the viscosity of the solution as it is being stretched. The solubility of the polymer in the solvent not only determines the viscosity of the solution but also the types of polymer that can be mixed together.

Solution conductivity

For electrospinning process to be initiated, the solution must gain sufficient charges such that the repulsive forces within the solution are able to overcome the surface tension of the solution. Subsequent stretching or drawing of the electrospinning jet is also dependent on the ability of the solution to carry charges.

Generally, the electric conductivity of solvents is very low (typically between 10^{-3} to 10^{-9} ohm^{-1} m^{-1}) as they contain very few free ions, if any, which are responsible for the electric conductivity of solution. The presence of acids, bases, salts and dissolved carbon dioxide may increase the conductivity of the solvent. The electrical conductivity of the solvent can be increased significantly through mixing chemically non-interacting components. Substances that can be added to the solvent to increase its conductivity includes mineral salts, mineral acids, carboxylic acids, some complexes of acids with amines, stannous chloride and some tetraalkylammonium salts. For organic acid solvents, the addition of a small amount of water will also greatly increase its conductivity due to ionization of the solvent molecules [53]. This increase in the conductivity can help production of beadless fibers just because stretching of the solution has increased and to some degree fiber diameter decrease can be observed [49].

Surface tension

Surface tension (σ) is defined as force applied to the plane of the surface per unit length. In liquids, a small droplet falling through air takes a spherical shape. Surface property of the liquid which is known as surface tension causes this phenomenon. In electrospinning process, polymer solution has to have sufficient charge in order to overcome surface tension in the liquid solution. During electrospinning, beaded fiber formation can be observed within the polymer jet because of the effect of the high surface tension values. There are various ways to lower the surface tension of the polymer solution. One way is to use solvents having low surface tension. Beaded nanofibers were produced from water/poly(ethylene oxide) solution [78]. Addition of ethanol to the water/poly(ethylene oxide) solution reduced the surface tension of the solution and production of smooth poly(ethylene oxide) nanofibers was obtained. The same effect was found also as in the study of Fong and his research team [79]. They found out that high surface tension causes beaded fibers. Poly(vinylpyrrolidone)(PVP)/N,N-dimethylformamide (DMF) and PVP/dichloromethane (MC) resulted in beaded fibers since they have high surface tension. On the other hand, smooth fibers without bead formation were seen in PVP/ethanol solutions, having a lower surface tension. Another way is to add surfactant to the spinning solution. Surfactant contribution to the spinning solution is expected to decrease surface tension. Zeng and his coworkers used insoluble surfactant and observed a decrease in the surface tension [80]. Using soluble surfactants improved fiber formation and decreased the fiber diameter. Insoluble surfactant was even more effective. None or only a slight decrease on the surface tension was observed when a non-ionic surfactant was used. However, cationic surfactants helped in obtaining beadless fibers [81]. In addition to solvent and surfactants, temperature is another factros for surface tension. For a pure liquid system, the surface tension of the liquid would decrease with increasing temperature. When the temperature is raised, the equilibrium between the surface tension and the vapor pressure would decrease. At a critical point, the interface between the liquid and the gas disappears [82]. From the molecular point of view, at a higher temperature, the liquid molecules gain more energy and start to move more rapidly in the space. As a result, the fast moving molecules do not bound together as strongly as the molecules in a cooler liquid. With the reduction in the bonding between the

molecules, the surface tension drops. The effect of temperature on surface tension for pure liquid may be different from mixtures. For a mixture of methane and nonane, the surface tension actually increases with increasing temperature except at the lowest pressure. At a lower temperature, methane is more soluble than nonane and the effect of liquid mixture composition is more pronounce than temperature in the determination of the surface tension [83].

Dielectric effect

The dielectric constant of a solvent has a significant influence on electrospinning. Generally, a solution with a greater dielectric property reduces the beads formation and the diameter of the resultant electrospun fiber [84]. Solvents such as N,N-Dimethylformamide (DMF) may added to a solution to increase its dielectric property to improve the fiber morphology [85]. The bending instability of the electrospinning jet also increases with higher dielectric constant. This is shown by increased deposition area of the fibers. This may also facilitate the reduction of the fiber diameter due to the increased jet path [86]. The dielectric constant of some common solvents used in electrospinning is shown in Table 2.2.

The relationship between the diameter of resultant fiber and dielectric constant of the polymer solution were studied and at the this study, it has been found out that resultant fibers from solutions which have higher dielectric constant have thinner diameter.

Solution viscosity

There are several factors affecting solution viscosity. Molecular weight, polymer chain entanglement, concentration, and temperature are accepted as the main factors. Molecular weight of a polymer is directly related to viscosity of the solution. Generally, when a polymer of higher molecular weight is dissolved in a solvent, its viscosity will be higher than solution of the same polymer but of a lower molecular weight. One of the conditions necessary for electrospinning to occur where fibers are formed is that the solution must consists of polymer of sufficient molecular weight and the solution must be of sufficient viscosity. As the jet leaves the needle tip during electrospinning, the polymer solution is stretched as it travels towards the collection plate. During the stretching of the polymer solution, it is the entanglement of the molecule chains that prevents the electrically driven jet from breaking up thus

maintaining a continuous solution jet. As a result, monomeric polymer solution does not form fibers when electrospun [87].

Table 2.2 : Dielectric constants of solvents [53].

Solvent	Dielectric constant
Water	80.02
Acetonitrile	35.92-37.06
Dimethylformamide	36.71
Methanol	32.6
Trifluoroethanol	27.0
Ethanol	24.55
Acetone	20.7
2-propanol	18.3
Pyridine	12.3
m-Cresol	11.8
Dichloromethane	8.93
Tetrahydrofuran	7.47
Acetic acid	6.15
Ethyl acetate	6.0
Chloroform	4.8
Toluene	2.4

The molecular weight of the polymer represents the length of the polymer chain, which in turn have an effect on the viscosity of the solution since the polymer length will determine the amount of entanglement of the polymer chains in the solvent. Another way to increase the viscosity of the solution is to increase the polymer concentration [53]. Increasing solution concentration shows almost same effect as using higher molecular weight polymer. Polymer chain entanglement of the polymer solution is improved in either case. At higher concentrations, viscosity of the solution becomes higher and it prevents the jet having larger bending instabilities. This causes small deposition on the collecting media for fibers and the resultant fiber diameter is thickened. At low viscosities, there will be less amount of chain entanglement in polymer solution. The forces from surface tension become dominant and bead formation occurs along the string of electrospun fibers. At high viscosities, jets can

be stretched fully and beadless fibers can be obtained. This situation can be observed from Figure 2.9. High viscosity values also provoke splitting of jets into smaller fibers. Moreover, pumping of the polymer solution becomes difficult and drying of the solution on the tip of the pipette can be observed [49].

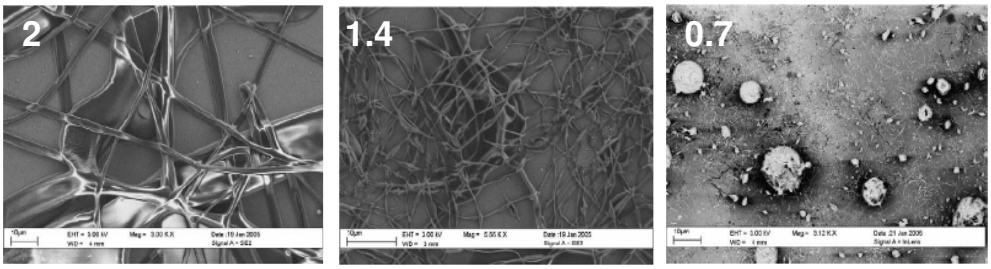

Figure 2.9: SEM images of the samples at different PMMA concentrations [88].

Many experiments have shown that a minimum viscosity for each polymer solution is required to yield fibers without beads [78,93]. At a low viscosity, it is common to find beads along the fibers deposited on the collection plate. When the viscosity increases, there is a gradual change in the shape of the beads from spherical to spindle-like until a smooth fiber is obtained [78]. At a lower viscosity, the higher amount of solvent molecules and fewer chain entanglements will mean that surface tension has a dominant influence along the electrospinning jet causing beads to form along the fiber. When the viscosity is increased which means that there is a higher amount of polymer chains entanglement in the solution, the charges on the electrospinning jet will be able to fully stretch the solution with the solvent molecules distributed among the polymer chains. With increased viscosity, the diameter of the fiber also increases [89-93]. This is probably due to the greater resistance of the solution to be stretched by the charges on the jet [90].

Volatility of the solvent

Solvent volatility is an important factor in electrospinning. Since electrospinning requires a quick evaporation rate and phase separation, vapor pressure of solvent affects the drying time and evaporation rate. Other parameters affecting evaporation rate are:

- Boiling point, Specific heat, Enthalpy and heat of vaporization, Rate of heat supply, Interaction between solvent molecules, Surface tension of liquid, Air movement above the liquid surface [53].

Solvent volatility is also an important factor in determining the properties of fibrous structures produced by electrospinning. In the electrospinning process, solvent evaporation occurs while the jet travels from the tip of the pipette to the collector. If all of the solvent evaporates on the way, fibers can be formed and deposited on the collector. However, if some solvent still remained on the polymer, instead of dry fibers, wet fibers or thin films can be produced [94]. It is claimed that solvent volatility plays an important role on the formation of pores in the fibers [93 ve 95]. A decrease in the solvent volatility resulted in smoother fiber surface. However, low boiling point solvents are desirable because evaporation of the solvent is enhanced and deposition of the fibers becomes easier. Matthews and his coworkers chose a volatile solvent having a low boiling point in their study [96]. Solvent volatility can also affect the shape of the fibers produced. Rapid evaporation rate of the solvent can cause the fibers to form as ribbons with various cross sections [97].

2.6.2.2 Polymer processing parameters

Another important parameter that affects the electrospinning process is the various external factors exerting on the electrospinning jet. This includes the voltage supplied, the feedrate, temperature of the solution, type of collector, diameter of needle and distance between the needle tip and collector. These parameters have a certain influence in the fiber morphology although they are less significant than the solution parameters [53].

Applied voltage

Applied voltage determines the amount of charges carried by the jet of the polymer. The high voltage will induce the necessary charges on the solution and together with the external electric field, will initiate the electrospinning process when the electrostatic force in the solution overcomes the surface tension of the solution. Generally, both high negative or positive voltage of more than 6kV is able to cause the solution drop at the tip of the needle to distort into the shape of a Taylor Cone during jet initiation [98]. Depending on the feedrate of the solution, a higher voltage may be required so that the Taylor Cone is stable. The columbic repulsive force in the jet will then stretch the viscoelastic solution. If the applied voltage is higher, the greater amount of charges will cause the jet to accelerate faster and more volume of solution will be drawn from the tip of the needle. This may result in a smaller and

less stable Taylor Cone [99]. When the drawing of the solution to the collection plate is faster than the supply from the source, the Taylor Cone may recede into the needle [92].

Applied voltage has also effects on the morphology and the resultant fibers. Increase in the applied voltage results with a decrease in the fiber diameter. Generally, high voltage results with higher bead formation, but increased jet stretching leads to fewer amounts of beads [90]. At lower voltage, due to the weaker electrostatic force, flight time may last longer. Longer flight time lets the jet to elongate and stretch stronger and longer resulting with reduced fiber diameter. Wang and his research team measured both jet diameter and fiber diameter and investigated the effect of voltage difference [100]. They found out that both jet diameter and fiber diameter decreased slightly. Also, better chain orientation within electrospun fibers was seen by an increase in the applied voltage. A proportionality relation between applied voltage and fiber diameter was reached in a study [101]. In that study, fiber diameter became thicker as the voltage increased from 5 kV to 25 kV.

Flow rate

The flowrate will determine the amount of solution available for electrospinning. For a given voltage, there is a corresponding flowrate if a stable Taylor cone is to be maintained. When the flowrate is increased, there is a corresponding increase in the fiber diameter or beads size . This is apparent as there is a greater volume of solution that is drawn away from the needle tip [99,102]. However, there is a limit to the increase in the diameter of the fiber due to higher flowrate [102]. If the flowrate is at the same rate which the solution is carried away by the electrospinning jet, there must be a corresponding increased in charges when the flowrate is increased. Thus there is a corresponding increase in the stretching of the solution which counters the increased diameter due to increased volume. Due to the greater volume of solution drawn from the needle tip, the jet will takes a longer time to dry. As a result, the solvents in the deposited fibers may not have enough time to evaporate given the same flight time. The residual solvents may cause the fibers to fuse together where they make contact forming webs. A lower flowrate is more desirable as the solvent will have more time for evaporation [103].

Distance

The distance between the tip of the needle and the collector has a significant effect on the strength of the electric field and the flying time of the jet throughout electrospinning path. If the distance between two polar ends is short, solvents may not find the required time to be vaporized entirely before the jet arrives at the collector. The resultant fibers may include some solvents left on them. These residual solvents may cause fibers to stick together, and can result in merging of the fibers. Shorter distance between the tip and the collector may lead to an increase in the strength of electric field. This increase accelerates the velocity of the polymer jets. It also reduces the flight time of the polymer jet that is electrospun. Reducing the distance does not affect size and shape of the fibers, but, inhomogeneously distributed beads can be observed [93]. These beads can be due to increase in the electric field strength. If the distance between the tip and the collector is longer, solution jet finds more time for the evaporation of the solvent and jet can be stretched sufficiently before it lands to the collecting media. Increasing the working distance enhances both the number of beads and the density of the fibers [90]. Jet diameter dependence on the working distance is studied [100]. They concluded that increasing working distance caused a decrease on the jet diameter.

Effect of collector

In the electrospinning process, usually conductive material is used to cover collecting media. Aluminium foil is one of the most common conductive materials that are used for collection of fibers onto it. By the help of the conductive material covering, stable potential difference can be obtained between the tip and the collector. Conductive collectors attract more jets on the surface of collector resulting in a higher amount of fiber deposition. For nonconductive collectors, less fiber deposition is seen because charges on the polymer jet flows on the collector due to fast accumulation of the charges. Gathered fibers on the collection area have a lower packing density compared to using a conductive material. Fiber structures and honey comb structures can be obtained by using a non-conducting collective media. Using a porous collector has also an effect on the resulting fibers. The packing density is usually low in porous collectors. This is mainly due to the rate of evaporation of the residual solvents on the fibers deposited. Fiber morphology can be improved by using a

dynamic collector. Rotating cylinders are utilized for the production of aligned fibers. One advantage of using rotating collector is that solvents have more time for evaporation [49].

Diameter of needle

In electrospinning process, inner diameter of the needle or pipette also has some effects. Decreasing the inner diameter can cause an observable decrease in: Clogging, The number of beads and Final fiber diameter.

The decrease in the inner diameter creates an increase in the surface tension of the drops on the tip of the needle or pipette. This means that greater amount of electrostatic force is needed to start the formation of a jet. If no voltage changes occur in the process, jet acceleration decreases and gives more time for stretching and elongating of the jet before it reaches to the collector. Too small inner diameter needle is not desired due to not being able to form droplets at the tip [53]. Zeng and his coworkers studied three different capillary diameters [80]. They found that increasing the internal diameter of the capillary increased both the driving voltage necessary for electrospinning and the diameter of fibers deposited on the collecting mesh.

2.6.3 Applications of nanofibers

In the constructions made by nanofibers, the high volume to weight ratio, soft handling, and high strength and to form barrier to microorganisms and small particlesetc. are the main reasons for using them in many applications. These advantages of nanofibers make them very appealing for a broad array of potential applications in many industry segments. Nanofiber applications are shown in Figure 2.10.

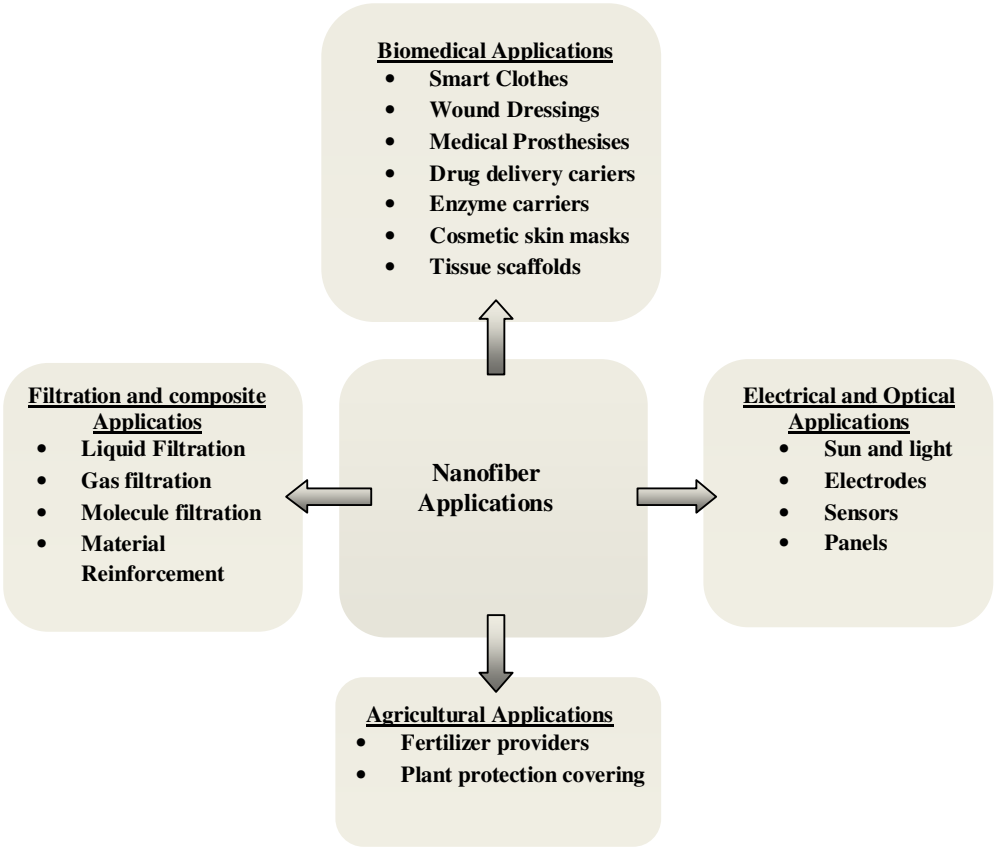

Figure 2.10 : Application areas of Nanofibers.

2.6.3.1. Filtration applications

Filters have been widely used in both households and industry for removing substances from air or liquid. Filters for environment protection are used to remove pollutants from air or water. In military, they are used in uniform garments and isolating bags to decontaminate aerosol dusts, bacteria and even virus, while maintaining permeability to moisture vapour for comfort. Respirator is another example that requires an efficient filtration function. Similar function is also needed for some fabrics used in the medical area [78].

For a fiber-based filter, removal of particles is determined by different mechanisms. Large particles are blocked on the filter surface due to the sieve effect. Particles that are smaller than the surface-pores will penetrate into the filter, which could still be collected by the fibers, via either interception or impaction, or static electrical attraction. Also, very fine particles could be captured due to the Brownian motion effect. The filtration efficiency is normally influenced by the fitler physical structure

(fiber fineness, matrix structure, thickness, pore size, etc), fiber surface electronic properties, and its surface chemical characteristic (e.g. surface free energy). The particle collecting capability is also related to the size range of particles being collected. Besides the filtration efficiency, other properties such as pressure drop and flux resistance are also important factors to be evaluated for a filter media [78].

Electrospun nanofibers for filtration application have started about 20 years ago A company in US (Donaldson) has produced electrospun nanofiber-based filter products for industry, consumer and defense applications (Figure 2.11), and its Ultra-web® nanofiber filter has been developed for nonwoven and filtration industry for a wide range of applications. Recently another company (AMSOIL) has also developed a nanofiber- based fuel filter for automobile applications. DuPont has electrospun fabric products for HVAC, automotive and liquid filtration, bedding protection and apparel applications.

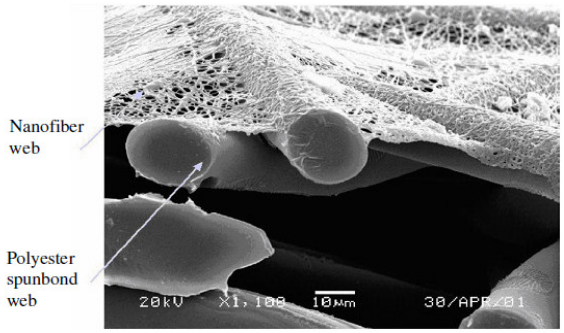

Figure 2.11 : Filter system that formed by electrospun nanofibers on the polyester spunbond nonwoven [104].

Electrospun nanofiber membrane provides dramatic increases in filtration efficiency at relatively small decreases in permeability. In comparison with conventional filter fibers at the same pressure drop, nanofibers with a diameter finer than half a micron have a much higher capability to collect the fine particles, because the slip flow around the nanofibers increases the diffusion, interception and inertial impaction efficiencies [104].

Both experimental measurements and theoretical calculations revealed that electrospun nanofiber mats were extremely efficient at trapping airborne particles (0.5—200 μm) [105]. A very thin layer of electrospun nanofibers sprayed onto a porous substrate was sufficient to eliminate the particle penetration. The air flow

resistance and aerosol filtration properties correlate with the add-on weight of the electrospun fiber coating. Also, electrospun layers present minimal impedance to moisture vapour diffusion, which is very important for protection clothing in decontamination applications. A comparison study between a nylon-6 electrospun membrane (thickness 100 μm, pore size 0.24 μm) and a commercial high efficiency particulate air (HEPA) filter (thickness 500 μm, pore size 1.7 μm) using 300 nm test particles indicated that the thin nanofiber membrane had a slightly higher filtration efficiency (99.993%) than the HEPA filter (99.97%) [106].

Besides solid particles, tiny liquid droplets within a liquid-liquid immiscible system could also be removed by a nanofiber membrane (liquid-liquid coalescence filtration). Polystyrene (PS) nanofibers (diameter about 600 nm) were electrospun from a recycled expandedpolystyrene (EPS), and mixed with micro glass fibers to form a filter media for removal of water droplets from a water-in-oil emulsion [107]. The addition of small amount of PS nanofibers was reported to significantly improve the capture efficiency (from 68% to 88%), but the pressure drop of the filters was increased considerably. In another work, electrospun nylon nanofibers were also blended with glass fibers (diameter 5 μm) for the coalescence filtration, and addition of an optimal amount of nanofibers (1.6 wt%) to the coalescence filter improved the capture efficiency, but did not cause excessive pressure drop [108].

Nanofibers were used as a supporting scaffold in ultrafiltration (UF) for oil/water emulsion separation. The reported UF membrane has a three-tier composite structure consisting of a nonporous hydrophilic top layer, a crosslinked poly(vinyl alcohol) (PVA) electrospun nanofibrous mid-layer and a conventional nonwoven microfibrous substrate [109,103]. The electrospun nanofibrous substrate provided a well interconnected porous network with a large specific surface area, so the UF filter has a high flux rate and excellent organic solute rejection capability.

Other works related to the filtration applications include effects of operating parameters in electrospinning on fiber morphology and pore structure for filter media [110], nanofiber membrane for separation of micro particles from liquid [111], and pre-filter nanofiber membrane for particulate removal [112].

2.6.3.2 Nanocomposites

The use of reinforcing fillers and fibers in polymers to improve their mechanical properties is commonly encountered in polymer technology. Conventional fibers such as carbon fibers, glass fibers, gel-spun polyethylene fibers, and aramids are routinely used in composites of a range of different polymers (113). The improvement in modulus and strength achieved by using even low levels of a reinforcing fiber in a composite is impressive. Some of this improvement is due to the properties at the fiber/matrix interface and therefore dependent on the surface area of the interface. Nanofibers, with their very high specific surface area, should therefore deliver particularly good composite characteristics. For instance (poly(2,20(m-phenylene)-5,50-dibenzimidazole)) (PBI) electrospun nanofiber filler in epoxy EPON 828 (Shell Chemical Company) and rubber matrices has been studied by Kim and Reneker (1999a). Even at the 10 phr level, the nanofibers increased the modulus of styrene-butadiene rubber (SBR) tenfold! Nanofibers of nylon-4,6 used in an epoxy matrix that yielded a transparent composite have also been reported (114).

2.6.3.3 Biomedical applications

From biological viewpoint, almost all of the human tissues and organs are deposited in nano fibrous forms or structures. Examples include: bone, dentin, collagen, cartilage, and skin. All of them are characterized by well organized hierarchical fibrous structures realigning in nanometer scale. As such, current research in electrospun polymer nanofibers has focused one of their major applications on bioengineering. We can easily find their promising potential in various biomedical areas [115]. Biomedical applications of nanofibers are medical prostheses, smart clothes, drug delivery carriers, wound dressings, cosmetic skin masks, and tissue scaffolds.

One of the sub-sections of the biomedical application of nanofibers is to cure for wound and burnings in human skin. It can be designed for especially haemostatic tools. Electrospun biodegradable polymers can be spun onto the wound skin. They form a thin web onto the skin. This web protects skin from microbe. Moreover, it helps to heal the wound quickly. Finally, it minimizes the possibility of scar. Electrospun nanofiber equipment used in wound healing is shown in Figure 2.12.

Figure 2.12 : Application of electrospun nanofibers used in wound covering and healing [116].

Similarly, nano fibrous mats are being explored as biomedical grafts and wound dressings. It has been found that cells can adhere to and proliferate into the mats with a great deal of success. Also, because of the extremely small size of the nano-fibers, the potential exists for layering of different polymers with specific functionalities [117].

2.6.3.4 Agricultural, electrical, optical and other applications

Plants are covered with a web that produced by electrospun nanofibers. One of the functions of this web is protection against harmful insects and chemicals. It can be used as a greenhouse covering. Furthermore, fertilizers, which were injected to the web before, can be given by the help of nanofiber web. The study about nanofiber web for plant done in our department is shown in Figure 2.13.

Figure 2.13 : A plant covered with nanofiber web [118].

In military applications, protecting clothes are expected especially to hold the possibility of survival, enable long term protection, stand heavy weather conditions, endure nuclear, chemical, and biological effects and increase efficiency. Protecting clothes now being used have made of heavy fabrics. The light and high porous fabrics which absorb the air and air vapor can easily react with chemical gases that cause fabric to decompose. Because of the higher surface area and low pore size of the nanofibers, fabrics, produced by them, are suitable for protecting clothes. Additionally, neutralization can be provided with these fabrics. Also, it allows the clothes to breath. Nanofibers which have high numbers of pores with small pore sizes provide high resistance to penetration of the chemicals into the fabrics. In military applications, it is benefited from nano sensors for work of finding trace, from nano electronics for various controls, from nano composites for platforms that need to lightness [51].

Production of nanofibers which have the ability to transmit electricity creates many advantages. These nanofibers are used in the production of the small electronic devices and in the fabrication of some machines. Because surface area of the electrodes is proportional to the chemical reaction speed, electrospun nanofiber membranes are used appropriately in the production of improved high performance batteries.

Nanofibers also used for sensors because of their high specific area allows them to sorb and/or react rapidly with low levels of analytes in the air [119-122]. It is reasonable to therefore expect better performance from nanofiber sensors.

The other potential applications of nanofibers are wires, capacitors, transistors and diodes for information technology and enzyme carriers. The application of nanofibers in textiles is not aimed only at specialized industries involved in technical textiles [117].

2.6.4 Literature review of PMMA and fluorinated nanofibers

Generally, acrylic polymers were used for automobile windshields, but poly(methyl methacrylate) sheet (Plexiglas, Lucite) soon became the principal use of acrylic plastics. Poly(methyl methacrylate) (PMMA) has a wide variety of applications and uses from thermoformed signs, aircraft windshields, bathtubs [19], electron beam or ion beam resists in the manufacture of microelectronics chip [20,21] due to the it has

a light transmittancy of about 92% , good resistance to weathering and good mechanical properties. There are many researches carried out related to electrospinning of PMMA for different purposes.

Uyar et al. reported PMMA electrospun fibers with different concentration in DMF solution. They have been demonstrated that polymer concentration increases, the diameter of the nanofibers increase and beads form dissapeared [123].

Piperno et al. reported nanofibers of PMMA and they have been demonstrated that increasing the PMMA concentration the fiber number and their homogeneity grow, while the beads, that are characteristic of the lowest concentration solution, disappear. Moreover, increasing the polymer concentration, increasing the diameter of the nanofibers s are determined [88].

Wang et al the nanofibers of PMMA, PMAA and poly(MMA-co-MAA) copolymers by electrospining technic. 6% (wt) electrospinning solutions prepared in DMF, and bead-free nanofibers have been obtained for PMMA, but bead-fiber of PMAA and copolymer have been obtained [124].

Up until now, There are many researches carried out related to electrospinning of PMMA and copolymers of PMMA, but not researches carried out related to electrospinning of P(BA-co-MMA). Therefore, this study will be first example related to electrospinning of P(BA-co-MMA).

Hydrophobicity of a material is a key property that depends on both surface chemistry and surface roughness [125-127]. Hydrophobic polymers (with water contact angle above 90°) are useful in many applications such as inert biomaterials, environmentally resistant coatings, and lowfriction devices, whereas superhydrophobic materials (with water contact angles above 150°) are of special interest as self-cleaning surfaces and stain-resistant textiles [128,129].

Deitsel et al. reported P(MMA-r-TAN) electrospun fibers with contact angles of 76^{o} for pure PMMA and that of 103^{o} for the unannealed 90:10 P(MMA-r-TAN) film and 107^{o} for the annealed the same sample film [92].

Actay et al. reported superhydrophobic surfaces by electrospinning low molecular weight poly- (acrylonitrile-*co*-R,R-dimethyl-m-isopropenylbenzyl isocyanate) with a perfluorinated linear diol [130]. A contact angle of 167° was observed for a polymer film with predominantly bead morphology.

Polymethylsilsesquioxane (PMSQ) surfaces prepared by electrospinning method. The contact angle was found to be 151^o as repoted by Xiang et al. [131]. Polystyrene (PS) and polyvinyl chloride (PVC) micro-nano fibers were also obtained by electrospinning method. The diameter of fibers were between 200-500nm and that of PS were between 400nm-1.25µm for PVC and PS, respectively. A high contact angle were reported(i.e 144^o for PVC, 156^o for PS) [132]. Water contact angle of spin coated and electrospun PAN nanofbers were found to be 72^o and 151^o, respectively [133].

Yano et al. reported the nanofiber and flat surfaces using PMMA-co-PBIEM and PMMA-co-PBIEM-g-PFA-C_8 copolymers by electrospining and spin coated technics. The water contact angle increased from 76^o to 127^o with nanofiber synthesized when PMMA-co-PBIEM copolymer was used. However, the water contact angles were reported as 129^o for spin coated and 150^o for electrospining by grafting 2-(perfluorooctyl)ethyl acrylate part [134]. Similarly, Hardman et al. reported the superhydrobhobic fluoroalkyl end functionalized PS fibers with 158^o of water contact angle when the fluoroalkyl end functionalized group content of the polymer as 4 % (wt). The water contact angle of PS fiber was reported 140^o without any floropolymer content [135]. Electrospun poly(caprolactone) (PCL) was coated by perfluoroalkyl ethyl methacrylate (PPFEMA) with coated chemical vapor deposition. The contact angles were reported as 139^o and 172^o before and after coating by Ma.et al. [136]. Han et al. reported the first Teflon (PTFE) electrospun fibers by coaxial electrospinning with Teflon AF sheat and poly(ε-caprolactone)(PCL) core materials. They reported the water contact angle 69^o and 120^o for spin coated PCL and Teflon AF film, respectively. Increase in the roughness by electrospining resulted in increase in the water contact angle as 125^o for PCL fiber membrane and 158^o for PCL/Teflon fiber membrane [137].

The significance of this approach is that it yields polymer mats with either hydrophobic or superhydrophobic surfaces. Moreover, this work is one of the few examples in which nanofibers of a highly fluorinated polymer have been produced because most hydrophobic fluoropolymers are too insoluble to allow electrospinning to be used.

3. EXPERIMENTAL PART

3.1 Materials

Methyl Methacrylate (MMA), Butyl Acrylate (BA) and poly(methyl methacrylate) (PMMA), Dimethylformamide (DMF), *Tetrahydrofuran (THF), Sodium Dodecyl Sulfate (SDS) and Potassium Peroxydisulfate* (KPS) were purchased from Sigma Aldrich. Acetone [$(CH_3)_2CO$] and Ethyl alcohol [(C_2H_5OH)] were obtained from Merck. They were used without further purification and all chemicals were analytical grade. Fluorinated copolymers (BT-1, BT-4 and BT-9) were supplied from GYTE.

3.2 Synthesis of P(BA-co-MMA)

0.5 g emulsifier sodium dodecyl sulfate (SDS) was dissolved in 80 ml water and then 50 g of a mixture of monomers of MMA and BA (25:25 wt MMA:BA) were dropped into the reactor, the mixture was stirrred for 30 minutes. Monomers were shown in Figure 3.1. At the same time, 0.25 g KPS is dissolved in 20ml pure water. After the 30 minutes, dissolving KPS is added to the mixture [138]. Copolymer Structure were shown in Figure 3.2.

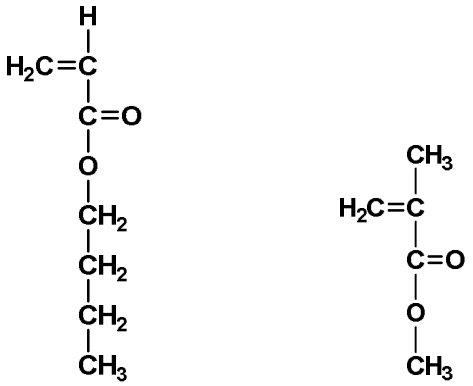

Butyl Acrylate (BA) Methyl Methacrylate (MMA)

Figure 3.1 : Monomers used in synthesis of P(BA-co-MMA).

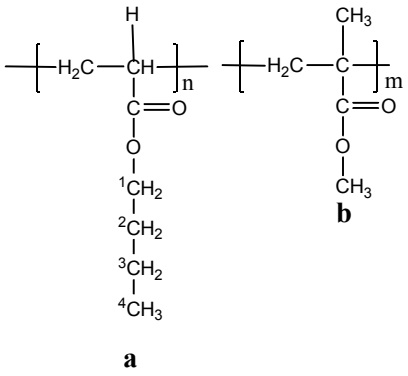

Figure 3.2 : P(BA-co-MMA) structure.

Reaction continued for 3 h at 80 C. Experimental setup of the polymerization was demonstrated in Figure 3.3. After the 3 hours, reaction was stopped with addition of 300ml ethanol. Then the mixture was washed with ethanol and water and copolymer was dried at 50°C for 24h in vacuum drying-oven.

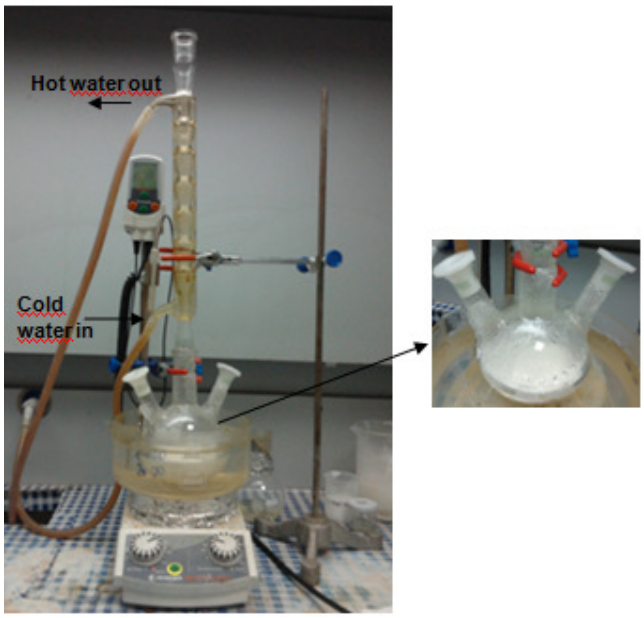

Figure 3.3: Experimental setup for synthesis of P(BA-co-MMA).

3.3 Florinated Copolymers

Statistical copolymers of poly(PFMA-ran-MMA-ran-BA) were synthesized in supercritical carbon dioxide at 200 bar and 80 ^{o}C using AIBN as an initiator in a heterogeneous free radical copolymerization medium at Gebze Institue of

Technology [27] which represented as BT-1, BT-4 and BT-9. These Florinated polymers (BT-1, BT-4 and BT-9) used for Electrospinning which copolymer structure and compositions shown in Figure 3.4 and Table 3.1, respectively.

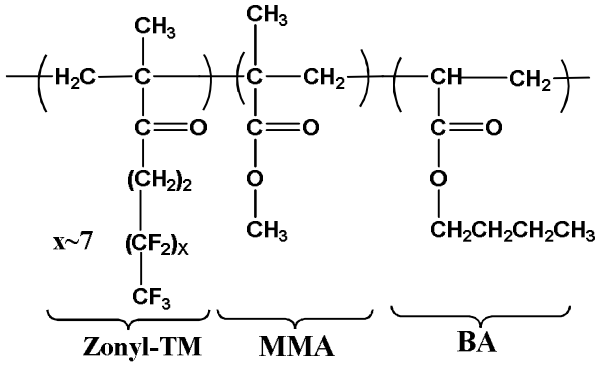

Figure 3.4: Fluorinated polymer structure.

Table 3.1 : Zonyl-TM, BA and MMA composition in feed and copolymer

Copolymer	Feed Monomer Mole Fraction (mol %)			Copolymer Mole Fraction (mol %)[a]			
	X_{FMA}	X_{BA}	X_{MMA}	X_{FMA}	X_{BA}	X_{MMA}	Yield[b] (%)
P(BA-co-MMA)	-	50	50	-	17.85	82.1	60
BT1	5	25	70	9.2	30.7	60.1	80
BT4	5	20	75	8.6	25.8	65.6	88
BT9	5	5	90	6.6	10.6	82.8	85

[a]:Determined from ^{1}H-NMR
[b]:Calculated gravimetrically

3.4 Preparation of Electrospinning Solutions

3.4.1 Electrospinning of P(BA-co-MMA)

Five series of polymer solutions with different concentration of P(BA-co-MMA) dissolved in DMF which are 1%(w/v), 3%(w/v), 5%(w/v), 8%(w/v) and 10%(w/v) P(BA-co-MMA) polymer solutions. At the same time, the electrospinning solutions for 5% (w/v) P(BA-co-MMA) were prepared in various solvent systems (Table 3.2 and Figure 3.5). For each solutions were stirred at room temperature with the speed of 400 rpm for 3 h. Then the solutions were filtered therefore impurities were removed from the solutions. The electrospinning apparatus consists of a syringe pump (NE-500 model, New Era Pump Systems, Inc., USA) and DC power supplier (ES50 model, Gamma High Voltage Inc., USA). The solutions were then loaded into

a 2.5 ml syringe. Obtained fibers were characterized by FTIR-ATR, DSC and SEM measurements.

Table 3.2 : P(BA-co-MMA) polymer solutions used for various solvents

Polymer	Polymer Concentration (wt%)	Solvents	Mixture ratio of solvents (wt%)
P(BA-co-MMA)	5	DMF	-
P(BA-co-MMA)	5	THF	-
P(BA-co-MMA)	5	Acetone	-
P(BA-co-MMA)	5	DMF/Acetone	50/50
P(BA-co-MMA)	5	THF/Acetone	50/50
P(BA-co-MMA)	5	DMF/THF	25/75
P(BA-co-MMA)	5	DMF/THF	50/50
P(BA-co-MMA)	5	DMF/THF	75/50

Figure 3.5 : Prepared electrospinning solutions

3.4.2 Electrospinning of flourinated copolymers

15 wt% PMMA, 8 wt% P(BA-co-MMA), 0.03M BT-1, 0.015M BT-9, and 0.0075M BT-4 polymer solutions were prepared in DMF. For this purpose each solution were stirred at room temperature with the speed of 400 rpm for 5 h. Then the solutions were filtered therefore impurities were removed from the solutions. The solutions were then loaded into a 2,5 ml syringe. The distance between the tip of syringe needle and Al plate collector was varied from 10 cm to 15 cm and the flow rate of the solution was varied from 0.5 to 2 ml/h, while electrical potential between the needle tip and the Al plate voltage was also varied from 15 to 20 kV. The outline of the experimental procedure for the preparation of Electrospinning solutions are

illustrated in Figure 3.6. Obtained fibers were characterized by FTIR-ATR spectra, DSC, SEM and Contact Angle measurements.

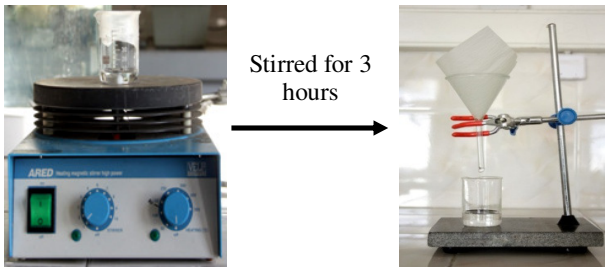

Figure 3.6 : Schematical representation of preparation of Electrospinning solutions.

3.5 Process setup and electrospinning

In electrospinning process, the setup consisted of a DC high voltage power supply from GAMMA High Voltage Research Inc., USA (Model no: ES50) with an electrical potential range from 0 to 30 kV, and a syringe pump (New Era Pump Systems Inc., USA Model no: NE-500). The metal collector was covered with an aluminum foil. The setup was kept in a plexiglass box for experimenter's safety. All experiments were carried out under atmospheric pressure and at room temperature. The positive electrode wire was hooked at the metal part of the needle and negative part of the electrode was attached to the metal collector 5 to 60 minutes of operation time was sufficient for the deposition of fibers on aluminum foil. A horizontal setup was chosen for electrospinning process. A picture that was captured during electrospinning is illustrated in Figure 3.7.

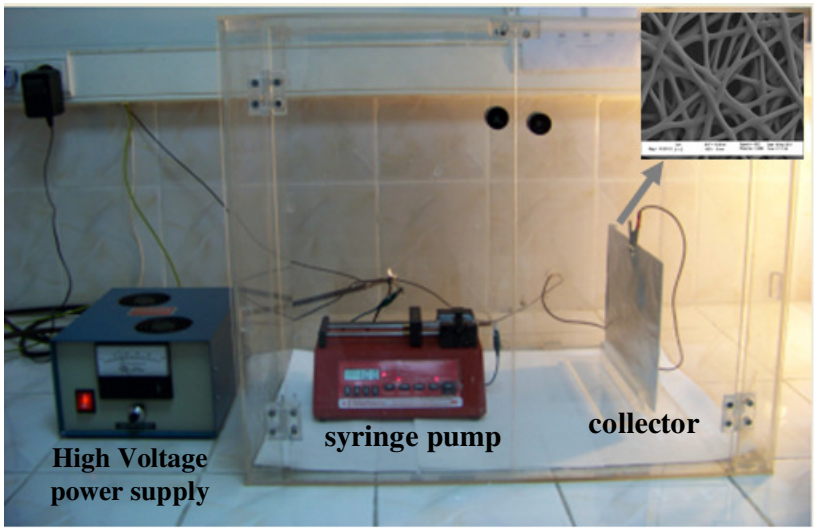

Figure 3.7 : A representative picture taken during electrospinning.

3.6 Characterization of P(BA-co-MMA), PMMA and Florinated Copolymers

The structure of the copolymers was characterized by means of ^{1}H NMR spectroscopy and Fourier Transform Infrared-Attenuated Total Reflectance (FTIR-ATR) spectroscopy.

- FTIR analysis of P(BA-co-MMA) nanofibers were carried out with FTIR-ATR reflectance spectrophotometer (Perkin Elmer, Spectrum One, with a Universal ATR attachment with a diamond and ZnSe crystal).
- ^{1}H NMR spectroscopy by using a 250 MHz Brucker AC Aspect 3000 NMR spectrometer with $CDCl_3$ as a solvent. Values were recorded as ppm relative to internal standard (TMS).
- Number average (M_n) and weight average (M_w) molecular weights were determined in ultra pure THF solvent using GPC (Agilent 1200 series, BIC RID detector) equipment. The calibration was done by using the different molecular weight of PS standards (M_w=2000 to 800,000) and the passage time of the solvent was 0.3 mL/min.
- The DSC measurements were carried out on TA Q1000 DSC instrument calibrated with poly(methyl methacrylate). DSC measurement of polymers were operated with 4 cycles. First cycle was heating from -30°C to 150°C, second cycle was cooling from 150°C to -30°C, third cycle was heating from -30°C to 250°C and fourth cycle was heating from -250°C to -30°C. Third cycles were considered for DSC analysis. Each sample was scanned at a heating rate of 10 °C min^{-1}.
- Resulting fibers were also characterized as morphological by Scanning Electron Microscope (two diffrent SEM devices are used, firstly Philips XL30 and lastly, LEO SUPRA 35 VP) and the samples for the SEM measurements are prepared by coating of gold (Ion Sputter Metal Coating Device, MCM-100).
- Static contact angles of fiber surfaces under air were measured by using a KSV-CAM 200 contact angle meter with a PC controlled motorized syringe within ±1° precision (Figure 3.8).

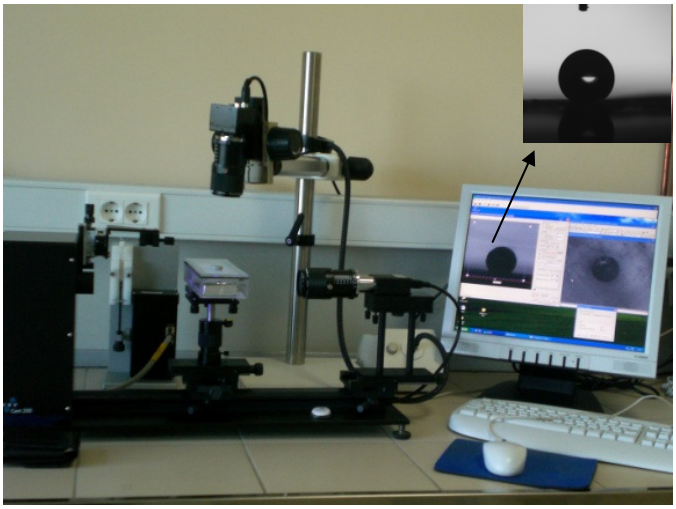

Figure 3.8 : Contact Angle Meter, KSV CAM 200.

4. RESULTS AND DISCUSSION

4.1. Copolymer Characterization

4.1.1 FTIR-ATR spectrophotometric analysis of P(BA-co-MMA)

The FTIR-ATR spectra of PMMA and P(BA-co-MMA) are shown in Figure 4.1 and it was recorded in the absorbance mode.

Figure 4.1 shows the peaks at 2950 cm^{-1}, 1728 cm^{-1}, 1435 $cm^{-1}$and 1149 cm^{-1} are assigned to CH stretching, C=O stretching, CH_3 stretching and O-CH_3 stretching vibrations, respectively, in PMMA. PBA and PMMA have similar molecular backbones, only slight differences can be found in their FTIR spectra. Absorption at 962 cm^{-1} was the characteristic peak of BA in P(BA-co-MMA) FTIR-ATR spectrophotometric results. These results are in agreement with literature [139].

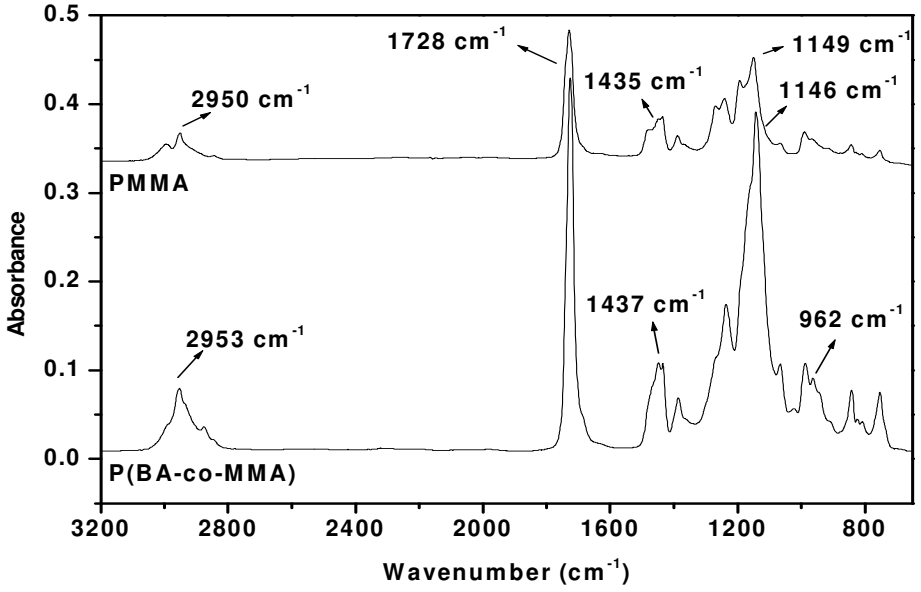

Figure 4.1 : FTIR-ATR spectra of pure PMMA and pure P(BA-co-MMA).

Figure 4.2 and Figure 4.3 shows the FTIR-ATR spectrums of prepared 5 wt.% DMF solution electrospinning solution, and DMF solvent. According to the this graph, FTIR-ATR spectrums for both of them approximately are the same due to the rich in DMF content in the solution. The CH_3 symmetric stretching mode can be observed at 2928 cm^{-1}, C-H stretching mode at 2855 cm^{-1}, C=O stretching mode at 1661 cm^{-1}, C-N stretching mode at 1504 cm^{-1}, O=C-N stretching mode at 657 cm^{-1} for peaks of DMF solvent. However, FTIR-ATR spectra of 5 wt.% DMF solution different from just one peak which at 1729 cm^{-1} is assigned to C=O stretching in P(BA-co-MMA).

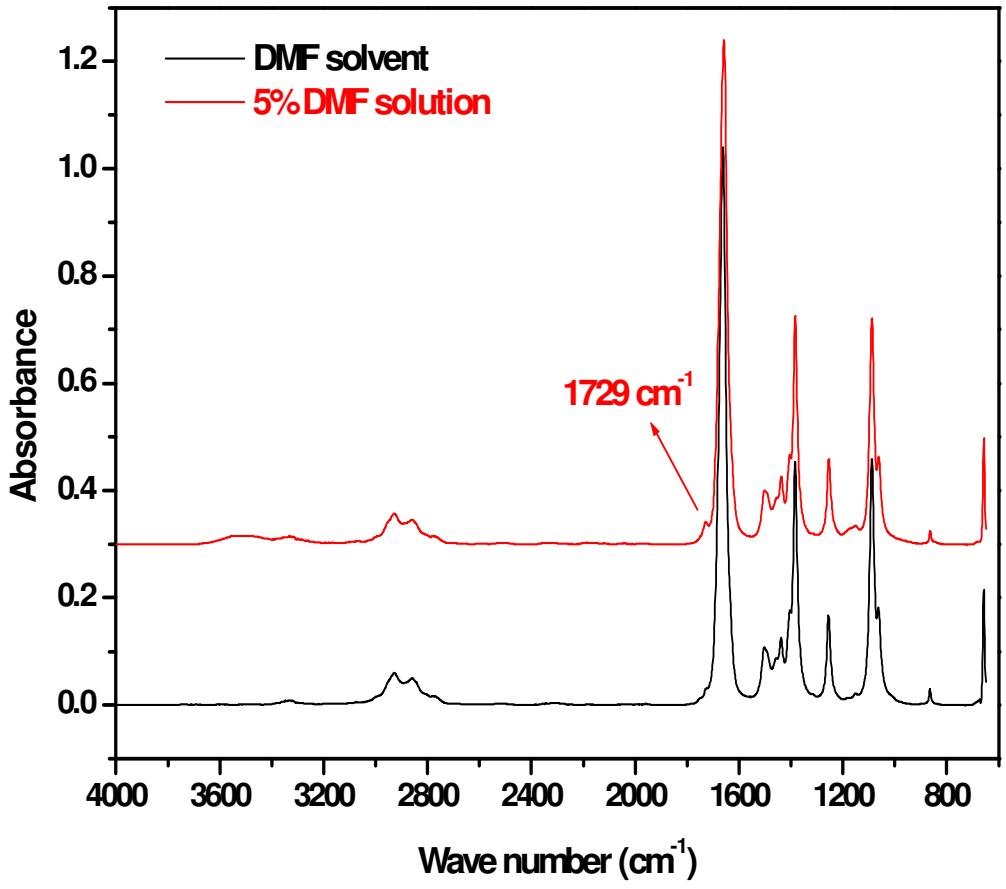

Figure 4.2 : FTIR-ATR spectra of prepared 5 wt % DMF solution for electrospinning solution (red line), and DMF solvent (black line) [4000-600 cm^{-1}].

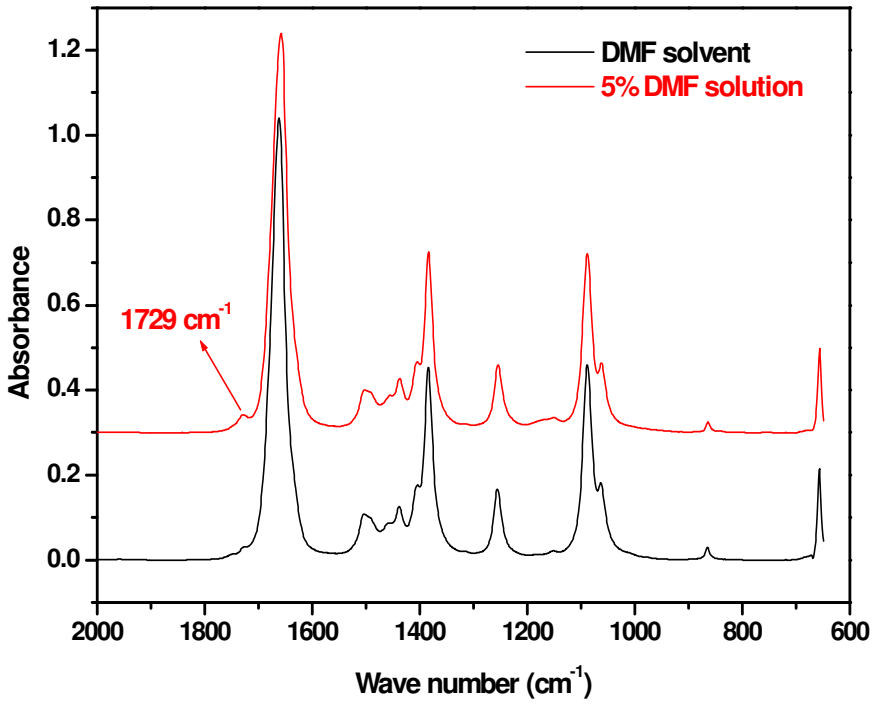

Figure 4.3 : FTIR-ATR spectra of prepared 5 wt % DMF solution for electrospinning solution (red line), and DMF solvent (black line) [2000-600 cm^{-1}].

Figure 4.4 and Figure 4.5 shows the FTIR-ATR spectrums of prepared 5 wt % DMF solution for electrospinning solution, and obtained nanofibers from this solution. The peaks at 2953 cm^{-1}, 1728 cm^{-1}, 1437 cm^{-1}, 1146 cm^{-1} and 962 cm^{-1} are assigned to CH stretching, C=O stretching, CH_3 stretching, O-CH_3 stretching vibrations and the characteristic peak of BA, respectively in P(BA-co-MMA). However, new peaks are observed FTIR-ATR spectrum of 5 wt.% DMF solution at 1661 cm^{-1}, 1504 cm^{-1} and 657 cm^{-1} are belong to C=O stretching, C-N stretching and O=C-N stretching, respectively. These peaks are characteristic peaks for the DMF solvent [140]. FTIR-ATR spectrum of DMF solution approximately are the same that of DMF solvent due to the copolymer concentration lower than the solvent concentration. Therefore, peaks of copolymer are not good observed in DMF solution. However, DMF characteristic peaks disappear after the electrospinning process due to the solvent

evaporates during the electrospinning for the FTIR spectra of obtained nanofibers from this solution

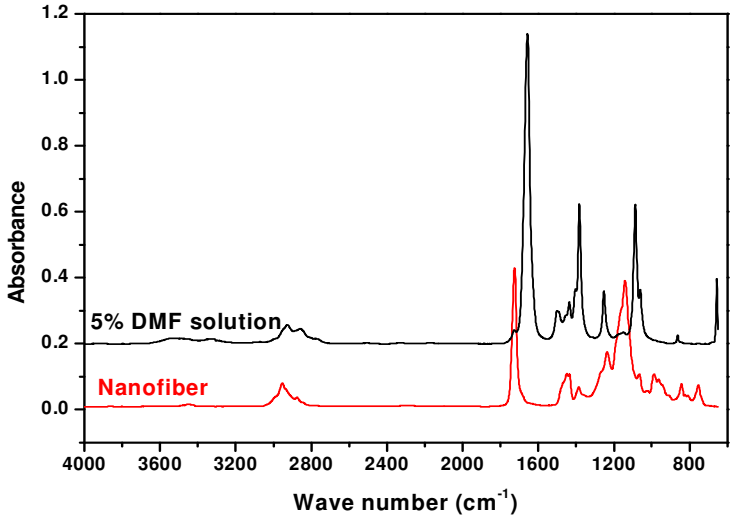

Figure 4.4 : FTIR-ATR spectra of prepared 5 wt.% DMF solution for Electrospun solution, and obtained nanofibers from this solution [2000-600 cm^{-1}].

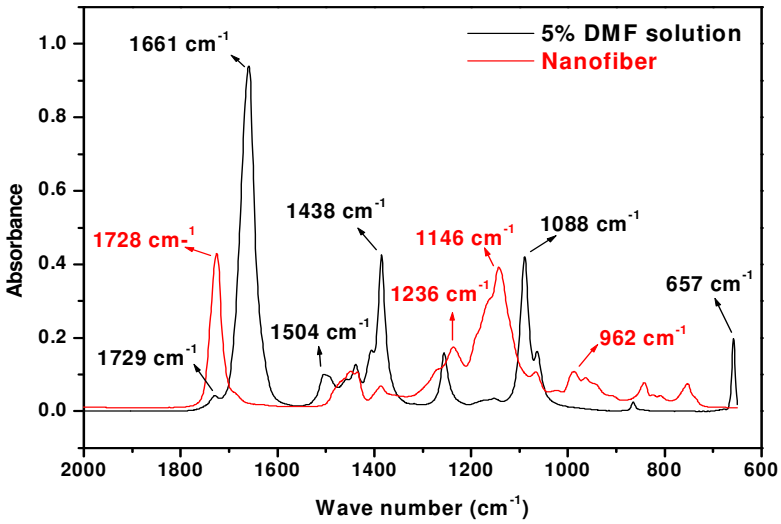

Figure 4.5 : FTIR-ATR spectra of prepared 5 wt.% DMF solution for electrospun solution, and obtained nanofibers from this solution [2000-600 cm^{-1}].

Figure 4.6 shows the FTIR-ATR spectrums of pure P(BA-co-MMA) and nanofibers of this copolymer in different solutions. At the same time this graph indicates that the solvents are completely evaporated during the electrospinning process because all peaks were almost identical although different solvents were used for the preparation electrospinning solution.

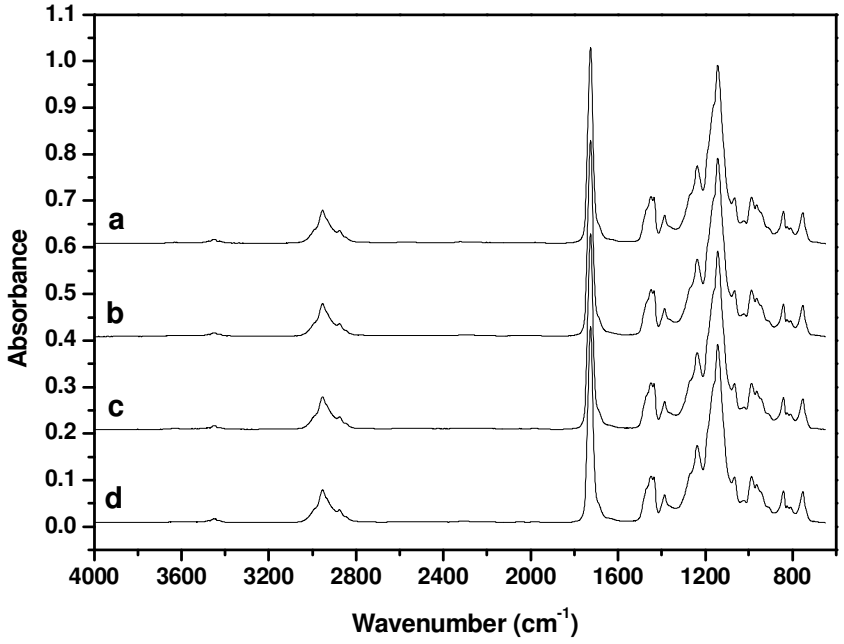

Figure 4.6 : FTIR-ATR spectra of (a) pure P(BA-co-MMA) and Obtained nanofiber from (b) 5 wt. DMF solution, (c) 5 wt. THF solution, (d) 5 wt. Acetone solution.

4.1.2 Nuclear magnetic resonance (NMR) spectroscopy of P(BA-co-MMA)

Figure 4.7 shows the ^{1}H-NMR spectra of copolymers recorded in $CDCl_3$ using TMS as the internal standard. The peak at δ=3.99 ppm is due to the $–OCH_2$ groups of BA and the peak at δ=3.64 ppm is due to $–OCH_3$ group of MMA. Observing other peaks δ=2.03 ppm due to α-CH, at δ=1.38 ppm $-^{2}CH_2-$, at δ= 1.57 ppm $-^{3}CH_2-$ and δ=0.91 ppm due to the $-^{4}CH_3-$ of n-butyl acrylate and δ=1.08 ppm and δ=1.22 ppm to α-CH_3 of methyl methacrylate, respectively and δ=7.24 ppm is due to $CDCl_3$. Moreover, a peak is observed at δ=3.46 is due to ethanol in remaining copolymer structure.

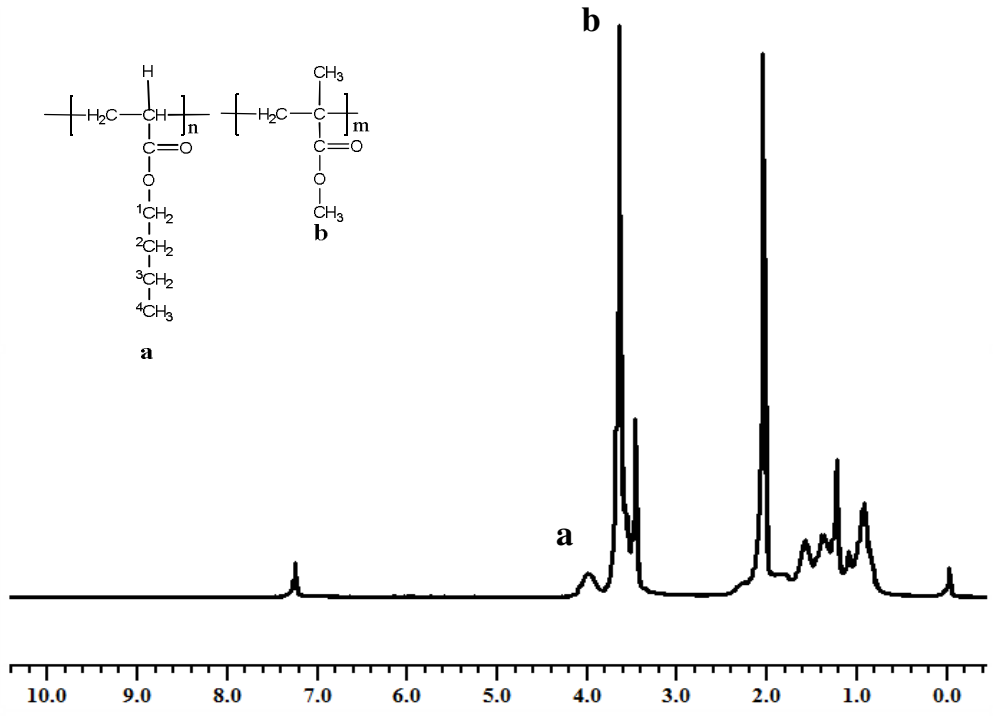

Figure 4.7: NMR spectrum of P(BA-co-MMA).

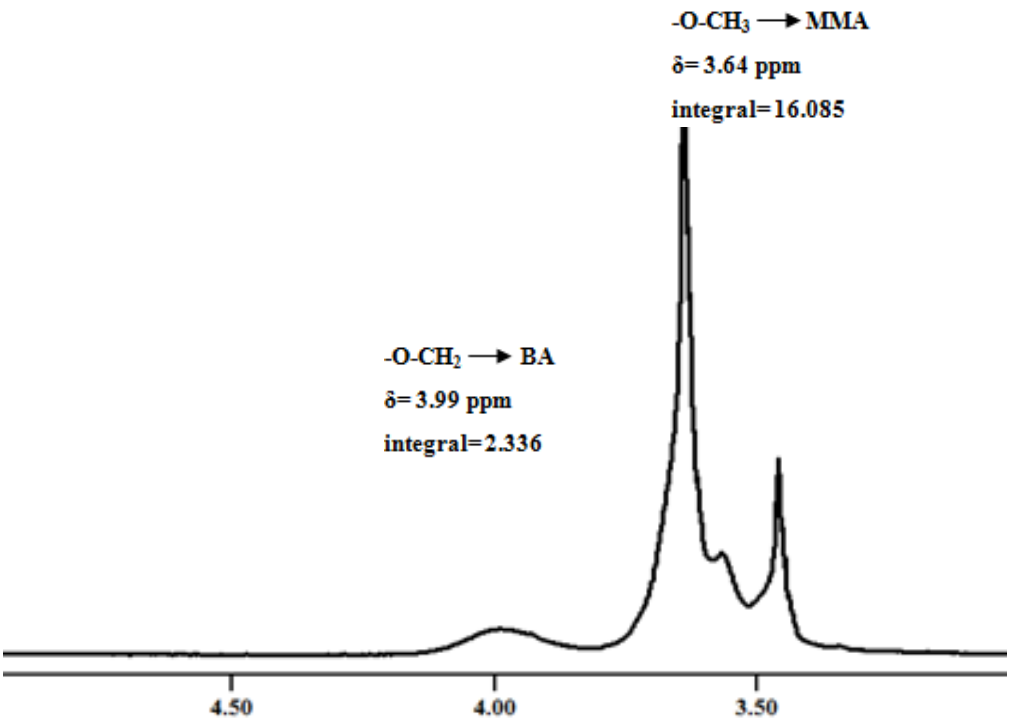

Figure 4.8: NMR Spectrum of P(BA-co-MMA) (0.0-5 ppm)

The quantatity of MMA and BA in the copolymers was calculated from the integral ratio of methyl protons (-$COOCH_3$) and methylene protons (-$COOCH_2$) originated from MMA and BA respectively and these peak domains included methyl and methylene protons obtained from ^{1}H-NMR spectrum in agreement with the literature [141, 142]. The mole fraction of MMA in the copolymer (F_{MMA}) can be determined using the following relationship [143];

$$F_{MMA} = \frac{2A(-OCH_3)}{2A(-CH_3)+3A(-OCH_2)} \quad \textbf{(4.1)}$$

Where A(-OCH_3) and A(-OCH_2) stand for the total peak areas of -OCH_3 and -OCH_2, respectively. A(-OCH_3) was shown in Figure 4.8 and F_{MMA} calculated as 0.821; A(-OCH_2) was shown in Figure 4.8 and F_{BA} calculated as 0.178. According to the literature MMA has a higher reactivity ratio (Table 4.1), so its tends to react with itself more than BA during polymerization.

Table 4.1: Reactivity ratios for the P(BA-co-MMA).

r_{MMA}	r_{BA}	initiator	medium	polymerization	Ref.
0.920	0.130	SDS	Water	Emulsion	144
1.871	0.291	AIBN	Toluene	Free radical	145
2.279	0.395	AIBN	Toluene	Free radical	146
2.24	0.414	AIBN	n-Butyl acetate	Free radical	147
2.55	0.36	AIBN	toluene	Bulk	148

This difference in reactivity ratios will lead to longer sequences of MMA, making the glass transition temperature of the copolymer higher than expected for this copolymer.

4.1.3 Differential scanning calorimetry measurement (DSC) of P(BA-co-MMA)

T_g values of the PMMA and P(BA-co-MMA) were determined as 117.92 °C and 48.48 °C (Figure 4.9), respectively and it is realized that the presence of the BA content in the copolymers caused a decrease in the T_g values due to the increase in the number of -CH_2- group in the copolymer.

T_g value of PMMA homopolymer was reported as 105 ^oC [149] and *T*g value of poly(BA-co-MMA) copolymer was reproted as 41.8°C [150] and 53 °C [151].

According to the literature, incraese in the polymer of BA contents of the copolymer resulted in decrease in the Tg values of the copolymers. Decreasing trend of *T*g value

with BA content is due to increase in main chain flexibility. These results are in agreement with the literature [152].

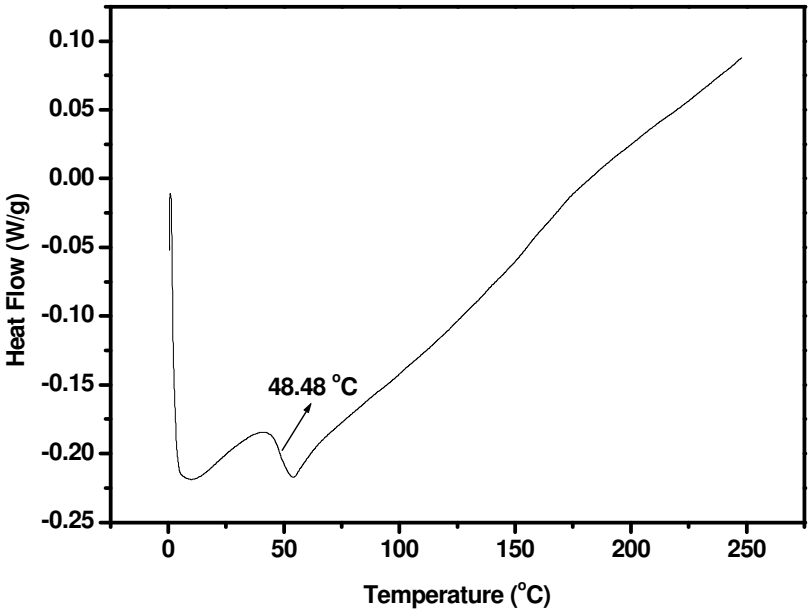

Figure 4.9 : DSC graph of P(BA-co-MMA).

4.1.4 Molecular weight determination

M_n and M_w results obtained from GPC are given in Table 4.2. Polydispersity index (PDI) of copolymers which were calculated from (M_w/M_n) and the copolymer intrinsic viscosities (η) in chloroform solutions were determined by using an Ubbelohde-type viscometer were also given in Table 4.2

Table 4.2 : M_n, M_w, PDI and η results.

Copolymer	η^a (dL/g)	$M_w{}^b$ (kg/mol)	$M_n{}^b$ (kg/mol)	PDI
P(BA-co-MMA)	178	663	518	1.29

4.2 Morhology of Fibers

4.2.1 Effect of concentration of solution on nanofibers

Five different samples have been prepared, changing the concentration of P(BA-co-MMA) in DMF: 1 wt.%, 3 wt.% 5 wt.%, 8 wt.% and 10 wt.% of P(BA-co-MMA) in DMF. In this section, concentration effects on the diameters of nanofibers were

examined. Therefore electrospinning parameters have been hold same for all solutions (Table 4.3).

Table 4.3: Electrospinning conditions and diameters of nanofibers.

P(BA-co-MA)/DMF solutions (wt%)	Flow rate (ml/h)	Distance (cm)	Applying Voltage (kV)	Diameters of Nanofibers (nm)
1	1	15	15	Fibers not produced
3	1	15	15	390±30
5	1	15	15	600±50
8	1	15	15	1780±100
10	1	15	15	2240±40

Figure 4.10 shows the scanning electron microscopy (SEM) images of P(BA-co-MMA) nanofibers electrospun from 3%, 5%, 8% and 10% (w/v) P(BA-co-MMA) solution in DMF. The average diameter of electrospun fibers of different concentrations is determined by using Adobe Acrobat 8 Professional to randomly measure the diameters of 50 individual fibers shown in SEM images with x5000 magnitude. The diameters of the fibers increase slightly as the concentration of the P(BA-co-MMA) solution is increased (Table 4.3). An increased in the concentration results in greater polymer chain entanglements within the solution which is necessary to maintain the continuity of the jet during electrospinning. We find that the P(BA-co-MMA) solutions yielded Bead-free nanofibers due to the greater polymer chain entanglements and viscosity of the solutions, but fibers did not observed for 1% (w/v) P(BA-co-MMA) solution due to the smaller polymer chain entanglements and surface tension effects could be dominant with decreased polymer concentration/solution viscosity. So, the concentration of P(BA-co-MMA) solution is increased to 3% (w/v) uniform bead-free P(BA-co-MMA) nanofibers were obtained with a diameter of 390±30 nm. This shows that a high concentration/viscosity is required to produce uniform bead-free P(BA-co-MMA) nanofibers.

Many experiments have shown that a minimum viscosity for each polymer solution is required to yield fibers without beads [93,78], but the 5 wt.% P(BA-co-MMA) solution was determined the best electrospinning solutions because of the continuous electrospinning process for this study.

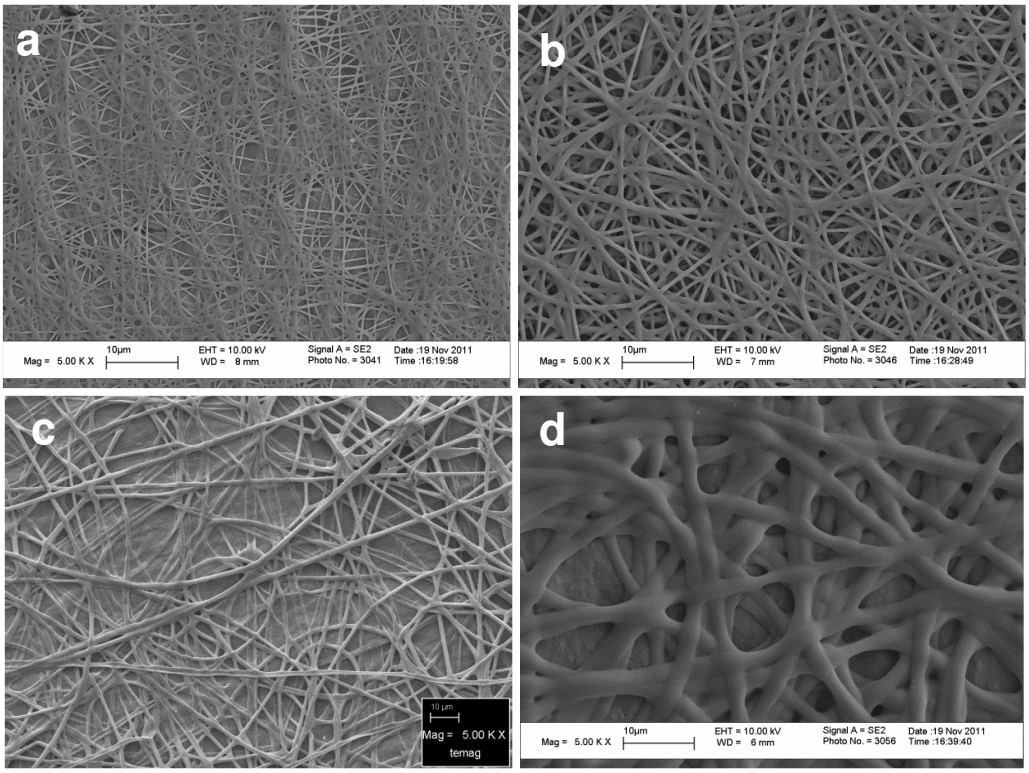

Figure 4.10 : SEM images of the samples at different P(BA-co-MMA)/DMF concentrations: 3 wt.% (a), 5 wt.% (b), 8 wt.% (c) and 10 wt.% (d).

4.2.2 Effects of dielectric constant of solvent mixture on nanofiber

In order to determine an optimum solvent system for electrospinning P(BA-co-MMA), different single and solvent mixture systems were studied. Three solvents with different electrical conductivities were used to prepare P(BA-co-MMA) solution at a fixed polymer concentration of 5 wt%. Dielectric constant values of Solvent mixture were calculated by the following equation;

$$\varepsilon_m = \varepsilon_1 x_1 + \varepsilon_2 x_2 \qquad \textbf{(4.2)}$$

where ε_1 is the dielectric constant of the solvent and x_1 is the corresponding volume fraction [153].

Dielectric constants of different solvents and diameter of resulting nanofibers prepared in these solvents shown in Table 4.4.

Table 4.4 : Dielectric constants of different solvents and diameter of resulting nanofibers prepared in these solvents.

Polymer Concentration (wt%)	Solvents	Dielectric Constant	Diameter of Nanofibers (nm)
5	DMF	36.71	600±20
5	Acetone	20.7	870±40
5	THF	7.47	1600±80

(*Electrospinning conditions are the same for all samples. Flow rate: 1ml/h, Distance:15cm, Applying Voltage: 15kV)

Figure 4.11 shows the scanning electron microscopy (SEM) images of P(BA-co-MMA) nanofibers electrospun from 5% (w/v) P(BA-co-MMA) solution in different solvents (DMF, Acetone and THF).

Bead-free nanofibers can be obtained for the polymer solutions having high dielectric constant. Figure 4.11(a) shows the nanofibers of 5% DMF solution. It has the lowest diameters of nanofibers among the others due to its highest dielectric constant. Figure 4.11(c) shows the beaded nanofibers of THF solution which has the highest diameters of nanofibers due to its lowest dielectric constant. Comparison of Figure 4.11(a) and Figure 4.11(b), In Figure 4.11(a) shows that production of nanofiber and electrospinnability are easier because of solution dielectric constant. In general, SEM images indicate that the bead-free nanofibers are obtained except for obtaining nanofibers from THF solution shown in Figure 4.11(c) in this study.

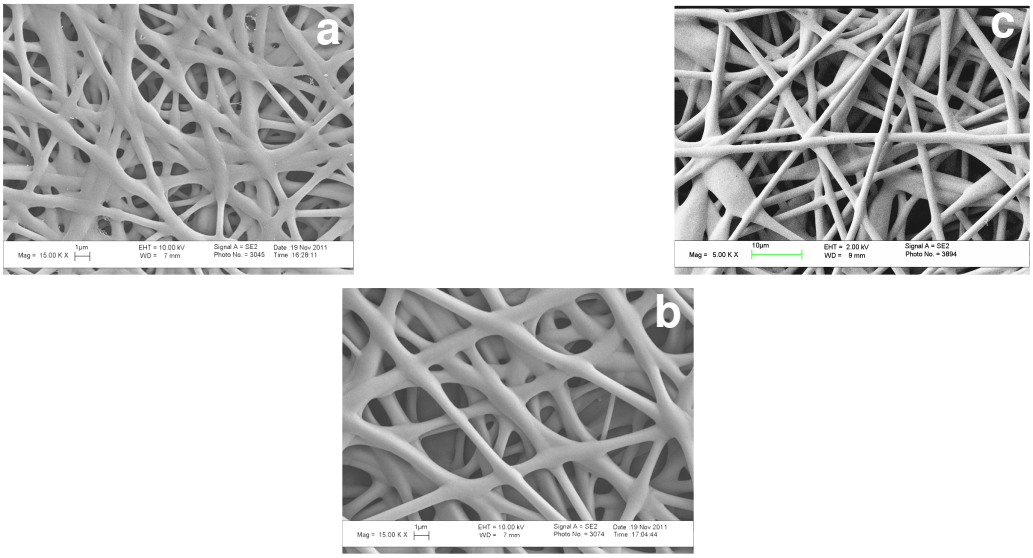

Figure 4.11: SEM images of- nanofibers from (a) 5%DMF solution (b) 5%Acetone solution and (c) 5% THF solution.

To show the dielectic effect of solvents on fiber formation , solution mixtures consist of DMF with the same ratio of THF and Acetone were also studied (Table 4.5). Generally, dielectric of a solution reflects a charge density on a jet thus elongation level of a jet by an electrical force. Therefore, under the same flow rate (1 ml/h), applied voltage (15kV) and spinning distance (15 cm), a solution with a higher electrical conductivity may cause higher elongation of a jet along its axis and thus electrospinning fibers with smaller diameter.

Table 4.5 : The dielectic effect of further solvent mixtures on fiber formation , solution mixtures consisting of DMF with the same ratio of THF and Acetone.

Polymer ConcTentration (wt%)	Solvents	Mixture ratio of solvents (wt%)	Dielectric Constant	Diameter of Nanofibers (nm)
5	DMF/Acetone	50/50	28.705	720±25
5	DMF/THF	50/50	22.09	790±30
5	THF/Acetone	50/50	14.085	1200±40

Figure 4.12 shows the (SEM) images of P(BA-co-MMA) nanofibers electrospun from 5% (w/v) P(BA-co-MMA) solution in different solvents mixtures. Increasing the dielectric constant results a decrease in the fiber diameter and improve the fiber morphology. THF/Acetone mixture has the lowest dielectric constant, so it exhibited the highest fiber diameters (Figure 4.12 (C)).

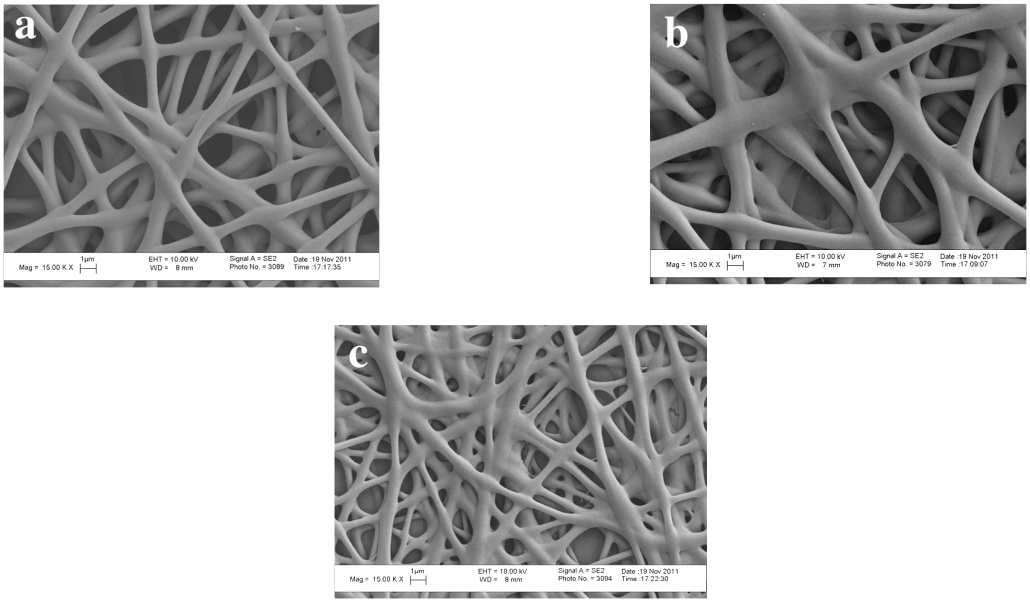

Figure 4.12: SEM images of nanofibers from (a) DMF/Acetone , (b) DMF/THF , (c) THF/Acetone solution mixtures.

DMF/THF at various volume ratios such as 25/75, 50/50 and 75/25 and neat THF significantly changed the fiber morphology provided other experimental parameters remained constant.

Table 4.6 indicates the effect of solvent mixture ratio on dielectric constant and fiber diameter by using DMF/THF solution mixture. Increase in the DMF content causes an increase in dielectric constant which results a decrease in the fiber diameter and improve the fiber morphology. These results are in agreement with in literature [111].

Table 4.6: Effect of solvent Mixture ratio and dielectric constants of DMF/THF solutions on nanofiber diameters.

Polymer Concentration (wt%)	Solvents	Mixture ratio of solvents (wt%)	Dielectric Constant	Diameter of Nanofibers (nm)
5	DMF/THF	25/75	14.78	995±50
5	DMF/THF	50/50	22.09	800±30
5	DMF/THF	75/25	29.40	680±40

Effect of solvent Mixture ratio DMF/THF solutions on nanofiber diameters are shown in Figure 4.13. Solvent evaporation is also important factor on the fiber morphology. P(BA-co-MMA) solution at higher ratios of the THF and DMF solvent mixtures, more solvent evaporation occured due to the higher vapor pressure of THF and was predicted to evaporate right from the tip of the capillary. On the other hand, since DMF has lower vapor pressure, it was expected to evaporate slowly especially likely after deposition of fibers on the target. Therefore, at lower DMF/THF (25/75) ratios, rate of the solvent evaporation from the fiber surface increased due to the large volume of THF in the polymer solution and caused the fiber diameters increase. The THF solvent affected the bead formation (Figure 4.11(c)). It was known that the formation of beads and beaded fibers was driven by the surface tension coefficient depended on the polymer and solvent . During the electrospinning of P(BA-co-MMA) with increased THF ratios in DMF/THF mixture, the solution was noticed to lose the capability to form more fibers than beaded due to higher THF evaporation rate. It was expected that surface tension of DMF/THF (25/75) gradually increased and thus the solution lost the capability to form more fibers against the relatively higher surface tension. As a result, increasing THF amount in the mixture caused by increasing fiber diameter and beads occur with fibers in only THF (Figure 4.11(c)).

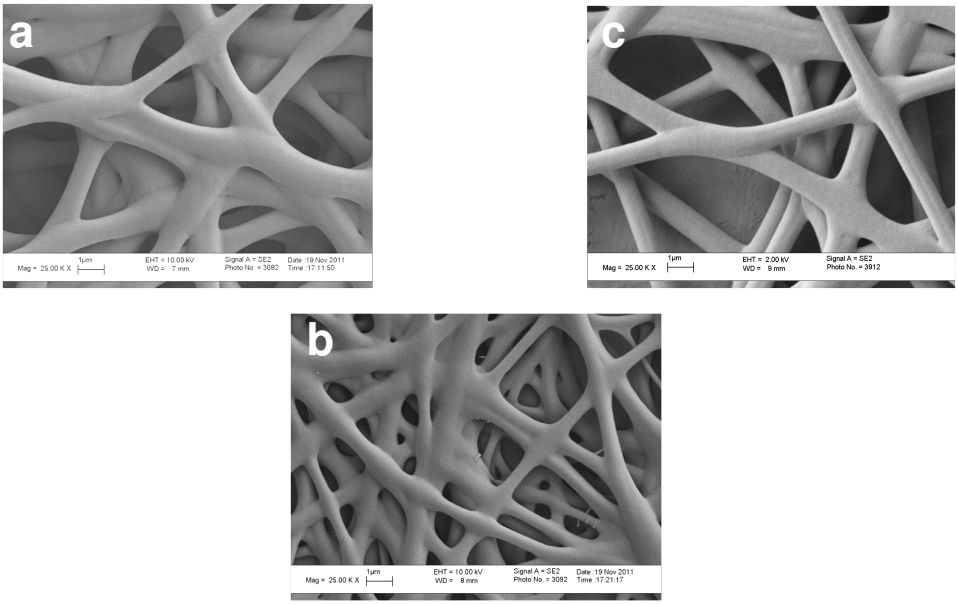

Figure 4.13 : SEM images of nanofibers from (a) DMF/THF (%25/75), (b) DMF/THF (%50/50) and (c) DMF/THF (%75/25) solution mixtures.

Significant changes in fiber diameter and morphology with various processing parameters including solvent evaporation and dielectric constant was realized. By using different solvents and solvent mixtures different fiber diameters have been observed. Figure 4.14 shows relationship between dielectric constant and diameter of nanofibers. As it can be seen, increasing dielectric constant caused a decrease in fiber diameter.

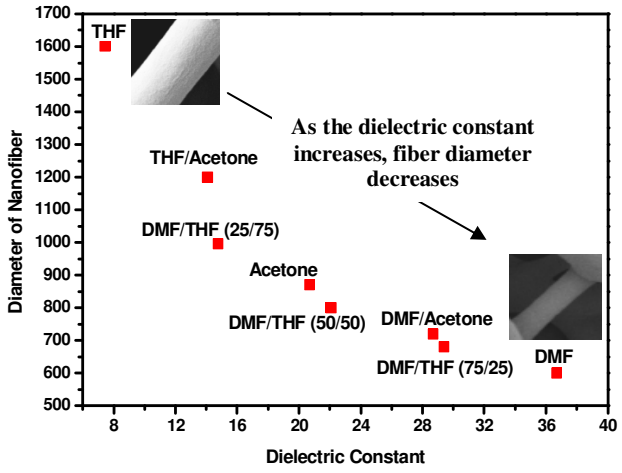

Figure 4.14: Relationship between Diameter of nanofibers and Dielectric constant.

4.2.3 Effect of flow rate on nanofiber

To study effects of Flow rate on morphology of electrospun fibers, DMF was used as a solvent for dissolving P(BA-co-MMA) given in Table 4.7.

Table 4.7: Electrospinning conditions of P(BA-co-MMA) in DMF with different flow rate.

P(BA-co-MMA)/DMF solutions (wt%)	Flow Rate (ml/h)	Distance (cm)	Applying Voltage (kV)	Diameters of Nanofibers
5	1	15	15	600±20
5	3	15	15	820±40
5	5	15	15	990±50
5	7	15	15	1180±80

In Fig. 4.15 the SEM images of the four samples are reported. All the images show the presence of nanofibers. When the flow rate is increased, a corresponding increase in the fiber diameter was observed as shown in Table 4.7. This is apparent that there is a greater volume of solution fiber is drawn away from the needle tip [99,102]. The diameter values range from 390 nm to 1180 nm for the P(BA-co-MMA) nanofibers. Figure 4.15 also shows that the morphology of the electrospun P(BA-co-MMA) fibers was not significantly changed except for diameters of nanofibers with varied volume flow rate.

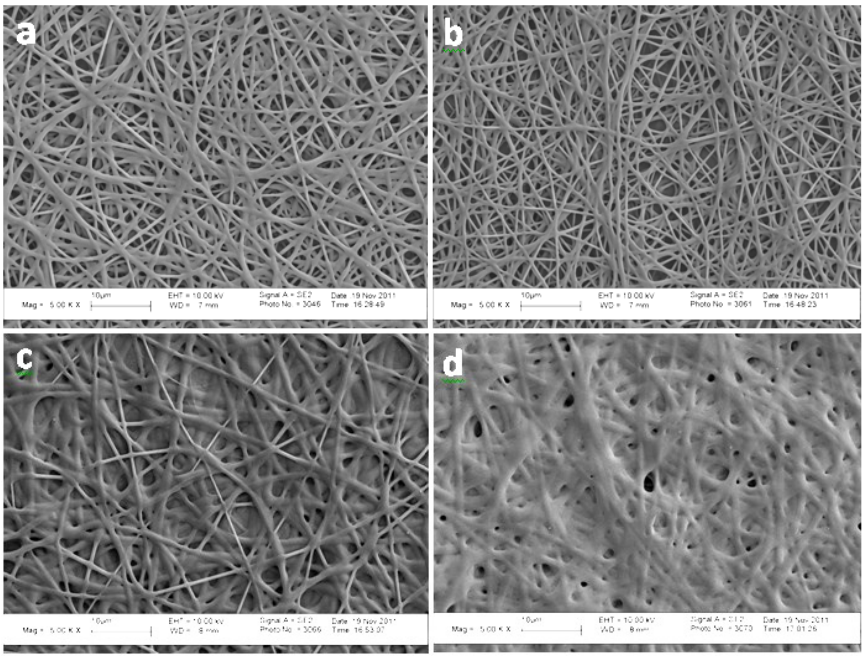

Figure 4.15 : SEM images of the samples at different Flow rates; (a) 1 ml/h, (b) 3 ml/h, (c) 5 ml/h, (d) 7 ml/h.

According to parameter studies presented, polymer concentration, and dielectric effects of solvents were found to play a significant role in controlling the morphology of the electrospun nanofibers while the voltage and the flow rate were less effective compared to those parameters. Therefore, it can be noted that the morphology of the electrospun nanofibers is primarily affected by polymer concentration, its molecular weight and dielectric of solvents (primary parameters), followed by the voltage and the feed rate (secondary parameters) [154].

4.3 Fluorine-Containing Acrylate, Butylacrylate and Methylmethacrylate Copolymer Characterization

4.3.1 FTIR-ATR spectrophotometric analysis

The FTIR-ATR spectra of nanofibers of BA,MMA and fluorine-containing acrylate copolymer are shown in Figure 4.16. FTIR-ATR spectra were recorded in the absorbance mode.

Figure 4.16 shows the peaks at 2950 cm^{-1}, 1728 cm^{-1}, 1435 $cm^{-1}$and 1149 cm^{-1} are assigned to CH stretching, C=O stretching, CH_3 stretching and O-CH_3 stretching vibrations, respectively, in PMMA. Absorption at 962 cm^{-1} was the characteristic peak of BA in P(BA-co-MMA), but 1726 cm^{-1} and 1145 cm^{-1} are assigned to CH stretching and CH_3 stretching respectively, in BT-9. The typical stretching vibration and wagging vibration of C-F bonds were at 1190 cm^{-1} and 690 cm^{-1} (Figure 4.16 and Figure 4.17) which did not appear for FTIR-ATR spectra of P(BA-co-MMA). Therefore, the FTIR-ATR spectra revealed that Zonyl-TM had effectively participated in polymerization. These results are in agreement with literature [45-48].

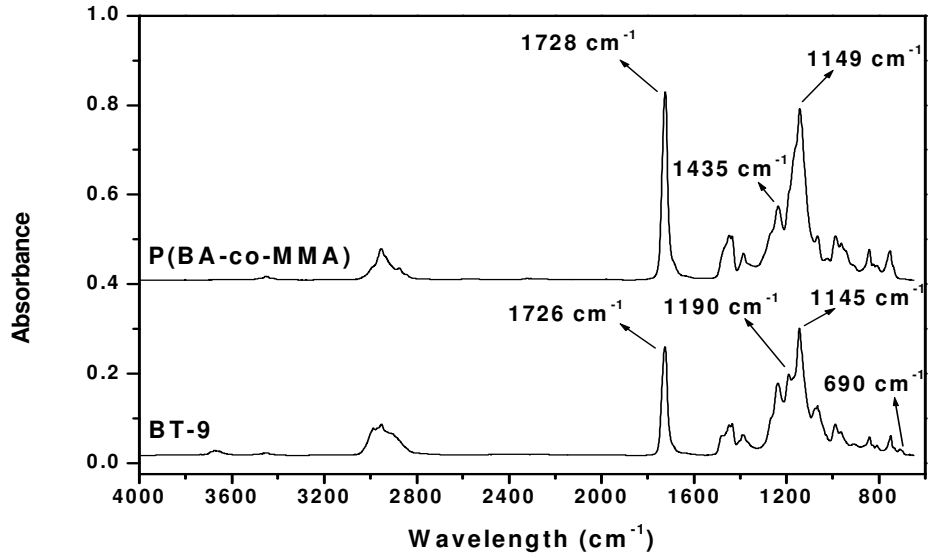

Figure 4.16 : FTIR-ATR spectrums of BA,MMA and fluorine-containg acrylate Copolymer [4000-600 cm^{-1}].

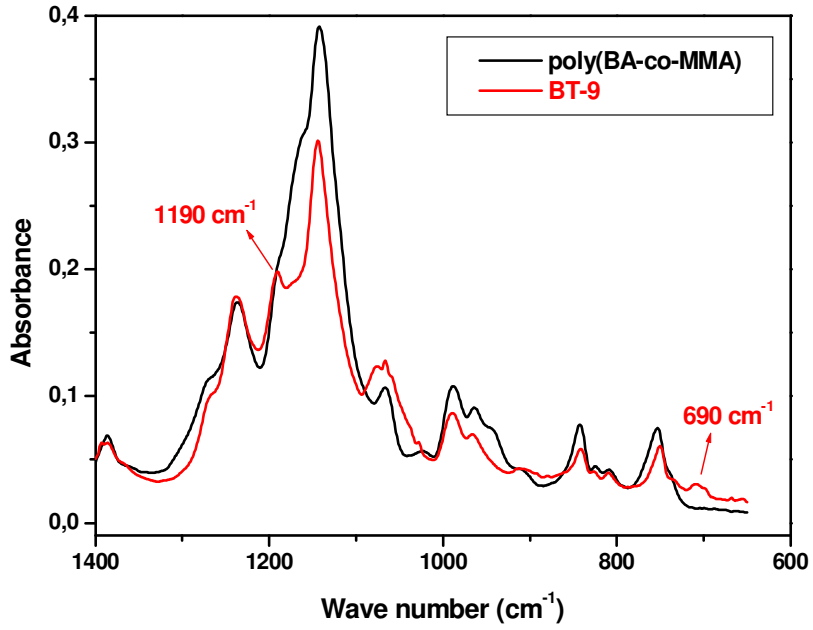

Figure 4.17 : FTIR-ATR spectrums of BA,MMAand fluorine-containing acrylate copolymer [1400-600 cm^{-1}].

Figure 4.18 shows the FTIR spectrum of the BT-1, BT-4 and BT-9 copolymers. This spectra indicates that by increasing the concentration of copoymers increases the absorbance. In these spectra, the characteristic stretching peaks of C–H and C=O group are obviously appeared at 2951 and 1726 cm^{-1}, respectively, resulting from the presence of BA, MMA and PFMA units all containing the CH_2 and C=O groups. In the fingerprint region, there is one medium band at 690 cm^{-1}, which is belong to C-F wagging vibration [44].

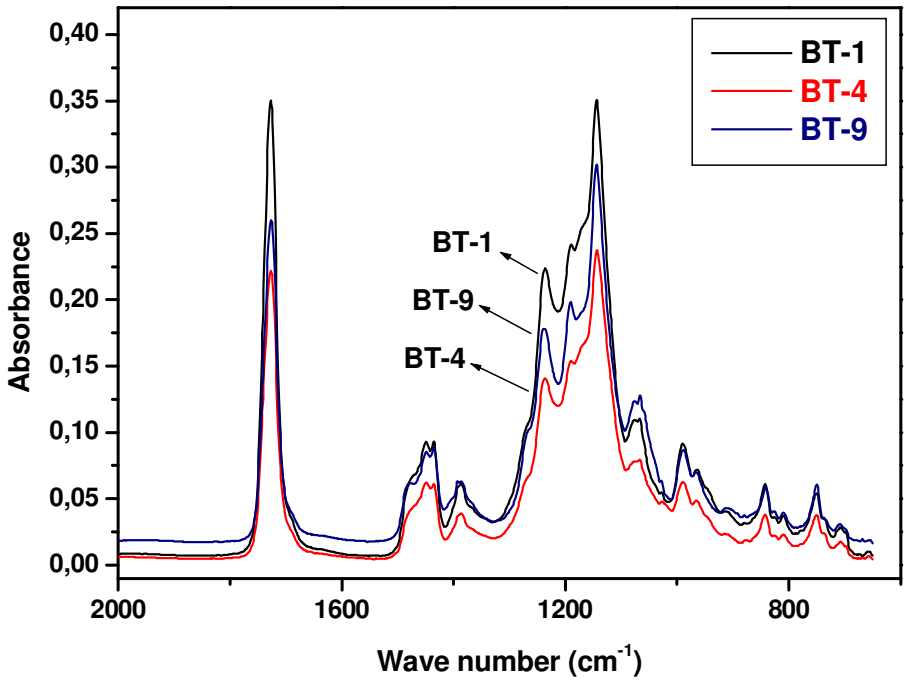

Figure 4.18 : FTIR-ATR spectrums of BT-1, BT-4 and BT-9 nanofibers.

The calibration curve is obtained from the data shown in Figure 4. In this graph absorbance ratio of C-F str (1190 cm^{-1})/ C-F str(1190 cm^{-1}) + C=O (1728 cm^{-1}) against the MMA content (wt%) was plotted determined by FTIR-ATR . Figure 4 helps to find the MMA content (wt%) of a PFMA-ran-MMA-ran-BA copolymer by using the main characteristic peaks of poly(PFMA-ran-MMA-ran-BA) using FTIR-ATR spectrophometer.-The reason for the deviation from linearity comes from the interference of peaks at the same wave numbers.

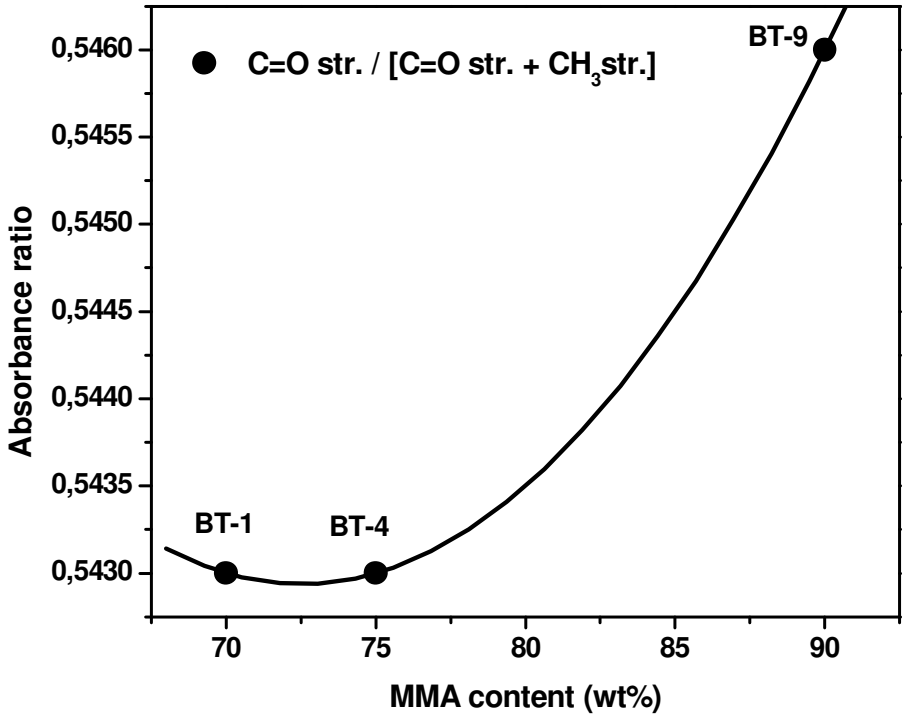

Figure 4.19 : Relationship between Absorbance ratio and MMA content (C=O str. 1726 cm^{-1}; CH_3 str. 1445 cm^{-1} is taken).

4.3.2 Nuclear magnetic resonance measurements (NMR) of perfluoromethacrylate copolymers

The indicative ^1H NMR spectra of BT-4 copolymer is given in Figure 1. The peak at 4.25 ppm (a) was attributed to the methylene attached to the carboxyl group bonded to the perfluorooctyl group in Zonyl-TM. The intensity of the peak at 3.6 ppm (b) resulting from the methyl group in MMA and the peak at 4.0 ppm (c) was attributed to the methylene attached to the carboxyl group in BA. The quantity of MMA, BA and Zonyl-TM in the copolymers was calculated from the integral ratio of methyl protons ($-COOCH_3$) and methylene protons ($-H_2R_f$) originating from PMMA, PBA and PFMA respectively, and these peak domains included methyl and methylene protons obtained from H-NMR spectrum in agreement with the literature [45].

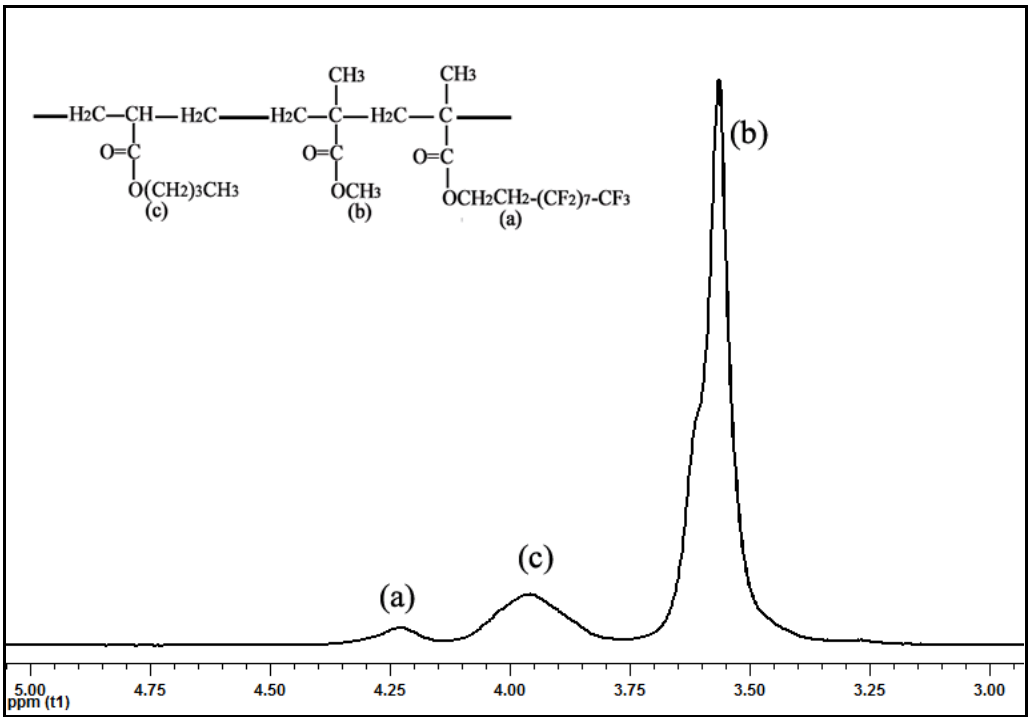

Figure 4.20 : Indicative ^{1}H-NMR spectrum of BT-4 copolymers.

4.3.3 Molecular weight determination of perfluoromethacrylate copolymers

M_n and M_w results obtained from GPC are given in Table 4.8. Polydispersity index (PDI) of copolymers which were calculated from (M_w/M_n) and the copolymer intrinsic viscosities in chloroform solutions were determined by using an Ubbelohde-type viscometer were given in Table 4.8. The higher molecular weight polymer exhibits higher viscosity, for this reason to obtain the same viscosity higher concentration of lower molecular weight polymer was used for the electrospinning [155]. Thus, the concentration of copolymers were chosen in a way that it balances its viscosity properties i.e., The concentration of BT-1 is taken maximum, and the amount of P(BA-co-MMA) is taken as minumum.

Table 4.8: Intrinsic viscometric measurement results and , M_v, M_n, and M_w values of the copolymers from GPC.

Copolymer	η^a (dL/g)	M_w^b (kg/mol)	M_n^b (kg/mol)	PDI	Concentration (mmole/L)
PMMA	-	75	-	-	2
P(BA-co-MMA)	178	663	513	1.29	0.13
BT1	9.9	20.4	12.1	1.69	300
BT4	35.0	80.4	26.4	3.05	7.5
BT9	14.9	32.0	11.8	2.71	15.0

[a] Determined from Ubbelohde-type viscometer
[b] Determined from GPC

4.3.4 Differential scanning calorimetry measurement (DSC) of perfluoromethacrylate copolymers

Park et al. reported that the homopolymers and the random copolymers of perfluoromethacrylate. MMA resulted a single peak in their DSC thermograms like our random copolymers, but the graft copolymer and mixture of the homopolymers exhibit two peaks [151]. Thus, our indicative DSC thermogram result of BT-9 samples showed that our copolymers were random (Figure 4.21). In Figure 4.22, T_g values of the PMMA, BT-1, BT-4 and BT-9 were determined as 117.92 °C, 53.53 °C, 57.38 °C and 67.83 °C, respectively and it is realized that the increase of the BA content in the copolymers caused a decrease in the T_g values due to the increase in the number of -CH_2- group in the copolymer.

T_g value of PMMA homopolymer was reported as 105 °C [149] however T_g value of the poly(Zonyl-TM) homopolymer which was synthesized in the heterogeneous CO_2 medium determined as 40 °C [27].and T_g value of poly(BA-co-MMA) copolymer was reported as 41.8 [150] and 53 °C [151] and for DFHMA-MMA-BA copolymer as 76 °C [155].

Previous study [27] indicated that the increase in the Zonyl TM content of the copolymer caused a decrease in the T_g value of copolymers. In this study, increase in the both of the long chain monomer of Zonyl TM and BA contents of the copolymer resulted in decrease in the T_g values of the copolymers. These results are in agreement with the literature [27,155]. Decreasing trend of T_g value with BA and Zonyl-TM content is due to increase in main chain flexibility.

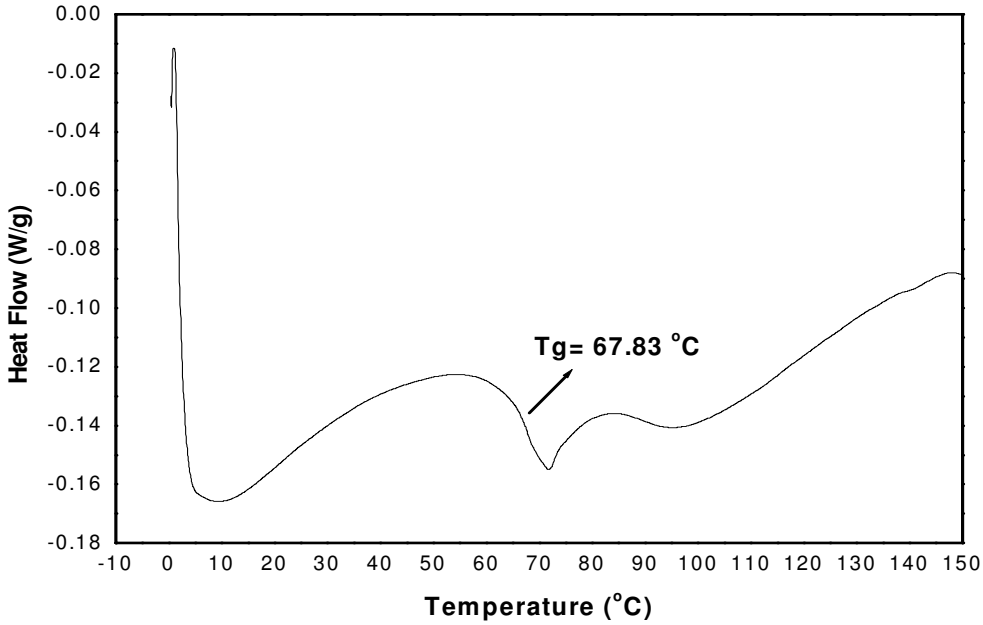

Figure 4.21 : Representative DSC thermogram of BT-9 samples.

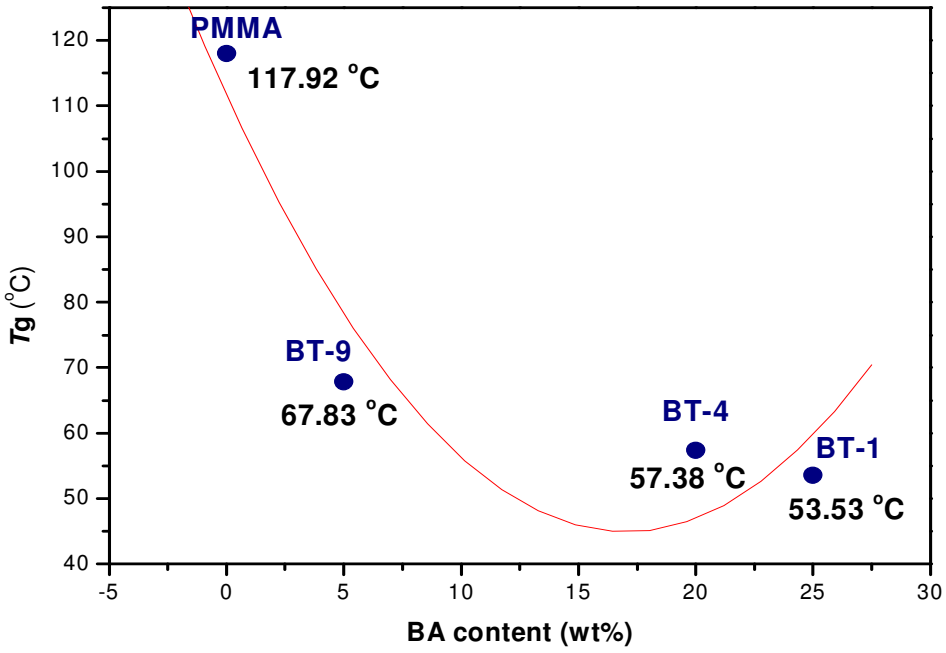

Figure 4.22 : Graph of Tg values versus BA content

4.3.5 Morphology of perfluoromethacrylate copolymer fibers

Table 4.9 shows the concentration, Diameter of nanofibers and electrospinning conditions. Feed flow rate values were adjusted according to following relationship between molar concentration and concentration by weight and inclusion of flow rate;

C_c[Concentration (mole/l)] .M[Molecular weight (g/mole)] = C_mConcentration as weight(g/l)

C_c [Concentration (mole/l)]. M [Molecular weight (g/mole)] .[flow rate (ml/h)]. (1 l/1000 ml) = FR [Feed flow rate (g/h)]

Feed flow rate (FR) (as weight) as weight for all samples were calculated accordingly. From Table 4.9 it can be concluded that as the concentration increase there is a n increase in the diameter of fibers.

Table 4.1 : Diameters of nanofibers and Electrospinning conditions.

Copolymer Code	Concentration (g/L)	Diameter of Nanofibers (nm)	Feed Flow rate (g/h)	Flow rate (ml/h)	Applying voltage (kV)
PMMA	150	240	0.150	1	15
Poly(BA-co-MMA)	80.0	1780	0.0810	1	10
BT-1	612.000	320.2	0.306	0.5	15
BT-4	603.000	839.5	0.603	1	20
BT-9	480.000	1071	0.960	2	15

*Distances were 15 cm for all samples except for BT-4 sample which was 10 cm

SEM images of all nanofibers were shown in Figure 4.23. The images indicate that the Mw and Zonyl-TM content of copolymer influences the formation of nanofibers. Increase in the Mw of copolymers, eases to electrospin process and the fiber number grows due to the viscosity. As the viscosity of the solution is too low, electrospinning may result polymer particles (beads) which are formed instead of fibers like BT-1. At lower viscosity the polymer chain entanglements are lower; the beaded fibers can be obtained instead of smooth fibers like BT-4 and BT-9 [53]. Concentration of BT-1 is the highest, but Mw of BT-1 is the lowest, hence, BT-1 solution could not be viscous enough, so beads are observed.

Code	SEM-3000x	SEM-10000x	SEM-20000x
Poly(BA-co-MMA)	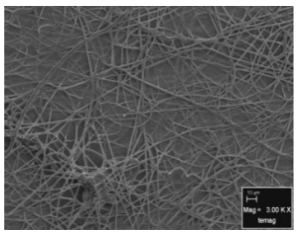	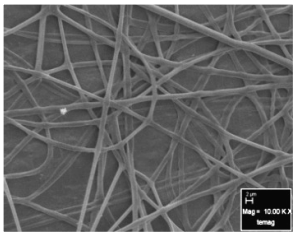	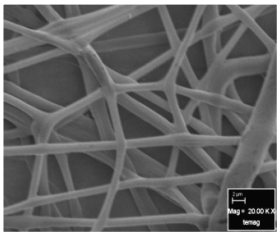
BT-1	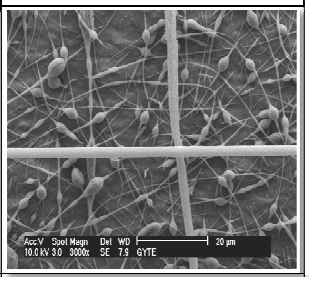	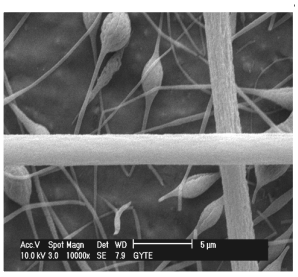	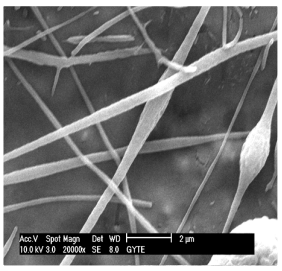
BT-4	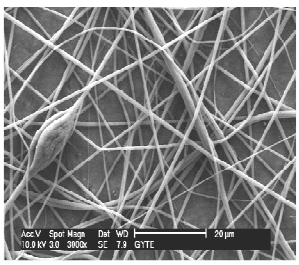	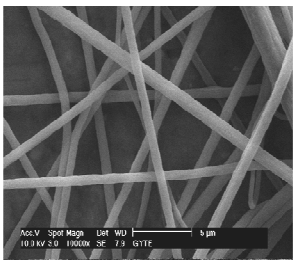	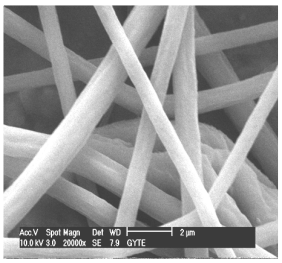
BT-9	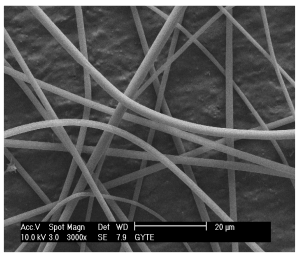	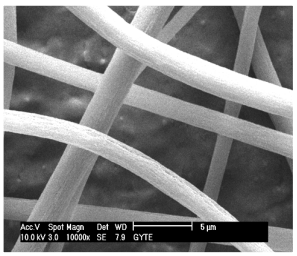	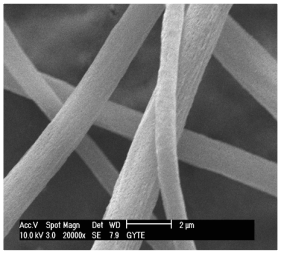

Figure 4.23 : SEM images of Poly(BA-co-MMA), BT-1, BT-4 and BT-9 nanofibers with diffrent magnification.

Figure 4.24 shows the effects of Fluorine content on the fiber diameter. Increasing in the Zonyl-TM content of the copolymer resulted in decrease in the fiber diameter due to the lowering solubility of the copolymer in organic solvent [42]. Therefore, reduces of viscosity of solution makes electrospinning process difficult. These results lead to observe hierarchical structure which has nanofibers and micro beads in the structure together. BT-1 has the highest Fluorine content and the lowest fiber diameter because of hierarchical structure. As it can be seen from Figure 4.24 an increasing Fluorine content caused by a decrease in diameter of nanofibers due to the viscosity.

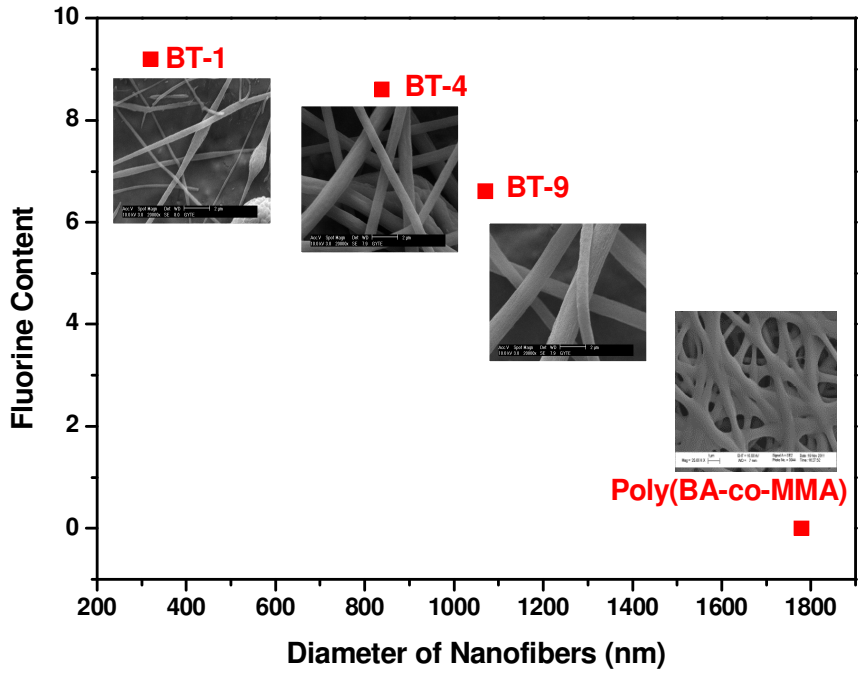

Figure 4.24 : Diameter of Nanofiber versus Fluorine Content Mole Fraction (mole %).

When the diameter of BT-1 and BT-9 nanofibers are compared, BT-9 has shown a higher fiber diameter due to the high feed flow rate although the other electrospinning process conditions are the same (Table 4.9). According to our investigation for the understanding of the presence of beads, we can conclude that the increasing flow rate causes greater volume of solution drawn from the needle tip and then the jet takes a longer time to dry. As a result, the solvents may not have enough time to evaporate and beads can be formed [138].

4.4 Contact angle measurement of perfluoromethacrylate copolymer fibers

Advancing (θ_a), receding (θ_r) and equilibrium (θ_e) contact angle results for water droplets and θ_e contact angle results for glycerol and ethylene glycol liquids on electrospun fiber surfaces are given in Table 4.10. These results indicated that, the electrospun copolymeric nanofibers were superhydrophobic with a water contact angle changed from153^o to 172^o depending on not only fiber size but also presence of bead. The nanofibers were also superoleophobic, when higher surface tension oils

were used (~45 mN/m) such as a glycerol and ethylene glycol contact angle of 167±1 and 163±1 were obtained, respectively. But when lower surface tension oils were used such as hexadecane (27.5 mN/m), only BT-1 sample can be measured with the contact angle of hexadecane drop as 70°, other samples were not measured due to the spriding fastly on the surfaces.

Table 4.2 : Equilibrium, Advancing, Receding Contact Angle and Contact Angle Hysteresis (CAH) Results of Water Drops and Equilibrium Contact Angle Results of Organic liquids on Nanofiber Polymeric Substrates by Electrospining.

Copolymer	Water (°)				Glycerol (°)	Ethylene Glycol (°)
	θ_e	θ_{adv}	θ_{rec}	CAH		
P(BA-MMA)	130	135	110	25	120	N/A
BT1	172	172	168	4	167	163
BT4	153	155	145	10	147	142
BT9	169	169	166	3	150	145

Figure 4.25 indicated that diameters of nanofiber have an effect on the contact angle (increase from 130° to 172°) and nanofiber diameter (from 320 nm to 1780 nm) and minumum contact angle and maximum nanofiber diameter can be obtained. Poly(BA-co-MMA) have exhibited the highest diameter but lowest contact angle.

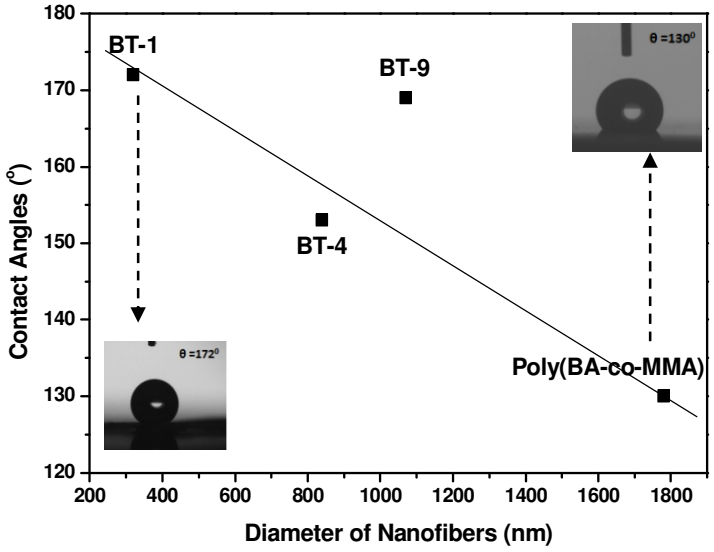

Figure 4.25 : The relationship between Contact Angle and Diameter of nanofibers for poly(BA-co-MMA) and fluorinated copolymers.

Increasing the Fluorine content of composite should have an effect on the contact angle due to the Fluorine content on nanofiber surface. The expectation is, higher the Fluorine content, higher the contact angle (see Table 4.10) as it can be seen from Table 4.10 for all samples it was the case except for BT-9.

The highest contact angle is found for BT-1 due to the contact angles of bead fibers are higher than that of bead-free fibers for the samples [156]. Quite number of nanofibers and micro beads appear on the BT-1 structure and such a micro-nano hierarchical structure (Figure 4.26) leads to a superhydrophobicity with a contact angle of 172^{o}.

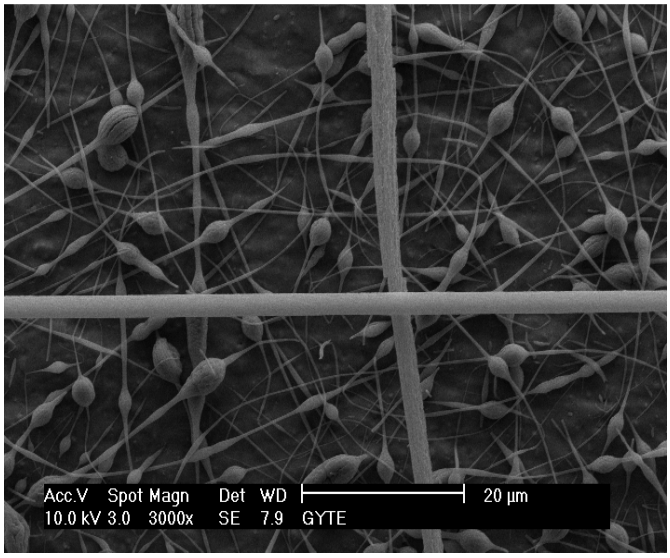

Figure 4.26 : SEM images of BT-1

According to the H. Xiang et al. and R. Asmatulu et al. smaller fibers have higher contact angle than that of larger fibers for the same samples [132,157]. However, in this study copolymer contents are variable and thus these phenomenons are exactly not the similar.

5.CONCLUSION

The first objective of this theses was to obtain Nanofibers of n-Butyl Acrylate/Methyl Methacrylate copolymer by electrospinning method. Thus, first n-Butyl Acrylate/Methyl Methacrylate copolymer was synthesized [P(BA-co-MMA)]by Emulsion polymerization in aqeuos medium. FTIR-ATR spectra and NMR spectrum revealed that BA and MMA had effectively participated in polymerization. SEM images indicate that the diameters of P(BA-co-MMA) nanofibers were strongly dependent on polymer solution concentrations, dielectric constant of solution and flow rate. Based on the parameter study, electrospun P(BA-co-MMA) fibers as small as 390±30 nm were successfully produced. The diameters of the fibers increase slightly as the concentration of the P(BA-co-MMA) solution is increased and Bead-free nanofibers and smaller fiber can be obtained for the polymer solutions having high dielectric constant. Moreover, processing conditions were examined and as the flow rate is increased, fiber diameter increases. This is apparent that there is a greater volume of solution fiber is drawn away from the needle tip. The diameter values range from 390 nm to 1180 nm for the P(BA-co-MMA) nanofibers.

The second objective of this theses was to produce nanofibers of acrylate-based copolymers with unique properties imparted by the presence of fluoroalkyl containing monomer, which we have succeeded to obtain nanofiber of poly(PFMA-ran-MMA-ran-BA) beaded fiber and bead-free fiber formation which was not the case in most of previous studies for similar structure. These results indicate that successful preparation of surfaces with fluorine containing copolymers are possible by using electrospinning technique. Such Electrospun nanofiber might open the possibility of designing new specific membranes, biomedical and reinforced composite applications. It was found that the molecular weight and feed flow rate of the copolymers has an important effect on nanofiber formation and less bead formation. Maximum feed flow rate resulted as 1,78 µm fiber diameter. Superhydrophobic surfaces are obtained by a simple one-step method of electrospinning of fluorinated copolymers. The hydrophobicity and superhydrophobicity seems to be related to the surface morphology. Such surface

formation (water-resistant coatings) indicated the superhydrophobicity ‘water-roll’ effect at an angle of about 0^{0},(water droplets on such surfaces rolles away). The results are comparable with the corresponding nonfluorinated copolymer.

REFERENCES

[1] **Huang, Z. M., Zhang, Y. Z., Kotaki, M., Ramakrishna, S.,** (2003). A review on polymer nanofibers by electrospinning and their applications in nanocomposites, *Comp. Sci. & Tech.,* vol.63, pp. 2223-2253.

[2] **Gonzalez, I., Asua, J. M., and Leiza J. R.,** (2007). The role of methyl methacrylate on branching and gel formation in the emulsion copolymerization of BA/MMA, *Polymer,* vol.48, pp 2542-2547.

[3] **Hong, S.L, Jin G.L., Jia M.R., Lin, F., Shi, Y.Y.,** (1996). Synthesis and characterization of novel fluorinated aromatic polyimides derived from1,1-bis(4-amino-3,5-dimethylphenyl)-1-(3,5-ditrifluoro methyl phenyl)-2,2,2-trifluoroethane and various aromatic dianhydrides, *J. Polym Sci Part A Polym Chem,* vol.44,pp 2665–2674.

[4] **Hougham, G., Cassidy, P.E., Johns, K., Davidson, T.,** editors. (1999) Fluoropolymers 1: Synthesis. Fluoropolymers 2: Properties, *New York, Plenum Press.*

[5] **Wang, F., Ma, C., Sun, W., Li, A., Zhao, Y., Zhang, H.**, (2004). 32-Channel arrayed-waveguide-grating multiplexer using fluorinated polymers with high thermal stability, *Microwave Optl Technol Lett,* vol.42, pp 192–196.

[6] **Mahua G. Dhara, M. G., and Banerjee, S.,** (2010). Fluorinated high-performance polymers: Poly(arylene ether)s and aromatic polyimides containing trifluoromethyl groups, *Progress in Polymer Science, vol.*35, pp 1022–1077.

[7] **Singh, A., Steely, L., and Allcock, H. R.,** (2005). Poly[bis(2,2,2-trifluoroethoxy)phosphazene] Superhydrophobic Nanofibers, *Langmuir,* Vol. 21, pp 11604-11607.

[8] **Nuyken, O., and Lattermann, G**., (1991). Handbook of Polymer Synthesis Part A, 1st ed, (Kricheldorf, H. R., ed.), *Marcel Dekker, New York, p. 223* ISBN: 978-0-8247-5473-0.

[9] **Warson, H. and Finch, C.A.,** (2001). Applications of Synthetic Resin Latices: Fundamental chemistry of latices and applications of adhesives*, John Wiley & Sons Inc.* ISBN 0-471-95268-0.

[10] **Fittig, R., and Paul, L.,** (1887). *Justus Liebigs Ann. Chem.,* 188: 55.

[11] **Fittig, R., and Engelhorn, F. R.,** (1880). *Justus Liebigs Ann. Chem.,* 200: 70.

[12] **Kahlbaum, G. W. A.,** (1880). Über polymere Acrylsäuremethylester, *Ber. Dtsch. Chem. Ges.,* 13: 2348.

[13] **Röhm, O.,** (1901). *On the Polymerization Products of Acrylic Acid*, Ph.D. thesis.

[14] **Röhm, O.,** (1914). U.S. patent 1,121,134; CA (1914), 09: 395 A.

[15] **Barker, A. L., and Skinner, G. S.,** (1924). *J. Am. Chem. Soc.,* 46: 403.

[16] **Riddle, E. H.,** (1954). Monomeric Acrylic Esters, *Reinhold, New York.*

[17] **Kautter, C. T.,** (1975). *Plastics Handbook, Polymethacrylate (Polymethacrylates) Kunststoff Handbuch,* Vol. 9, p. 1., Edited by R. Vieweg and F. Esser. Carl Hanser Verlag, München.

[18] **Kine, B. B., and Novak, R. W.,** (1985) Encyclopedia of Polymer Science and Engineering, *2nd ed.,* (Mark, H. F., Bikales, N. M., Overberger, C. G., and Menges, G., eds.), p. 234. *Wiley,* New York.

[19] **Charles E. Carraher, Jr.,** (2003) Giant molecules; Essential Materials for everyday living and problem solving*, 2nd Ed. John Wiley & Sons Inc*. ISBN 0-471-27399-6.

[20] **Thompson, L. F., C. G. Willson, and J. M. J. Frechet.,** (1984) Materials for Microlithography: Radiation-Sensitive Polymers, *American Chemical Society*, vol. 266, pp 5026–5026.

[21] **Htoo, M. S.,** *(1989*). Microelectronic Polymers, *Marcel Dekker, Inc., New York..*

[22] **Semegen, S. T.,** (1991). Encyclopedia of Physical Science and Technology*, Polymers, 3rd ed.,* pp. 395-405, *Academic Press*.

[23] **Sardar, D., Radcliffe, S. V., and Baer, E.,** (1968) *Polym. Eng. Sci. Vol.*8, pp 290.

[24] **Sookne, A. M., and Harris, M.,** (1945). *Ind. Eng. Chem.* vol.37, pp 478.

[25] **Chern, C. S.,** (2008). *Principles and Applications of Emulsion Polymerization* pp 129, *John Wiley & Sons, Inc.,* ISBN 978-0-470-12431-4.

[26] **Painter, P. C., and Coleman M. M.,** (2009). Essentials of Polymer Science and Engineering, pp 517, *DEStech Publications,Inc., ISBN* 978-1-932078-75-6.

[27] **Cengiz, U., Gengec, N. A., Kaya, N. U., Erbil, H. Y., and Sarac, A. S.,** (2011). Mechanical and thermal properties of perfluoroalkyl ethyl methacrylate–methyl methacrylate statistical copolymers synthesized in supercritical carbon dioxide, *Journal of Fluorine Chemistry,* vol.132, pp 348–355.

[28] **Hartmann, P., Collet, A., and Viguier, M.,** (2006). Acrylic Copolymers with perfluoroalkylated biphenyl side groups, correlation structure-surface properties, *Macromolecules*, vol.39, pp 6975–6982.

[29] **van de Grampel, R. D., Ming, W., Gildenpfennig, A., van Gennip, W. J. H., Laven, J., Niemantsverdriet, J. W., Brongersma, H. H., de With, G., van der Linde, R.,** (2004). The outermost atomic layer of thin films of fluorinated polymethacrylates, *Langmuir,* vol.20, pp 6344-6351.

[30] **Liu, J.J., Moore, G., and Pellerite, G. I**., (2010). 3M Innovative Properties Company, *US Patent*, 7,682,771.

[31] **Huang, P.Y., Chao, Y.C., and Liao, Y.T.,** (2004). Preparation of fluoroacrylate nanocopolymer by miniemulsion polymerization used in textile finishing, *J. Appl. Polym. Sci.,* vol.94, pp 1466-1472.

[32] **Choi, D.I., Yeom, E.H., Park, M., Kim, J. K., and Byoung, C. K., (**2004). *J. Appl. Polym. Sci*., vol.93, pp 2082–2089.

[33] **DeSimone, J.M., and Z. Guan, C.S.,** (1992). *Elsbernd, Science,* vol.257, pp 945–947.

[34] **Park, I.J., Lee, S.B., and Choi, C.K.,** (1997). Synthesis of fluorine-containing graft copolymers of poly(perfluoroalkylethyl methacrylate)-g-poly (methyl methacrylate) by the macromonomer technique and emul-sion copolymerization method, *Polymer,* vol. 38, pp 2523–2527.

[35] **Hillmyer, M.A. and Lodge, T.P**., (2002). Synthesis and self-assembly of fluorinated block copolymers, *J. Polym. Sci. Part A:Polym Chem.*, vol.40, pp 1-8.

[36] **Baykal, L.,** (2007). M. Sc. Thesis, *Istanbul Technical University*.

[37] **Zisman W.A., (**1964). Relation of the Equilibrium Contact Angle to Liquid and Solid Constitution, *Advances in Chemistry*, Vol.43, pp. 1-51.

[38] **Li, D., Neumann, A.W.,** (1992). Contact Angles on Hydrophobic Solid Surfaces and Their Interpretation, *Adv. Colloid Interface Sci.*, Vol.148, pp. 190-200.

[39] **Li, D., Neumann, A.W.,** (1992). Equation of State for Interfacial Tensions of Solid Liquid Systems, *Adv. Colloid Interface Sci.*, Vol.39, pp. 299-345.

[40] **Kwok, D.Y., Neumann, A.W., (**1999). Contact Angle Measurement and Contact Angle Interpretation, *Adv. Colloid Interface Sci.*, Vol.81, pp. 167-249.

[41] **Fowkes, F.M., (**1964). Dispersion Force Contributions to Surface and Interfacial Tensions, Contact Angles, and Heats of Immersion, *Advances in Chemistry,* Vol.43, pp. 99-111.

[42] **Driedger, O., Neumann, A.W., Sell, P.J.,** (1965). An Equation of State for Surface Free Energies II, *Kolloid-Z. u. Z. Polym.,* Vol.204, pp. 101-105.

[43] **Neumann, A.W., Good, R.J., Hope, C.J., Sejpal, M.J., (**1974). An Equation-of-State Approach to Determine Surface Tensions of Low-Energy Solids from Contact Angles, *J. Colloid Interface Sci.,* Vol.49, pp. 291-304.

[44] **Spelt, J.K., Li, D.,** (1996). The equation of state approach to interfacial tensions in: **Neumann A.W., Spelt, J.K.** *Applied Surface Thermodynamics*, Marcel Dekker Inc, New York, pp. 239-292.

[45] **Van Oss, C.J., Chaudhury, M.K., Good, R.J.,** (1988). Additive and nonadditive surface tension components and the interpretation of contact angles, *Langmuir,* Vol.4, pp. 884-891.

[46] **C.N.C. Lam, R.Wu, Li, D., Hair, M.L., and Neumann**, **A.W.,** (2002). Study of the advancing and receding contact angles: liquid sorption as a

cause of contact angle hysteresis, *Advances in Colloid and Interface Science,* Vol.96, pp 169-191.

[47] **Erbil, H.Y.,** (2006). Surface Chemistry of Solid and Liquid Interfaces, *Blackwell Publishing,* pp 352.

[48]**Baykal, L., (**2007). Fluorine Containning Copolymers, M.Sc thesis, *Istanbul Technical Unıversity*

[49] **Göktaş, A.,** (2008). Electrospinning of Polystyrene/Butyl Rubber Blends: A Parametric Study' *Postgraduate thesis.*

[50] **Roco, M.C., William, R.S. and Alivisatos, P. (Eds.),** (1999). The Interagency Working Group on Nanoscience, Engineering and Technology, *Vision for Nanotechnology Research and Development in the Next Decade.*

[51] **Daşdemir, M.,** (2006). Electrospinning of Thermoplastic Polyurethane (TPU) for Producing Nanofibers**,** *Postgraduate thesis.*

[52] **Huang, Z. M., Zhang, Y. Z., Kotaki, M., Ramakrishna, S.,** (2003). A review on polymer nanofibers by electrospinning and their applications in nanocomposites, *Comp. Sci. & Tech.,* vol.63, pp. 2223-2253.

[53] **Ramakrishna, S., Fujihara, K., Teo, W.E., Ma, Z.W. and Lim, T.C.,** (2005). An Introduction to Electrospinning and Nanofibers, *World Scientific Publishing Co. Pte. Ltd., ISBN* 981-256-415-2.

[54] **Feng, L., Li, S., Li, H., Zhai, J., Song, Y., Jiang, L., and Zhu, D.,** (2002). SuperHydrophobic Surface of Aligned Polyacrylonitrile Nanofibers, *Angew. Chem. Int. Ed.,* vol.41, pp. 1221-1223.

[55] **Martin, C. R.,** (1995). Template Synthesis of Electronically Conductive Polymer Nanostructures, *Acc. Chem. Res.,* vol.28, pp. 61-68.

[56] **Martin, C. R.,** (1996). Membrane-Based Synthesis of Nanomaterials, *Chem. Mater.,* vol. 8, pp. 1739-1746.

[57] **Huczko, A.,** (2000). Template-based synthesis of nanomaterials, *Appl. Phys.,* vol.70, pp. 365-376.

[58] **Kataphinan, W.,** (2004). Electrospinning and Potential Applications, *PhD Thesis, The Graduate Faculty Of The University Of Akron.*

[59] **Formhals, A.** (1934). *US Patent.* 1,975,504.

[60] **Formhals ,A.,** (1939). *US Patent* 2,160,962.

[61] **Formhals, A.,** (1940). *US Patent*. 2,187,306.

[62] **Formhals ,A.,** (1943). *US Patent*. 2,323,025.

[63] **Formhals, A**., (1944). *US Patent*. 2,349,950.

[64] **Huang, M.Z., Zhang, Y.Z., Kotaki, M. and Ramakrishna, S. A. (**2003). Review On Polymer Nanofibers By Electrospinning and Their Applications in Nanocomposites, *Composites Science And Technology*, vol.63, pp. 2223-2253.

[65] **Vonnegut, B., and Neubauer R.L.** (1952). Production of monodisperse liquid particles by electrical atomization, *Journal of Colloid Science,*vol.*7*, pp. 616-622.

[66] **Drozin, V.G.,** (1955). The electrical dispersion of liquids as aerosols, *Journal of Colloid Science*, vol.10, pp. 158-164.

[67] **Simons, H.L**., 1966: *US patent.* 3,280,229.

[68] **Baumgarten, P.K., (**1971). Electrostatic spinning of acrylic microfibers, *Journal of Colloid and Interface Science*, vol.36, pp.71–79.

[69] **Yarin, A.L., Koombhongse, S. and Reneker, D.H.,** (2001). Taylor cone and jetting from liquid droplets in electrospinning of nanofibers, *Journal of Applied Physics*, vol.90, pp. 4837-4846.

[70] **Reneker, D.H., Yarin, A.L., Koombhongse, S. and Fong, H., (**2000). Bending instability of electrical charged liquid jets of polymer solutions in electrospinning, *Journal of Applied Physics, vol.*87, pp. 4531-4547.

[71] **Reneker, D.H. and Chun, I.,** (1996). Nanometre diameter fibres of polymer, produced by electrospinning, *Nanotechnology, vol.***7**, pp. 216-223.

[72] **Koombhongse, S., Liu, W., Reneker, D. H.,** (2001). Flat ribbons and other shapes by electrospinning, *J. of Poly. Sci. Poly. Phys. Ed.,* vol.39, pp. 2598-2606.

[73] **Diaz de Leon, M. J.,** (2001). Electrospinning Nanofibers of Polyaniline and Polyaniline/(Polystyrene and Polyethylene Oxide) Blends, *Proc. of Nat. Con. Undergrad. Res., Lexington, Uni. Of Kentucky.*

[74] **Frenot, A., and Chronakis, I. S.,** (2003). Polymer nanofibers assembled by electrospinning, *Cur. Opi. in Col. and Inter. Sci.,* vol.8, pp. 64-75.

[75]**Cetiner, S., Kalaoglu, F., Karakas, H., Sarac, A.S., (**2010). Electrospun Nanofibers of Polypyrrole-Poly(Acrylonitrile-co-Vinyl Acetate), *Textile Research Journal.* vol.80, pp. 1784-1792.

[76] **Taylor, G. I.,** (1969). Electrically Driven Jets, *Proc. of Roy. Soc.*, vol.313, pp. 453-475.

[77] **Subbiah, T., Bhat, G. S., Tock, R. W., Parameswaran, S., and Ramkumar, J. S.,** (2005). Electrospinning of Nanofibers, *J. of Appl. Poly. Sci.,* vol.96, pp. 557-569.

[78] **Fong, H., Chun, I., and Reneker, D. H.,** (1999). Beaded nanofibers formed during electrospinning, *Polymer,* vol.40, pp. 4585-4592.

[79] **Yang, Q., Li, Z., and Hong, Y.,** (2004). Influence of Solvents on the Formation of Ultrathin Uniform Poly(vinyl pyrrolidone) Nanofibers with Electrospinning, *J. of Poly. Sci.:Part B:Poly. Phys.,* vol.42, pp. 3721-3726.

[80] **Zeng, J., Xu, X., Chen, X., Liang, Q., Bian, X., Yang, L., and Jing, X.,** (2003). Biodegradable electrospun fibers for drug delivery, *J. of Cont. Rel.,* vol.92, pp. 227-231.

[81] **Lin, T., Wang, H., Wang, H., Wang, X.,** (2004). The charge effect of cationic surfactants on the elimination of fibre beads in the electrospinning of polystyrene, *Nanotechnology*, vol.15, pp. 1375-1381.

[82] **Clark, A.L., (**1938). The Critical State of Pure Fluids, *Chem Rev., vol.*23, pp. 1-15.

[83] **[109] Deam, J. R. and Maddox, R. N., (**1970). Interfacial Tension in Hydrocarbon Systems, *J. Chem. Eng. Data.,* vol.15, pp. 216-222.

[84] **Son, W. K, Youk, J. H, Lee, T. S. and Park, W. H.**, (2004a). The effects of solution properties and polyelectrolyte on electrospinning of ultrafme poly(ethylene oxide) fibers, *Polymer*, vol.45, pp. 2959-2966.

[85] **Lee, K.H., Kim, H.Y., Ra, Y.M. and Lee, D.R.,** (2003b). Characterization of nanostructured poly(e-caprolactone) nonwoven mats via electrospinning, *Polymer,* vol.44, pp. 1287-1294.

[86] **Hsu, C. M., and Shivakumar, S.**, (2004). N,N-Dimethylformamide Additions to the Solution for the Electrospinning of Poly(e-caprolactone) Nanofibers, *Macromol. Mater. Eng.* vol.289, pp. 334-340.

[87]**Buchko, C. J, Chen, L. C, Shen, Y. and Martin, D. C.** (1999). Processing and microstructural characterization of porous biocompatible protein polymer thin films, *Polymer*, vol.40, pp. 7397-7407.

[89]**Baumgarten, P. K.,** (1971). Electrostatic Spinning of Acrylic Microflbers, *J. Colloid Interf. Sci., vol.*36, pp. 75-79.

[90] **Jarusuwannapoom, T., Hongrojjanawiwat, W., Jitjaicham, S., Wannatong, L., Nithitanakul, M., Pattamaprom, C, Koombhongse, P., Rangkupan, R. Amd Supaphol, P.,** (2005). Effect of solvents on electro-spinnability of polystyrene solutions and morphological appearance of resulting electrospun polystyrene fibers, *Euro. Polym. J.*, vol.41, pp. 409-421.

[91] **Demir, M. M., Yilgor, I., Yilgor, E. and Erman, B.,** (2002). Electrospinning of polyurethane fibers, *Polymer*, vol.43, pp. 3303-3309.

[92] **Deitzel, J.M., Kosik, W., McKnight, S.H., Tan, N.C.B., DeSimone, J.M. and Crette, S.,** (2002). Electrospinning of polymer nanofibers with specific surface chemistry, *Polymer*, vol.43, pp. 1025-1029.

[93] **Megelski, S., Stephens, J.S., Chase, D.B. and Rabolt, J.F.,** (2002). Micro- and nanostructured surface morphology on electrospun polymer fibers, *Macromolecules*, vol.35, pp. 8456-8466.

[94] **Subbiah, T., Bhat, G. S., Tock, R. W., Parameswaran, S., and Ramkumar, J. S.,** (2005). Electrospinning of Nanofibers, *J. of Appl. Poly. Sci.,* , vol..96, pp.557-569.

[95] **Zheng, J., He, A., Li, J., Xu, J., and Han, C. C., (**2006). Studies on the controlled morphology and wettability of polystyrene surfaces by electrospinning or electrospraying, *Polymer*, vol.47, pp. 7095-7102.

[96] **Matthews, J. A., Wnek, G. E., Simpson, D. G., and Bowlin, G. L.,** (2002). Electrospinning of Collagen Nanofibers, *Biomacromolecules*, vol.3, pp. 232-238.

[97] **Koombhongse, S., Liu, W., Reneker, D. H.,** (2001). Flat ribbons and other shapes by electrospinning, *J. of Poly. Sci. Poly. Phys. Ed.,* vol.39, pp. 2598-2606.

[98] **Taylor, G.,** (1964). Disintegration of Water Drops in an Electric Field, *Proc. R. Soc. Lond.,* vol.280, pp. 383-397.

[99] **Zhong, X. H., Kim, K. S., Fang, D. F., Ran, S. F., Hsiao, B. S. and Chu, B.,** (2002). Structure and process relationship of Electrospun bioabsorbable nanofiber membranes, *Polymer,* vol.43, pp. 4403-4412.

[100] **Wang, C., Hsu, C. H., and Lin, J. H.,** (2006). Scaling Laws in Electrospinning of Polystyrene Solutions, *Macromolecules*, vol.39, pp. 7662-7672.

[101] **Baker, S. C., Atkin, N., Gunning, P. A., Granville, N., Wilson, K., Wilson, D., Southgate, J.,** (2006). Characterisation of electrospun polystyrene scaffolds for three-dimensional in vitro biological studies, *Biomaterials*, vol.27, pp. 3136-6146.

[102] **Rutledge, G. C, Li, Y., Fridrikh, S., Warner, S. B., Kalayci, V. E. and Patra, P. (**2000). Electrostatic Spinning and Properties of Ultrafine Fibers, *National Textile Center, Annual Report (M98-D01),* pp. 1-10.

[103] **Yuan, X., Zhang, Y., Dong, C. and Sheng, J.,** (2004). Morphology of ultrafine polysulfone fibers prepared by electrospinning, *Polym. Int.* Vol.53, pp. 1704–10.

[104] **Kosmider K., and Scott J.,** (2002). Polymeric nanofibres exhibit an enhanced air filtration performance, *Filtr Separat.,* vol.6, pp. 20—22.

[105] **Gibson P., Schreuder-Gibson H., Rivin D.,** (2001). Transport properties of porous membranes based on electrospun nanofibers, *Coll Surf A: Physicochem Eng Asp,* vol.8, pp. 469—481.

[106] **Barhate R S, Ramakrishna S.**, (2007). Nanofibrous filtering media:Filtration problems and solutions from tiny materials, *J Membrane Sci.,* vol.1-2, pp. 1—8.

[107] **Shin C., Chase G. G., and Reneker D. H.,** (2005). Recycled expanded polystyrene nanofibers applied in filter media, *Coll Surf A: Physicochem Eng Asp*, 262(1-3): pp. 211-215.

[108] **Shin C., Chase G. G., and Reneker D. H., (**2005). The effect of nanofibers on liquid- liquid coalescence filter performance, *AIChE J*, 51(12), pp. 3109-3113.

[109] **Wang X, Chen X, Yoon K, et al.** (2005). High flux filtration medium based on nanofibrous substrate with hydrophilic nanocomposite coating, Environ Sci Tech, vol.39, pp. 7684-7691.

[110] **Barhate, R. S., Loong, C. K., Ramakrishna S.,** (2006). Preparation and characterization of nanofibrous filtering media, *J Membrane Sci,* , vol.283, pp. 209-218.

[111] **Gopal, R., Kaur, S., Ma, Z., Chan, C., Ramakrishna, Matsuura, T.,** (2006). Electrospun nanofibrous filtration membrane, *J Membrane Sci.,* vol. 281, pp. 581-586.

[112] **Gopal R, Kaur S, Feng C Y, Chan, C., Ramakrishna, Tabe, S., and Matsuura, T.,** (2007). Electrospun nanofibrous polysulfone membranes as pre-filters: Particulate removal, *J Membrane Sci.,* vol.289, pp. 210-219.

[113] **Chronakis, I. S.,** (2005). Novel nanocomposites and nanoceramics based on polymer nanofibers using electrospinning process-a review, *Journal of Materials Processing Technology,* vol.167, pp 283-293.

[114] **Bergshoef, M. M., and Vancso, G. J.,** (1999). Transparent nanocomposites with ultrathin, electrospun nylon-4,6 fiber reinforcement, *Advanced Materials* ,vol.11, pp. 1362-1365.

[115] **Luzhansky, M. D., (**2003). Qualıty Control In Manufacturıng Of Electrospun Nanofıber Composıtes. *International Nonwovens Technical Conference. Baltimore- Maryland, 1-7.*

[116] **Huang, M.Z., Zhang, Y.Z., Kotaki, M. and Ramakrishna, S. A.**, (2003). Review On Polymer Nanofibers By Electrospinning and Their Applications in Nanocomposites, *Composites Science And Technology*, vol.*63*, pp. 2223-2253.

[117] **Lyons, J., and Kaufmann, J.,** (2004). Electrospinning: Past, Present & Future, *Textile World,* vol.8, pp. 46.

[118] **Url-1 <***http://schwartz.eng.auburn.edu/research/picts/plant.jpg***>** accessed at 02.12.11.

[119] **Aussawasathien, D., Dong, J. H., and Dai, L.,** (2005). Electrospun polymer nanofiber sensors, *Synthetic Metals,* vol.154, pp. 37–40.

[120] **Dersch, R., Steinhart, M., Boudriot, U., Greiner, A., and Wendorff, J. H.,** (2005). "Nanoprocessing of polymers: applications in medicine, sensors, catalysis, photonics, *Polymers for Advanced Technologies,* vol.16, pp. 276-282.

[121] **Ding, B., Gong, J., Kim, J., and Shiratori, S.,** (2005b). "Polyoxometalate nanotubes from layer-by-layer coating and thermal removal of electrospun nanofibres, *Nanotechnology*, vol.16, pp. 785-790.

[122] **Virji, S., Huang, J. X., Kaner, R. B., and Weiller, B. H**., (2004). Polyaniline nanofiber gas sensors: examination of response mechanisms, *Nano Letters, vol.*4, pp. 491–496.

[123] **Uyar, T., Balan, A., Toppare, L., and Besenbacher, F.,** (2009). Electrospinning of cyclodextrin functionalized poly(methyl methacrylate) (PMMA) nanofibers, *Polymer,* vol.50, pp.475-480.

[124] **Wang, M., Hsieh, A. J., and Rutledge, G.C.,** (2005). Electrospinning of poly(MMA-co-MAA) copolymers and their layered silicate nanocomposites for improved thermal properties, *Polymer*, vol.46, pp. 3407–3418.

[125] **Blossey**, **R.,** (2003). Self-cleaning Surfaces-Virtual Realities, *Nature Mater.*, Vol.*2*, pp. *301-306*.

[126] **Lafuma, A., and Quere, D.,** (2003). Superhydrophobic states, *Nat. Mater. Vol.2*, pp. 457-460.

[127] **Patankar, N. A.,** (2004). Mimicking the lotus effect: Influence of double roughness structures and slender Pillars, *Langmuir,* vol.20, pp. 8209-8213.

[128] **Nakajima, A., Hashimoto, K., Watanabe, T., Takai, K., Yamauchi, G., Fujishima, A.,** (2000). Transparent superhydrophobic thin films with self-cleaning properties, *Langmuir*, vol.16, pp. 7044-7047.

[129]**Furstner, R.; Barthlott, W., Neinhuis, C., Walzel, P.,** (2005). Wettting and self-cleaning properties of artificial superhydrophobic surfaces, *Langmuir,* Vol.21, pp. 956-961.

[130] **Acatay, K.; Simsek, E., Yang, C. O., Menceloglu, Y. Z**., (2004). Stable Polymeric Surfaces by Electrospinning, *Angew.Chem. Int. Ed.* Vol.43, pp. 5210-5213.

[131] **Xiang, H., Zhang, L., Wang, Z., Yu, X., Long, Y., Zhang X., Zhao N., Xu J.,** (2011). Multifunctional polymethylsilsesquioxane (PMSQ)

surfaces prepared by electrospinning at the sol-gel transition: superhydrophobicity, excellent solvent resistance, thermal stability and enhanced sound absorption property, *Journal of Colloid and Interface Science,* Vol.359, pp 296-303.

[132] **Asmatulu, R., Ceylan M., Nuraje N.,** (2011). Study of superhydrophobic electrospun nanocomposite fibers for energy systems, *Langmuir,* Vol.27, pp 504–507.

[133] **Lim, H.S., Park S., Koo, S.H., Kwark Y.J., Thomas, E.L., Jeong, Y., Cho, J.H., (**2010). Superamphiphilic Janus fabric, *Langmuir,* Vol.26, pp 19159–19162.

[134] **Yano, T., Yah, W.O., Yamaguchi, H., Tereyama, Y., Nishihara, M., Kobayashi M., Takahara, A.,** (2011). Precise Control of Surface Physicochemical Properties for Electrospun Fiber Mats by Surface-Initiated Radical Polymerization, *Polymer Journal,* Vol.43, pp 838-848.

[135] **Hardman, S.J., Sarih, M.N., Riggs H.J., Thompson, R.L., Rigby, J., Bergius, W.N.A., Hutchings, L.R.,** (2011). Electrospinning superhydrophobic fibers using surface segregating end-functionalized polymer additives, *Macromolecules,* Vol.44, pp 6461-6470.

[136] **Ma, M., Mao, Y., Gupta, M., Gleason, K.K., Rutledge, G.C., (**2005). Superhydrophobic Fabrics Produced by Electrospinning and Chemical Vapor Deposition, *Macromolecules*, Vol. 38, pp 9742-9748.

[137] **Han, D., Steckl, A.J., (**2009). Superhydrophobic and oleophobic fibers by coaxial electrospinning, *Macromolecules*, Vol. 25, pp 9454-9462.

[138] **Yuan, X., Huo, D., and Qian, Q.,** (2010). Effect of annealing on the phase structure and the properties of the film formed from P(St-co-BA)/P(MMA-co-BA) composite latex, *Journal of Colloid and Interface Science,* vol.346, pp 72–78.

[139] **Ramesh, S., Leen, K.H., Kumutha, K., and Arof, A.K.,** (2007). *Spectrochimica Acta Part A*, Vol.66, pp 1237-1242.

[140] **Starkey, S.R., and Frech, R.,** (1997). *Electrochim. Acta* vol.42, pp 471.

[141] **Xie, H.Q., Liu, X.H., and Guo J.S.,** (2003). Synthesis and properties of amphiphilic copolymers of butyl acrylate and methyl methacrylate with uniform polyoxyethylene grafts, Journal of Applied Polymer Science, Vol.89, pp 2982-2988.

[142] **Taweerat' T., and Phattanarudee, S.,** (2010). Chitosan Encapsulation of Poly(*n*-butyl acrylate-*co*-methyl methacrylate) Particles, *Macromolecular Symposia,* Vol.296, pp 583-588.

[143] **Manders, B. G., Smulders, W., Aerdts, A. M., and Alex M., Herk, V.,** (1997). *Macromolecules,* vol.30*,* pp 322-323.

[144] **Kim,Y. S., Wright, J. B., and Grunlan, J. C.,** (2008). Influence of polymer modulus on the percolation threshold of latex-based composites *Polymer*, vol.49, pp 570-578.

[145] **Hua H.and Dube, M. A.,** (2001). Off-line Monitoring of Butyl Acrylate, Methyl Methacrylate and Vinyl Acetate Homo and Copoymerization in Toluene Using ATR-FTIR Spectroscopy, *Polymer,* vol.42, pp 6009-6018.

[146] **Aerdts, A. M., and German, A. L.,** (1994). Determination of the reactivity ratios, sequence distribution and stereoregularity of butyl acrylate-methyl methacrylate copolymers by means of proton and carbon-13 NMR, *Magnetic Resonance in Chemistry* vol.32, pp 80-88.

[147] **Chiefari, J., Jeffery, J., Julia Krstina, J., Moad, C. L., Moad, M., Postma, A., Rizzardo, E., and Thang, S. H.,** (2005). Binary Copolymerization with Catalytic Chain Transfer. A Method for Synthesizing Macromonomers Based on Monosubstituted Monomers, *Macromolecules,* vol.38, pp 9037-9054.

[148] **Buback, M., Feldermann, A., and Barner-Kowollik, C.,** (2001). Propagation Rate Coefficients of Acrylate-Methacrylate Free-Radical Bulk Copolymerizations, *Macromolecules* vol.34*, pp* 5439-5448.

[149] **Park, I.J., Lee, S.B., and Choi, C.K.,** (1997). *Polymer,* Vol. 38, pp 2523-2527.

[150] **Liu. Y., Haley, J.C., Deng, K., Lau, W., and Winnik, M.A.,** (2007). *Macromolecules*, Vol.40**,** pp 6422-6431.

[151] **Yu, H., Peng, J., Zhai, M., Li, J.,Wei, G., and Qiao, J.,** (2007). *Macromolecules,* Vol.76 pp 1746-1750

[152] **Roy, P., Jana, A.M., Das, D., and Nath, D. N.,** (2009). Study of magnetic field effect on Py-DMA exciplex luminescence in THF–DMF binary solvents: Evidence of multiple exciplex formation at higher bulk dielectric constant, *Chemical Physics Letters,* Vol.474, pp 297–301

[153] **Tan, S-H., Inai, R., Kotaki, M., and Ramakrishna, S.,** (2005). Systematic parameter study for ultra-fine fiber fabrication via electrospinning process, *Polymer* , Vol.46, pp 6128–6134.

[154] **Saidi, S.; Guittard, F.; Guimon, C.; Geribaldi, S., (**2006). *Journal of Applied Polymer Science***,** Vol. 99, pp 821-827.

[155] **Xiong, S., Gua, X., Li, L., Wu, S., Chu P.K., and Xu, Z. (**2010). *Journal of Fluorine Chemistry*, Vol.131, pp 417-425.

[156] **Xiang, H., Zhang, L., Wang, Z., Yu, X., Long, Y., Zhang, X., Zhao, N., J. Xu,** (2011). *Journal of Colloid and Interface Science* Vol. 359, pp 296-303.

[157] **Lim, H.S., Park, S., Koo, S., Kwark, Y.J., Thomas, E.L., Jeong, Y., Cho, J.H., (**2010). *Langmuir,* Vol.26, pp 19159–19162.

CURRICULUM VITAE

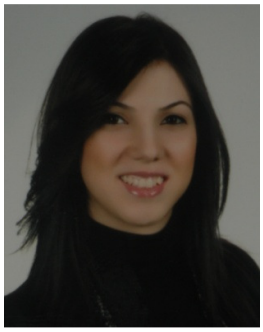

Name Surname: Merih Zeynep Avcı

Place and date of birth: Antalya- 21.04.1987

Address: Zeynep Kamil Mh. Divitciler Cd. Yeşil Artvin Apt. No: 30/9
Üsküdar/İSTANBULL

E-mail: mavci@itu.edu.tr/merih_avci07@hotmail.com

B.Sc.: Eskişehir Osmangazi University

M.Sc.: Istanbul Tehnıcal University

PUBLICATIONS/PRESENTATIONS ON THE THESIS

- **AVCI, M. Z., SARAC, A.S.,** 2011: Bütil Akrilat-Metil Metakrilat Kopolimerlerinden elektro lif çekim yöntemi ile nanolif eldesi, *1th Ar-Ge Proje Pazarı*, December 27-28, 2011 Yenibosna, Istanbul.

- **AVCI, M. Z., SARAC, A.S.,** 2011: Electrospun parameters of nanofibers of Poly(Butyl Acrylate-co-Methyl Methacrylate), *POLYCHAR 20 World Forum on Advanced Materials,* March 26-30,2012 Dubrovnik,CROATIA.